# Modeling and Simulation of a Combined Isomerization Reactor/Pressures Swing Adsorption Unit

by

Abdulhadi Abdullah Al-Juhani

A Thesis Presented to the

FACULTY OF THE COLLEGE OF GRADUATE STUDIES

KING FAHD UNIVERSITY OF PETROLEUM & MINERALS

DHAHRAN, SAUDI ARABIA

In Partial Fulfillment of the
Requirements for the Degree of

**MASTER OF SCIENCE**

In

**CHEMICAL ENGINEERING**

May, 2000

# INFORMATION TO USERS

This manuscript has been reproduced from the microfilm master. UMI films the text directly from the original or copy submitted. Thus, some thesis and dissertation copies are in typewriter face, while others may be from any type of computer printer.

**The quality of this reproduction is dependent upon the quality of the copy submitted.** Broken or indistinct print, colored or poor quality illustrations and photographs, print bleedthrough, substandard margins, and improper alignment can adversely affect reproduction.

In the unlikely event that the author did not send UMI a complete manuscript and there are missing pages, these will be noted. Also, if unauthorized copyright material had to be removed, a note will indicate the deletion.

Oversize materials (e.g., maps, drawings, charts) are reproduced by sectioning the original, beginning at the upper left-hand corner and continuing from left to right in equal sections with small overlaps.

Photographs included in the original manuscript have been reproduced xerographically in this copy. Higher quality 6" x 9" black and white photographic prints are available for any photographs or illustrations appearing in this copy for an additional charge. Contact UMI directly to order.

Bell & Howell Information and Learning
300 North Zeeb Road, Ann Arbor, MI 48106-1346 USA
800-521-0600

UMI®

# MODELING AND SIMULATION OF A COMBINED ISOMERIZATION REACTOR/PRESSURES SWING ADSORPTION UNIT

BY

**Abdulhadi Abdullah Al-Juhani**

A Thesis Presented to the

DEANSHIP OF GRADUATE STUDIES

**KING FAHD UNIVERSITY OF PETROLEUM & MINERALS**

DHAHRAN, SAUDI ARABIA

In Partial Fulfillment of the
Requirements for the Degree of

## MASTER OF SCIENCE

In

## CHEMICAL ENGINEERING

**May, 2000**

**KING FAHD UNIVERSITY OF PETROLEUM & MINERALS**

**DHAHRAN, SAUDI ARABIA**

**DEANSHIP OF GRADUATE STUDIES**

*This Thesis written by*

**Abdulhadi Abdullah Al-Juhani**

*Under the direction of his Thesis Advisor, and approved by his Thesis Committee, has been presented to and accepted by the Dean of Graduate Studies, in partial fulfillment of the requirements for the degree of*

**MASTER OF SCIENCE IN CHEMICAL ENGINEERING**

***Thesis Committee:***

Chairman (Dr. Kevin F. Loughlin)

Member (Dr. Jorge N. Beltramini)

Member (Dr. Ashraf I. Fatehi)

Dr. Abdullah A. Shaikh
Department Chairman

Dr. Abdullah M. Al-Shehri
Dean of Graduate Studies

Date: 23/5/2005

# ACKNOWLEDGMENTS

I will always remain thankful to my thesis committee chairman Dr. Kevin F. Loughlin for his sincere advise, valuable guidance and continuous assistance throughout the course of this work.

Thanks are also due to Dr Ashraf I. Fatehi and Dr. Jorge N. Beltramini, my thesis committee members, for their valuable help and guidance.

Acknowledgments are due to King Fahd University of Petroleum & Minerals, College of Graduate Studies and Chemical Engineering Department for granted me the opportunity and facilities to complete my M.S. Degree.

I wish also to express my deep thanks to Dr. Abdullah A. Shaikh, the chairman of chemical Engineering Department, for his continuous support and encouragement.

Finally, I thank all my friends who provide me all kinds of support I am ever in need of.

# CONTENTS

# LIST OF FIGURES

# LIST OF TABLES

# ABSTRACT


| | |
|---|---|
| NAME OF STUDENT | Abdulhadi Abdullah Al-Juhani |
| TITLE OF STUDY | Modeling and Simulation of a Combined Isomerization Reactor / Pressure Swing Adsorption Unit |
| MAJOR FIELD | Chemical Engineering |
| DATE OF DEGREE | May 2000 |



A novel process for isomerizing n-pentane to its branched isomers in a combined reactor/pressure swing adsorption unit (PSAR) is proposed. The unit is packed with two separate layers containing a catalyst (Pd/Y-zeolite) and an adsorbent (5A zeolite). The objective is to combine reaction with separation in one unit so that a significant cost saving in ancillary equipment may be achieved.

A mathematical model linking the catalyst layer and the adsorbent layer is developed. The model developed is general because it relaxes most simplified assumptions such as equilibrium theory, plug flow, constant velocity and frozen solid approximation. The model is used for predictions of the breakthrough curves for a fixed-bed adsorption/reaction column, with emphasis on the effects of temperature, total pressure, feed concentration, and catalyst/column length ratio. The catalyst/column length ratio has a stronger effect at lower temperatures. Also, the model is used to simulate a PSAR cycle with a configuration similar to the simple Skarstrom cycle. The simulation is conducted in the temperature range of 506-533 K. Adsorption/reaction step is conducted at high pressures (15-20 bar) and desorption/reaction step at low pressure (2 bar). It is found that the optimum catalyst/column length ratio is within the range of 0.4 to 0.6. Under the new configuration the blowdown stream has a considerable amount of isomers and could be considered as part of the product.

The proposed process is compared with the conventional isomerization process consisting of a tubular reactor followed by a PSA separation unit. The simulation results show that the proposed process is effective in accomplishing n-paraffin isomerization and separation.

# خـــــلاصة الـــــرسالة


اسم الطالب : عـبدالهادي بـــن عـبدالله الـجهني


عنوان الرسالة : نـمذجة ومـحاكاة مفاعـل الازمـرة تـحت الـضغط الـمتأرجح

التخصص : الهـــندسة الـكيميـائيـة

تاريخ الرسالة : مـــايـــو ٢٠٠٠ م


تم اقتراح طريقة مبتكرة لإجراء تفاعل لزمرة البنتان في وحدة تحتوي على طبقتين منفصلتين من محفـز كيميائي (فوجاسايت-بلاديوم) و ماص فيزيائي (٥أ زيولايت). الهدف هو دمج عمليتي التفاعل و الفصل في وحـدة واحدة, مما يؤدي إلى تقليل التكلفة العامة.

تم اشتقاق نموذج رياضي لوصف الطريقة المقترحة, وروعي في النموذج أن يكون عاماً بحيـث ألغـى معظم الفرضيات المبسطة. تم استخدام النموذج في توقع حالات التشبع و الانكسار لوحـدة مفـاعل الادمصـاص الثابت, مع دراسة تأثير درجة الحرارة, الضغط, تركيز اللقيم و طول طبقة المحفز الكيميائي. وجد أن طول طبقـة المحفز الكيميائي لها تأثير أقوى عند الحرارة المنخفضة. تم اسـتخدام النمـوذج أيضـاً لمحاكـاة دورة مفـاعل الادمصاص الضاغط المزدوج, الشبيهة بدورة سكارسترووم الأساسية. تمت المحاكاة في درجة حـرارة ٥٣٣-٥٠٦ ك, وتحت ضغط عالي ١٥-٢٠ بار, و ضغط منخفض عند ٢ بار. وجد أن القيمة المثلى لنسبة طول طبقة المحفز الكيميائي إلى الطول الكامل للوحدة ما بين ٠,٤ إلى ٠,٦ وأن الخليط الناتج من عملية تنظيف الوحدة يحتوي علـى نسبة كبيرة من ناتج الازمرة و يمكن اعتباره كجزء من المنتج النهائي.

تمت مقارنة العملية المبتكرة للازمرة مع العملية التقليدية المكونة من وحدتي مفاعل و فصـل بواسـطة الادمصاص. أظهرت النتائج أن العملية المقترحة فعالة لإجراء التفاعل و الفصل.


**درجة الماجستير في العلوم**

**جامعة الملك فهد للبترول المعادن**

**الظهران, المملكة العربية السعودية**

**مايو ٢٠٠٠**

# CHAPTER 1

# INTRODUCTION AND BACKGROUND

In this chapter a brief introduction to the topics discussed in this research thesis is given and the relevant literature on these topics is summarized.

## 1.1 INTRODUCTION

The isomerization of n-paraffins to high-octane number branched isomers is a method of upgrading naphtha to improve their utility as motor fuel components. For example, the unleaded research octane number (RON) for isopentane is 93 compared with 62 for n-pentane [28]. In the past, a lead compound was used as an additive to gasoline to increase its octane number. However, the use of lead now is restricted since it is known as a poisonous material and a strong air pollutant. Considering the available alternatives to upgrade gasoline-pool octane within the constraints of recent lead-reduction regulations, light straight-run naphtha isomerization is among the most effective [29].

Light straight-run naphtha, which consists mainly of n-pentane and n-hexane, is partially isomerized via an isomerization reactor. It is necessary to recycle the unreacted n-paraffins to the reactor. Separation by distillation is difficult and energy consuming because the n-/isoparaffins mixture is composed of components with close–boiling points. Alternatively, the separation is better done by selective adsorption using molecular sieves such as 5A zeolite, where the n-paraffins are adsorbed and the iso-paraffins are excluded [33,34].

This method is widely used in industry, such as the Total Isomerization Process (TIP) developed by Union Carbide in 1970 [19]. The flowsheet diagram and the block-flow diagram for the TIP process are shown in Figures 1.1 and 1.2, respectively. In the flowsheet diagram, the reactor (vessel#22) is typically operated most efficiently at high pressures (200-400 psia). The reaction must be conducted in the presence of hydrogen to avoid deactivation of the catalyst. Depending on the particular catalyst composition employed, the operating temperature of the isomerization reactor is generally within the range of 200 to 390$^{o}$ C. The TIP process employs a bifunctional catalyst, which consists of a noble metal such as platinum deposited on an acidic media such as Y-zeolite. The minimum hydrogen partial pressure required is also dependent on the catalyst used, and is usually in the range of

100 to 250 psia. Adsorber units (vessels 44, 46, 48, 50), however, have typically operated more efficiently at lower pressures (200-300 psia). Typical properties of the TIP process, as in the patent published by Gary [19], are summarized in Table 1.1.

## 1.2 n-PARAFFINS ISOMERIZATION REACTION

Paraffin isomerization requires a stable catalyst with high activity to take advantages of the higher equilibrium conversions to branched products at lower temperatures [29]. Selectivity is another important property for the catalyst where the undesired reaction is the cracking of alkanes [5].

Different isomerization catalyst systems have been developed, and a good summary of them is presented by Fujimoto *et al.* [18]. The catalyst systems can be classified into three groups: Friedel-Craft, bifunctional, and solid superacid catalysts. Up to 1956, commercial processes for the isomerization of light paraffins employed anhydrous aluminum chloride as the catalyst, which is known as Friedel-Craft catalyst. It possessed high activity for n-butane isomerization at low temperature below 90 $^{o}$C. However, because of its low selectivity, especially for n-$C_5$ and n-$C_6$ isomerization, poor structure stability, and strong corrosivity, it is out of use today.

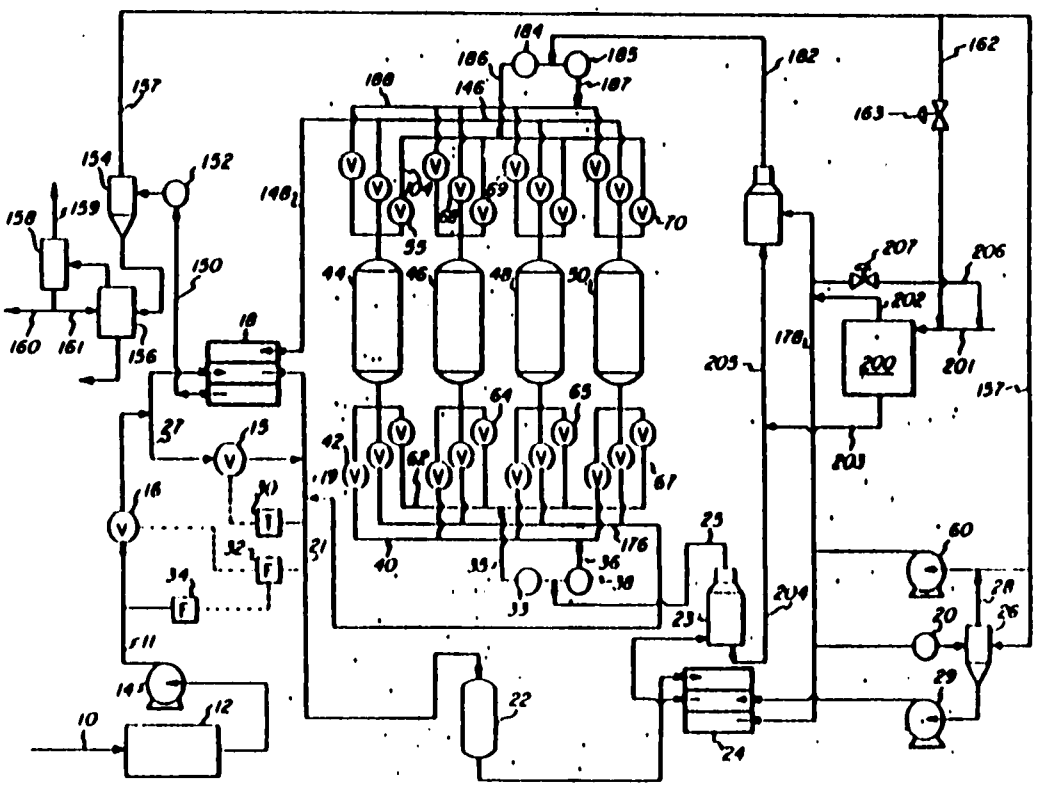

Figure 1.1. Flowsheet diagram for the Total Isomerization Process [19]

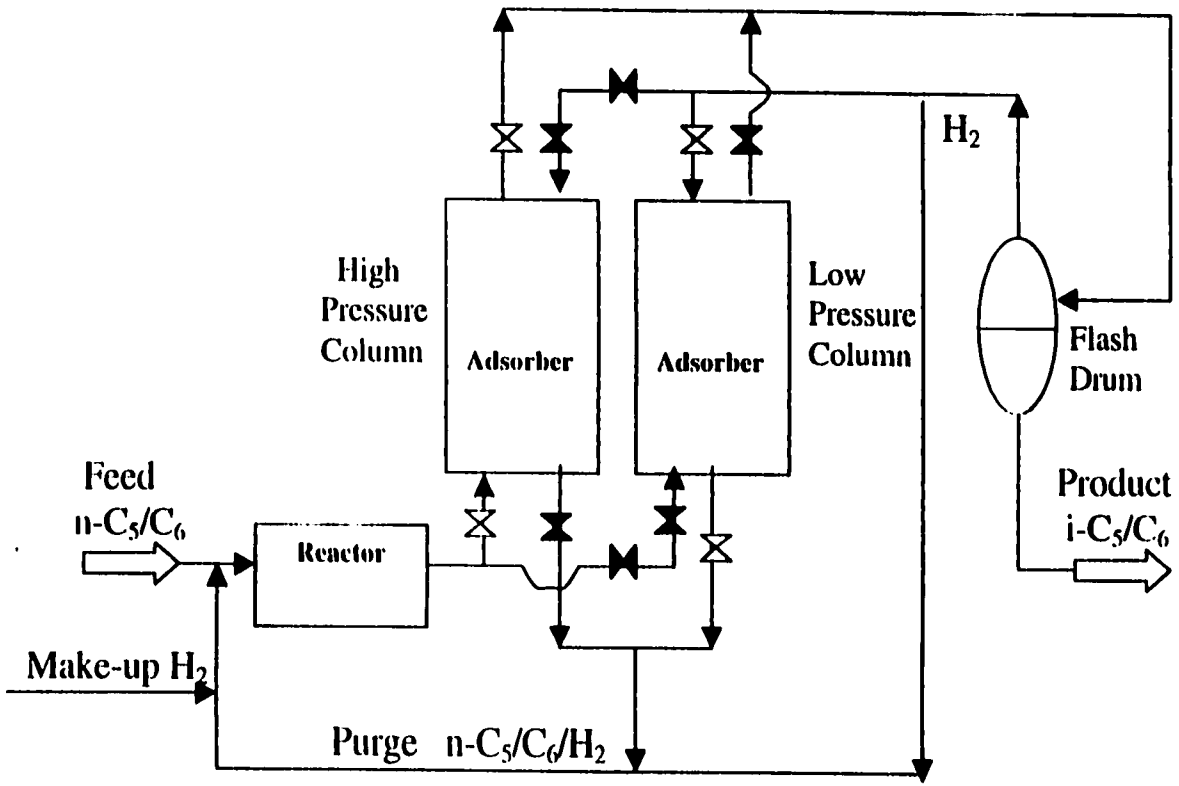


Figure 1.2 Block-flow diagram for the Total Isomerization Process

Table 1.1. Typical Properties of the Total Isomerization Process [19]

| | |
|---|---|
| ***Fresh Feedstock Composition :*** | |
| Components | Weight % |
| $C_4$ and lower | 4.1 |
| i-$C_5$ | 24.5 |
| n-$C_5$ | 27.8 |
| i-$C_6$ | 14.7 |
| n-$C_6$ | 27.4 |
| $C_7$ and higher | 1.5 |
| ***Reactor Condition:*** | |
| • Catalyst | 0.1-1.0 wt % Pt (Pd) / Y-zeolite |
| • Pressure | 14 – 28 bar |
| • Temperature | 200 – 390 $^0$C |
| • $H_2$ Partial Pressure | 7 – 14 bar |
| • $H_2$ feed composition | 50 – 70 mol % |
| ***Adsorbers Condition:*** | |
| • Adsorbent | 5A zeolite |
| • No. of beds | 4 |
| • No. of steps / bed | 4 (basic Skarstrom cycle) |
| • Pressure at adsorption step | 14 – 20 bar |
| • Temperature | 200 – 390 $^0$C |
| • Cyclic duration | 2 min/step; 8 min/cycle |

Then, bifunctional catalysts with a hydrogenation-dehydrogenation function (e.g., Pt or Pd) and an acid function (e.g., alumina, silica-alumina, or zeolites) were used. It is known that Pt-alumina is effective for the isomerization of n-$C_5$ and n-$C_6$, but it has to be used at high reaction temperature, usually between 455 and 510 $^{o}$C. To improve the performance and to lower the operating temperature, low temperature type bifunctional catalysts, which were Pt-alumina treated by $AlCl_3$ or organic chlorides, were developed and they have been widely used in the industry. Later, new kinds of bifunctional catalysts of noble metal/aluminosilicate and noble metal/zeolite were developed by Ribeiro in 1983, which produced a high conversion near to the equilibrium value at a medium temperature of 260 to 314 $^{o}$C [39].

The third group is solid superacid catalysts such as sulfated zirconia, which have been developed in recent years and are still under study. Most of these studies are for n-butane isomerization. A recent study was published in 1998 by Gates and Ryu for n-hexane isomerzation via sulfated zirconia [20]. Sulfated zirconia is shown to compromise the positive properties of the other two groups of catalysts. A summary comparing the three groups of catalysts is presented in Table 1.2.

Table 1.2. Properties of Isomerization Catalysts

| *CATALYST* | **Pt/Cl-Alumina** | **Pt/Zeolite** | **Solid Superacid** |
|---|---|---|---|
| *Reaction temperature* | Low (120-180 $^0$C) | Higher (250-280 $^0$C) | Low (180-220 $^0$C) |
| *Tolerance to feed contaminants (S, $N_2$,, water, oxygenates )* | Low | High | High |
| *Corrosion problem* | High | Low | Low |
| *Auxiliary equipment needed:* | | | |
| • *Cl injection* | Yes | No | No |
| • *HCl scrubber* | Yes | No | No |
| • *Feed dryers* | Yes | No | No |
| • *$H_2$ recycle* | No | Yes | Yes |

Hydroisomerization of n-paraffin on a bifunctional catalyst is considered to proceed through a mechanism whereby olefins are formed at the metallic site by dehydrogenation of the normal paraffin feed and are then adsorbed at an acidic site. At this acidic site, a carbonium ion is formed which undergoes skeletal rearrangement. The resulting isocarbonium ion is converted to an iso-olefin, which is then hydrogenated at the metallic site and desorbed. This is known as the classical Weisz bifunctional mechanism, which was first established by Weisz in 1962 [63]. This mechanism, shown schematically in Figure 1.3, dominated the explanation for hydroisomerization of n-paraffins for a long period. Different authors have proved that the skeletal isomerization of the reactive intermediate (i.e., the carbonium ion) is the rate-controlling step [5,8,9].

In 1982, Bryant and Spivey studied experimentally the hydroisomerization of n-$C_5$ / n-$C_6$ mixtures on a 0.5 wt% Pt/H-mordenite and a 0.5 wt% Pd/H-faujasite catalysts [9]. The rate constant values for a temperature range of 506 to 533 K have been published for the two catalyst systems. They have shown that mordenite is more active than faujasite. However, mordenite suffers from a high rate of deactivation [11,41,42]. Thus, faujasite is chosen as the catalyst for the present study, because catalyst deactivation is assumed negligible when modeling the process.

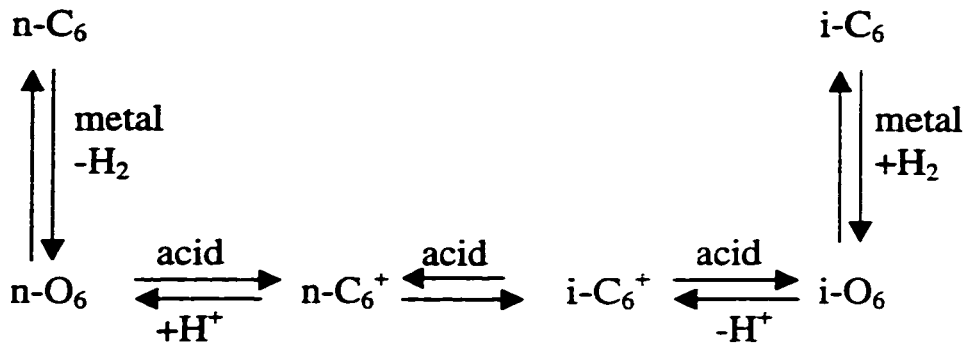


Figure 1.3. Weisz Bifunctional Mechanism [63]

($n\text{-}C_6$: n-hexane; $n\text{-}O_6$: n-hexene; $n\text{-}C_6^+$: n-carbonium ion; $i\text{-}C_6^+$: iso-carbonium ion; $i\text{-}O_6$: iso-hexene; $i\text{-}C_6$: iso-hexane )

## 1.3 PRESSURE SWING ADSORPTION (PSA) AND SEPARATION OF n-i/PARAFFINS MIXTURE

Pressure swing adsorption (PSA) is a process where one or more fixed beds are used to separate a gas or liquid mixture based on the differing affinities of individual components for a selected adsorbent. The selectivity may depend on a difference in adsorption equilibrium (equilibrium-based separation) or on a difference in sorption rates (kinetic-based separation). An example for the former is the production of oxygen by air separation on CaX zeolite, and an example for the latter is the production of nitrogen by air separation on 4A zeolite.

Modeling of PSA system is actually a process of linking up several models for sub-processes in the system. The PSA model should consider mass transfer, heat transfer, and physical equilibrium models. Reviews of these concepts are presented here.

### 1.3a EQUILIBRIUM ADSORPTION ISOTHERMS

Adsorption equilibria are described by isotherms, a relationship between adsorbed and bulk phase concentrations at constant temperatures. Different approaches are used to study the adsorption equilibrium isotherms on molecular sieve zeolites. The phenomena can be treated by

thermodynamic means using virial isotherms (e.g. Ruthven and Kaul [46]), by molecular models based on localized adsorption (e.g. Langmuir [30]; Nitta *et al.* [36]), or by empirical correlations (e.g. Yang [64]). Although a virial isotherm interprets data well from a thermodynamic point of view, it is unable to give insight into sorption events at the molecular level [4].

Sorption isotherms in zeolites generally follow type I in IUPAC classification. A representative and very well known isotherm for type I is Langmuir Isotherm [30], which is given by: $\theta = \frac{q}{q_{max}} = \frac{K_{ads}P}{1+K_{ads}P}$ ,

or alternatively : $K_{ads} = \frac{1}{P}\frac{\theta}{(1-\theta)}$

Nomenclature of the above expressions is presented at end of Chapter 2. In the above expression, Langmuir assumed that each adsorbed molecule occupies one active site, the surface is homogeneous, and no interaction exists between adsorbed molecules.

Based on Langmuir isotherm, Nitta *et al.* [36] developed the Multisite Langmuir (MSL) model, which is more reliable and accurate. Nitta *et al.* assumed that localized adsorption takes place where the adsorbed molecule occupies a certain number of active sites. n. They presented two types of isotherms for both homogeneous and heterogeneous surfaces. The expression for homogeneous surface is:

$$K_{ads} = \frac{1}{P}\frac{\theta}{(1-\theta)^n}$$

In the above expression, the interaction term between sorbed molecules is neglected. Also, if n equals 1, the expression is reduced to Langmuir isotherm. In 1997, Silva and Rodrigues proved experimentally that the Nitta *et al.* isotherm provides a good description of sorption of n-pentane and n-hexane in 5A zeolite. They found that n equals 5 and 6 for n-pentane and n-hexane, respectively [53,55].

The two models can be discriminated experimentally by plotting experimental data of $\frac{1}{P}\frac{\theta}{(1-\theta)^n}$ against $\theta$ at different temperatures. The appropriate model is the one that gives straight lines parallel to the $\theta$ axis.

### 1.3b KINETICS OF SORPTION

Zeolite molecular sieves consist of small microporous crystals formed in a macroporous pellet, as represented schematically in Figure 1.4. Therefore, there are three diffusion mechanisms: the gas-film diffusion around the pellet, the macropore diffusion into the pellets, and the micropore diffusions into the crystals. Under practical conditions of operation the external film resistance is negligible [47. 48]. Thus, the sorption rate is generally controlled by either macropore or micropore diffusion or by the

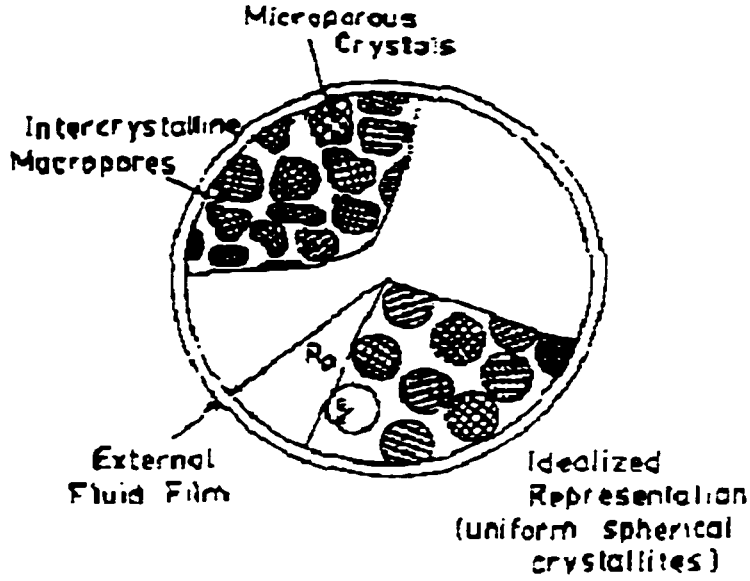


Figure 1.4. The resistance to mass transfer in a zeolite molecular sieve

combined effects of these resistances. Ruckenstein *et. al.* in 1971 proposed a bidisperse pore model for transient diffusion in bidisperse porous adsorbents, based on the assumption that the two mechanisms are in series [40]. Based on that model, Ruthven and Loughlin [45] developed a criterion for the relative importance of the diffusion mechanisms which is given by:

$$\gamma = \frac{(1+K)(D_c / r_c^2)}{(D_p / R_p^2)} \quad ,$$

where $R_p^2/D_p$ is the time constant for macropore diffusion, $r_c^2/D_c$ is the time constant for micropore diffusion, K is the capacity factor given by $(1-\varepsilon_p)H_{ad}/\varepsilon_p$ , and $H_{ad}$ is the dimensionless Henry's constant given by $\rho_s RTH / M_w$. Description to other notations is presented at end of Chapter 2. In the above expression, macropore diffusion is the controlling mechanism for $\gamma > 10$; crystal diffusion is the controlling mechanism for $\gamma < 0.1$. Between these limits, both mechanisms are important and should be taken into consideration.

The controlling diffusion mechanisms in zeolite molecular sieves can be determined experimentally by carrying out experiments in pellets with different sizes but with the same crystal size or pellets with the same size but with different crystals. If it is found that time constants for diffusion depend directly on pellet size and independent of crystal size, it can be concluded

that macropore diffusion is the controlling mechanism. If the reverse is observed, micropore diffusion is the controlling mechanism. Other options to determine the controlling mechanism experimentally are by studying the effects of purge gas, purge flow rate, and temperature on the desorption curves [53,55].

In 1997, Silva and Rodrigues [53] made a detailed experimental study on adsorption and diffusion of n-pentane in pellets of 5A zeolite. They made also a similar study for n-hexane [55]. They found that, in both cases, macropore diffusion is the controlling mass transfer mechanism for the pellets they were using. Diffusion and equilibrium sorption data were obtained from these experiments, including the pore diffusivity of n-pentane, the pore diffusivity of n-hexane, the isosteric heat of adsorption for n-pentane and for n-hexane, and the Henry constants.

### 1.3c PSA PROCESS AND MODELING

The unit operations of PSA process are operated in a cyclic manner by a combination of adsorption and desorption steps. High pressure favors adsorption and low pressure favors desorption. Therefore, the starting step in a PSA cycle is pressurization of the bed from low pressure of desorption step to a higher pressure. In the next step, feed gas passes through the column and

preferential retention of the strongly adsorbed component takes place and the weakly adsorbed component is collected at the other end of the column. When a specified saturation of the bed has occurred, feed is shut off, and pressure reduction is accomplished. This is known as the blowdown step and prepares the bed for the subsequent desorption of the adsorbed component. This desorption is carried out using a purge gas flowing countercurrently in the column, thus purging the solid phase. The bed is then re-pressurized. These four steps constitute the most rudimentary cycle developed by Skarstrom in the 1960's [58], which is based on two beds operating synchronously as shown in Figure 1.5.

To increase the efficiency of PSA separation several modifications of the Skarstrom cycle have been developed. Most of the differences are associated with cycles designed to conserve compression energy. In multiple bed systems, for example, beds are connected such that pressurization and depressurization occur in stages through equalization with other beds. A review of PSA modification can be found in references [48,64].

Theoretical modeling of a PSA system has been widely studied in the literature. The growth in PSA modeling has followed the route of gradual development by progressive elimination of the simplifying assumptions. A chronological summary for PSA models development is shown in Figure 1.6.

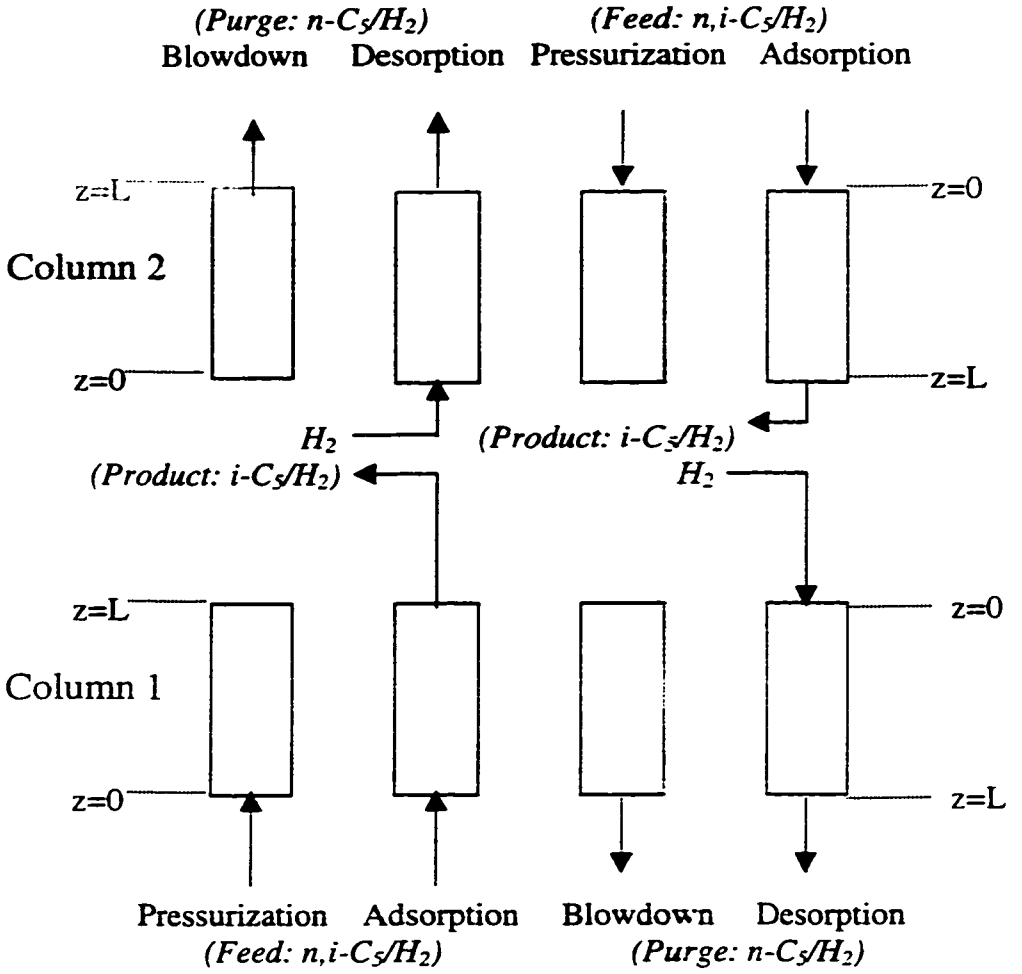


Figure 1.5. Steps for the n,i-$C_5$ PSA separation based on Skarstrom Cycle

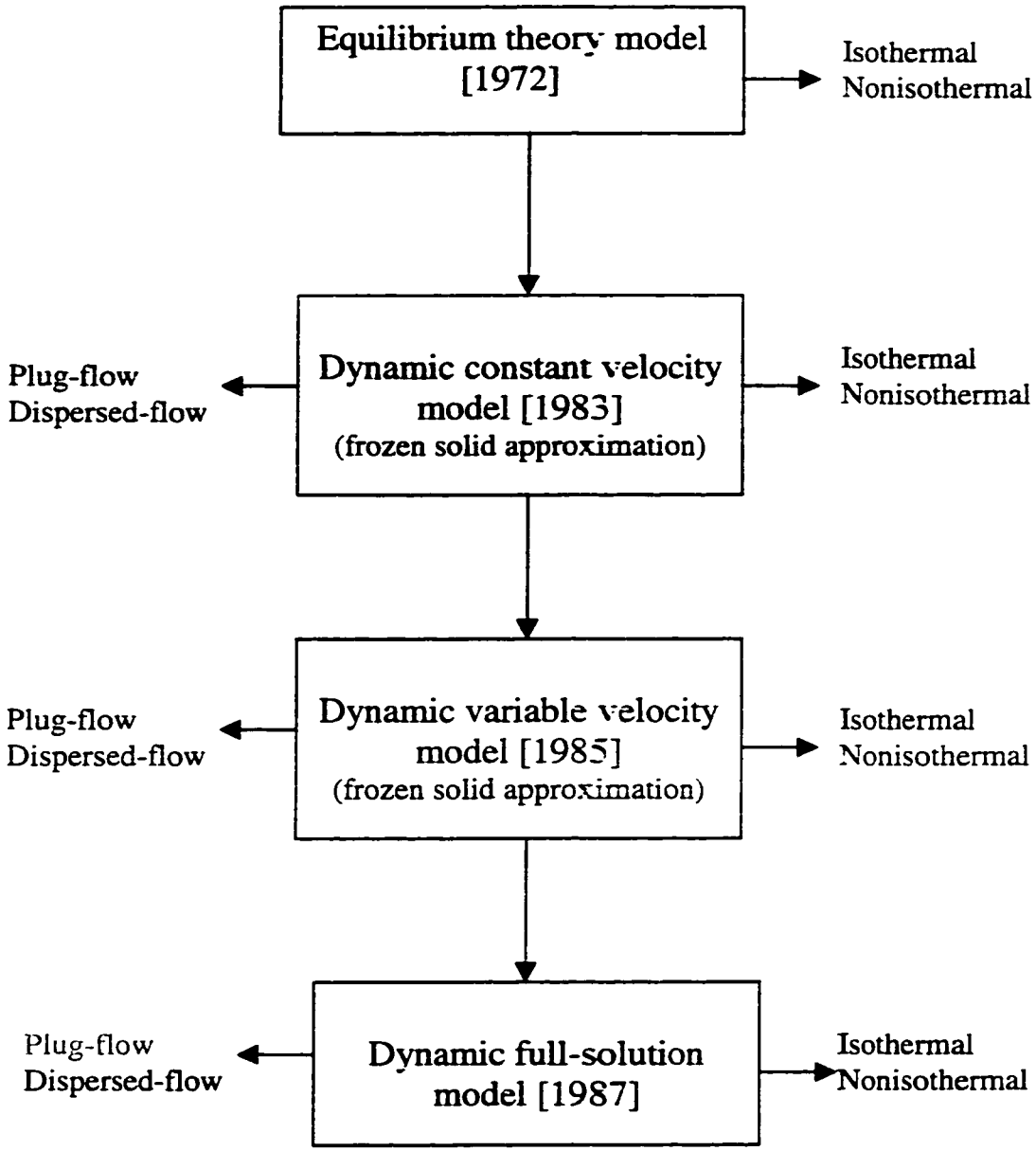


Figure 1.6 Summary for PSA models development

The first and simplest approach is by the equilibrium theory model, which is based on the assumption that local equilibrium always exists between the bulk and gas phases and hence mass transfer resistance is negligible. The concept was first published by Shendalman and Mitchell in 1972 [51]. An advantage of this approach is that it allows for analytical solution of the governing mass balance equation by the method of characteristics. However, the predictions by the equilibrium model are not accurate for real systems where the mass transfer resistance is considerable, especially for kinetic-based separation.

Dynamic modeling, the other approach of PSA modeling, allows for mass transfer resistance in the system, and the governing equations can be solved only by numerical methods. In 1983, Chihara and Suzuki developed a dynamic model based on the assumption that the velocity is constant along the column in adsorption and desorption steps [13]. They also assumed that mass transfer between bulk and solid phases is negligible during pressurization and blowdown steps. The second assumption is well known in literature as the frozen solid approximation. Constant velocity models are most useful for liquid systems or gaseous purification systems where the adsorbable components exist in the feed in trace amount. However, for bulk

gas separation, where the change in flow rate due to adsorption-desorption is significant, this assumption is clearly inappropriate.

Later on, Ruthven and Raghavan developed a variable velocity model in 1985, where they allow for velocity change in all steps [50]. However, they retained the frozen solid approximation. For purification processes, the frozen solid approximation is accepted. For bulk-separation processes, however, mass transfer between gas and solid phases during pressurization and blowdown steps is significant so that the frozen solid approximation is not accurate, especially for equilibrium-based separation [48].

Modeling by the equilibrium theory and the frozen solid approximation can be regarded as two extreme cases relative to the real situation. The former always gives predictions higher than reality, while the later always gives predictions lower than reality [64].

The first isothermal full solution model, which includes the dispersion term in the mass balance equation, allows for variable velocity during adsorption-desorption steps, and relaxes the frozen solid approximation, is the one published by Shin and Knaebel in 1987 [52]. Limited works have been published for developing the nonisothermal full solution model.

Both plug-flow and axially dispersed plug-flow conditions, isothermal and nonisothermal PSA systems are considered in PSA modeling

development, as shown in Figure 1.6. Heat effect in PSA modeling is treated in more detail in Chapter 4.

In pressurization and blowdown steps, the column pressure changes with time. One approach to account for this change in modeling is to assume that the pressure varies either linearly or exponentially over the period of the pressurization or blowdown step. An alternative approach is to assume instantaneous change of pressure followed by mass transfer (at constant high or low pressure) between the bulk and solid phases. The former is a good approximation for an equilibrium-based separation, while the latter is more appropriate for kinetic separation [48].

In order to determine the cyclic steady state, cycles are repeated until very minor differences are noticed in concentration profiles for all steps. This is called the successive substitution method, and used by most authors because of its simplicity, although in some cases the computation time is high. A new method is suggested by Alpay and co-workers in 1998, which is called the simultaneous discretisation method seems to be more efficient [3]. However, the user requires high experience in mathematics in order to apply it.

Most dynamic models developed so far have been solved numerically by either finite difference or orthogonal collocation techniques. The latter

method has been shown to be computationally much superior than the former [50]. Also, for the previous works all computer simulation codes have been developed in Fortran language. Nowadays there is a tendency in engineering applications to shift from FORTRAN to the more sophisticated language, MATLAB. This is because MATLAB is much easier and is used friendly, and the output can be directly visualized graphically [6]. Therefore, there is a need to develop a MATLAB computer simulation code that solves both isothermal and nonisothermal full solution PSA models.

## 1.4 PRESURE SWING ADSORPTION REACTOR (PSAR)

In conventional chemical reaction processes, the conversion is often limited by chemical equilibrium. In order to achieve higher conversions and improved overall energy efficiency, new chemical reactor configurations have been studied. In one, a conventional reactor is operated in a periodic mode [15]; other novel reactors can achieve simultaneous reaction and separation. The concept of combining reaction with separation is based on Le Chatelier's principle relating the conversion of reactants to products. The rate of forward reaction in an equilibrium-limited reaction can be increased by selectively removing some of the reaction products from the reaction zone [57]. Thus, a better conversion can be achieved. Another advantage of

applying this concept is that both capital and operating cost may be reduced because the downstream separation section can be minimized or eliminated from the conventional process.

Numerous applications of this concept have been published, such as membrane reactors, reactive distillation units, and others [17]. The pressure-swing reactor is a relatively new and untested device that combines reaction and product separation in a plant resembling a pressure swing adsorption (PSA) system [1,12,22,27]. In this device, a mixture of a catalyst and an adsorbent is filled in a chemical reactor. Mixing of the sorbent with the catalyst can be done in either a homogeneous or heterogeneous way [31]. In homogeneous units, the catalyst and the adsorbent are mixed uniformly, and one of the reaction products should be the strongly adsorbed component in order to get higher conversion by shifting the conversion to the right. Heterogeneous units are formed by dividing the unit into two separate regions; the catalyst-packed bed region followed by the adsorbent-packed bed region. Here, the strongly adsorbed component can be either the reactant or the product.

Combining reaction with pressure swing adsorption process is relatively a new area of interest and very limited works have been published. A good literature review on PSR systems was done by Sircar *et al.* [57], and some

outlines of the works done are briefly presented here. The first theoretical investigation of the PSR system is the one published by Vaporciyan and Kadlec in 1987 [59]. They considered a single rapid PSR column with extremely fast reaction and they applied the equilibrium theory model for adsorption. Two years later, they performed the first experimental evaluation of the PSR systems using Pt/alumina as the catalyst and 5A zeolite as the adsorbent in a rapid PSR process for oxidation of carbon monoxide [60]. Their patent was approved in 1993, which is the first patent in PSR systems [25]. They found that under certain operating conditions carbon dioxide production could be increased by up to 2 times the conventional reactor production. In 1994, Lu and Rodrigues proposed another mathematical model for the PSR system, and applied it on the dehydrogenation reaction of ethane [32]. However, they also used the equilibrium theory for their model. Dehydrogenation reaction of methylcyclohexane to toluene in a PSR unit has been studied experimentally by Alpay and co-workers in 1995 [2]. Also, applying the PSR concept to the water-gas shift reaction has been investigated experimentally by Sircar *et. al.* [57]. Both experimental studies have shown that equilibrium yields could exceed the values achieved by a conventional reactor. In a recent publication in 1998, Alpay *et. al.* have studied theoretically the rapid PSR concept, and applied it for a hypothetical

dissociation reaction [3]. They made detailed parametric studies, and applied the simultaneous discretisation method for determining the cyclic steady state. However, they retained the equilibrium theory assumption.

Isomerization process is a good example for applying the PSR concept for two reasons. First, the operating temperature and pressure for the reactor and the adsorber are similar. Second, both the reactor and the adsorber operate under hydrogen environment.

To date, all the previous studies considered homogeneous mixing of adsorbent and catalyst in the PSR unit. In these studies, the main objective of applying the homogeneous PSR concept is to increase the conversion to a value higher than the equilibrium value by shifting the equilibrium reaction to the right. For the current study, however, the heterogeneous PSR concept will be applied because the main objective here is to reduce the required unit operation equipment.

Also, most previous PSR models have applied the equilibrium theory concept for adsorption. However, separation of n,i-paraffins mixture is an example of a bulk-separation process. As mentioned before, the equilibrium theory model is not appropriate for this type of separation. Thus, there is a need to develop a full solution model for the PSAR system.

The performance of a PSAR unit can be affected by a number of design parameters, such as the bed length and the adsorbent/catalyst size; operating parameters, such as the duration of the various steps and the pressure level in each step; and physical/chemical parameters, such as adsorption isotherm relationship and reaction rate constant. The effects of these parameters are coupled so that it is difficult to arrive at an optimal design only by experimentation. Therefore, reliable mathematical modeling and computer simulations are required to obtain preliminary information about the performance of the PSAR process in order to insure that the capital and/or operating costs are minimized while satisfying technical specifications such as conversion, yield, and product purity.

The block-flow diagram of the PSAR system, taking the example of n-paraffins isomerization reaction, is shown in Figure 1.7. In this figure, the heterogeneous mixing system is employed and the reactant is the strongly adsorbed component. This flow diagram will be described in detail in Chapter 3.

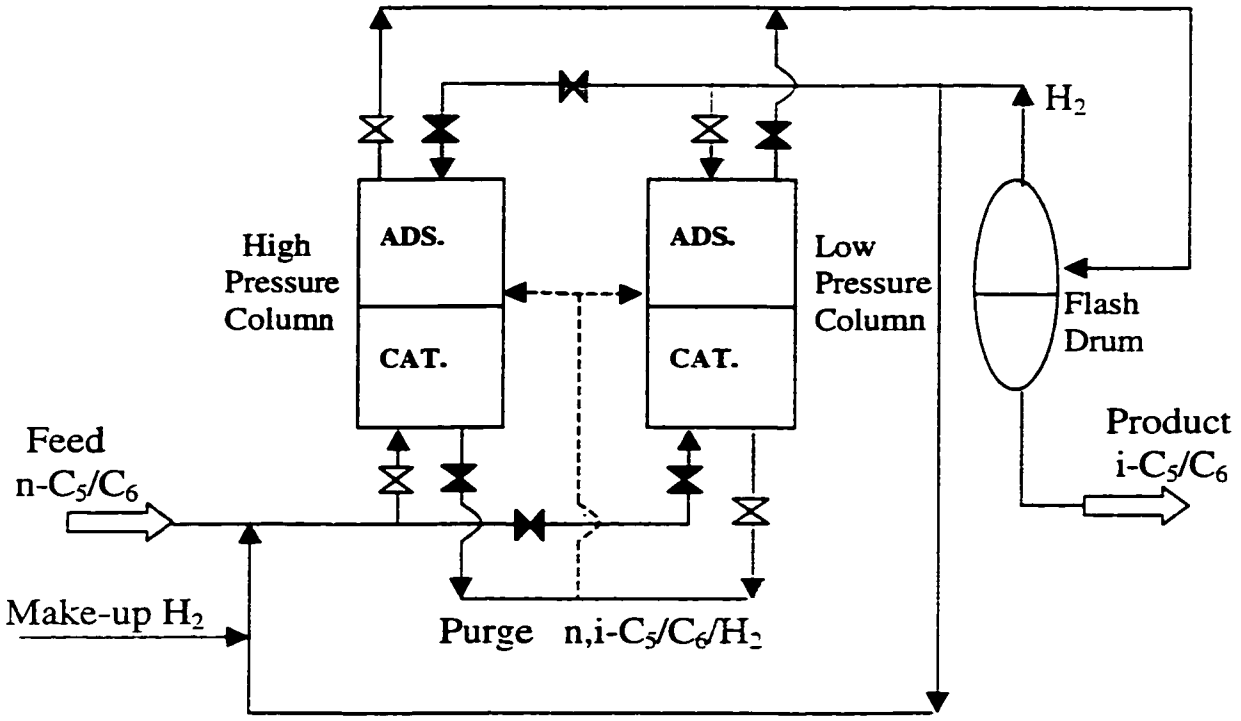


Figure 1.7 Flow Diagram for the Combined Isomerization Reactor/Adsorber Process

## 1.5 OBJECTIVES OF THE PRESENT RESEARCH

The objectives of this research work are:

1) To develop a model that describes the conventional n-pentane isomerization process, which consists of a steady state packed-bed reactor followed by a PSA unit. Both isothermal and nonisothermal PSA models are developed.

2) To develop and establish a model that describes a combined reactor / pressure swing adsorber unit (PSAR), for isomerizing n-pentane to its branched isomers. The PSA and PSAR models are to be full solution models. That is, most simplified assumptions are relaxed.

3) To generate computer simulation codes in MATLAB 5.2 language, which solve the above models.

4) To predict the breakthrough curves for the fixed-bed adsorber/reactor, and to study the effect of operating and design parameters on them.

5) To simulate the conventional and PSAR process, and perform comparison between them. The catalyst is Pd/Y- zeolite and the adsorbent is 5A zeolite. The operating temperature is in the range of 500 to 533 K. Adsorption/reaction step will be conducted at high pressure (15-20 bar) and desorption step at low pressure (2 bar).

# CHAPTER 2

# MODELLING AND SIMULATION OF THE BASE CASE

In order to compare the performance of the new PSAR process to that of a conventional process, a base case consisting of a reaction unit, a fixed-bed adsorption unit, and a PSA unit is first simulated. The reactor is considered to operate under steady state condition. The configuration of the PSA cycle is as shown in Figure 1.5. In practice, at least two beds in the PSA unit are needed in order to operate in a cyclic steady state manner. In the present case, however, simulation of one bed gives a complete picture since the purge gas stream here is an external source (pure hydrogen) rather than a portion of the product stream. Thus, only one PSA bed is considered in the simulation. For simplicity, the system is initially modeled as an isothermal process containing only three components (n-i/$C_5$/$H_2$).

## 2.1 MODEL ASSUMPTIONS

The dynamic model is based on the following assumptions:

1) The gas is ideal. Although in some simulation runs the pressure is high (15 bars and above), the gas is still an ideal system for two reasons: the

temperature is high (500 K and above), and the hydrogen content is high (above 50 %). To validate this assumption, the compressibility factor at high pressure is calculated to be close to unity by the Peng Robinson Equation of State.

2) The flow pattern is described by the axial dispersed plug flow model.

3) The gas and solids physical properties are independent of temperature.

4) The total pressure and the velocity are constants in the reactor. This is because, according to the reaction stoichiometry, one mole of n-pentane is consumed to produce one mole of isopentane.

5) The reaction is isothermal [41,42,43].

6) The reaction rate, expressed as moles of n-pentane consumed/hr/g. of catalyst, is given by: $(-r_A) = k_1[c_A - \frac{c_B}{K_C}]$ where subscripts A and B denote for n-pentane and iso-pentane, respectively. This expression assumes an elementary first-order reversible reaction, with isomerization of the reactive intermediate to be the rate-controlling step.

7) Deactivation of the catalyst is negligible. This is accepted for a faujasite (Y zeolite) catalyst, which has been chosen for the present study.

8) Hydrocracking products are negligible [16].

9) The total pressure is constant during the sorption-desorption steps.

10) Mass transfer between fluid and solid phases are considered for all PSA steps. The early PSA models assume that the solid phase remains frozen during pressurization and blowdown steps. As a consequence, the solid phase concentration profile is the same at the start of desorption as at the end of the adsorption step. During blowdown the gas phase concentration profile remains the same as at the end of the adsorption step. During pressurization the gas phase concentration profile is pushed forward in the column by a distance ratio equal to the pressure ratio. Gas composition behind this distance is the same as the feed composition and the composition ahead of this distance is equal to the average of gas phase composition at the end of the desorption step [50]. As mentioned before, the frozen solid approximation is not appropriate for bulk separation, especially those based on equilibrium selectivity.

11) The main resistance to mass transfer in the adsorbent region are external fluid film resistance and macropore diffusion in series. These two resistances are combined in a global resistance according to a lumped model suggested by Morbidelli et al. [35]. This is one type of mass transfer models that is well known as the Linear Driving Force (LDF) model. Although the other type, the pore diffusion model, is more realistic, the LDF model is highly preferred in PSA simulation

because of its simplicity in numerical formulation. For separation based on equilibrium selectivity, the LDF model approach is accurate and representative in almost all situations [48]. The other approach, the pore diffusion model, is necessary for separation based on kinetic selectivity.

12) The effect of pressure on the overall mass transfer coefficient is allowed for. This is necessary for a system where the controlling resistance to mass transfer is macropore diffusion [49,50].

13) The adsorption equilibrium is described by the Nitta et al. model [36].

14) A linear relationship represents the pressure profile during the pressurization and the blowdown steps.

15) The frictional pressure drop through the catalyst and the adsorbent beds is neglected.

16) Variation in the fluid velocity along the adsorber length is accounted for.

## 2.2 MODEL EQUATIONS

Subject to the above assumptions, the model equations for the base case system are as follows: [A=n-pentane, B=isopentane, I=inert ($H_2$), 1=reactor, 2=adsorber]

(Reactor Section):

Reactant mass balance is

$$-D_L\frac{d^2c_{A1}}{dz^2}+u_f\frac{dc_{A1}}{dz}+k_1[c_{A1}(1+\frac{1}{K_C})-\frac{c_{Af}}{K_C}-\frac{c_{Bf}}{K_C}]=0 \tag{2.1}$$

The concentration of the other species can be found by difference knowing that the ratio of $(c_{A1}+c_{B1})/c_{I1}$ is constant

$$c_{B1}=c_{Af}+c_{Bf}-c_{A1} \tag{2.2}$$

$$c_{I1}=c_{T1}-c_{A1}-c_{B1} \tag{2.3}$$

The boundary conditions are (Danckwert's boundary conditions)

$$-D_L\frac{dc_{A1}}{dz}\Big|_{z=0}=u_f(c_{Af}-c_{A1}\big|_{z=0}) \tag{2.4a}$$

$$\frac{dc_{A1}}{dz}\Big|_{z=L}=0 \tag{2.4b}$$

(PSA Section):

Step 1 (Pressurization)

Fluid phase mass balances are

$$-D_L\frac{\partial^2c_{A2}}{\partial z^2}+\frac{\partial(uc_{A2})}{\partial z}+\frac{\partial c_{A2}}{\partial t}+(\frac{1-\varepsilon}{\varepsilon})\rho_s\frac{\partial\langle q_A\rangle}{\partial t}=0 \tag{2.5}$$

$$-D_L\frac{\partial^2c_{B2}}{\partial z^2}+\frac{\partial(uc_{B2})}{\partial z}+\frac{\partial c_{B2}}{\partial t}=0 \tag{2.6}$$

$$-D_L\frac{\partial^2c_{I2}}{\partial z^2}+\frac{\partial(uc_{I2})}{\partial z}+\frac{\partial c_{I2}}{\partial t}=0 \tag{2.7}$$

The overall material balance is obtained by adding equations (2.5), (2.6) and (2.7), recognizing that the total concentration $c_{T2}$ defined as $c_{T2} = c_{A2} + c_{B2} + c_{I2}$ is a function of time and is not a function of $z$ (due to negligible pressure drop in the bed)

$$c_{T2}\frac{\partial u}{\partial z} + \frac{\partial c_{T2}}{\partial t} + (\frac{1-\varepsilon}{\varepsilon})\rho_s \frac{\partial \langle q_A \rangle}{\partial t} = 0 \tag{2.8}$$

The mass transfer rate is represented by the LDF expression

$$\rho_s \frac{\partial \langle q_A \rangle}{\partial t} = a_p k_{gl}(c_{A2} - \langle c_{A2} \rangle) \tag{2.9}$$

The adsorption equilibrium isotherm is

$$\langle c_{A2} \rangle RT = \frac{1}{K_{ads}} \frac{\theta_A}{(1-\theta_A)^n} \tag{2.10a}$$

where $K_{ads}$ is the adsorption equilibrium isotherm, calculated by

$$K_{ads} = K_0 \exp[(-\Delta H_{ads})/RT)] \tag{2.10b}$$

The boundary conditions are (Danckwert's boundary conditions)

$$-D_L \frac{\partial c_{A2}}{\partial z}\Big|_{z=0} = u\Big|_{z=0}(c_{A2.f} - c_{A2}\Big|_{z=0}) \tag{2.11a}$$

$$\frac{\partial c_{A2}}{\partial z}\Big|_{z=L} = 0 \tag{2.11b}$$

Similar boundary conditions apply to component B.

Boundary condition for velocity

$$u\Big|_{z=L} = 0 \tag{2.12}$$

Note that $c_{A2,f}$ appearing in equation (2.11a) is the exit concentration of the reactor.

Step 2 (Adsorption)

Fluid phase mass balances are

$$-D_L \frac{\partial^2 c_{A2}}{\partial z^2} + \frac{\partial (u c_{A2})}{\partial z} + \frac{\partial c_{A2}}{\partial t} + (\frac{1-\varepsilon}{\varepsilon}) \rho_s \frac{\partial \langle q_A \rangle}{\partial t} = 0 \tag{2.13}$$

$$-D_L \frac{\partial^2 c_{B2}}{\partial z^2} + \frac{\partial (u c_{B2})}{\partial z} + \frac{\partial c_{B2}}{\partial t} = 0 \tag{2.14}$$

$$-D_L \frac{\partial^2 c_{I2}}{\partial z^2} + \frac{\partial (u c_{I2})}{\partial z} + \frac{\partial c_{I2}}{\partial t} = 0 \tag{2.15}$$

The overall material balance is obtained by adding equations (2.13), (2.14) and (2.15), recognizing that the total concentration $c_{T2}$ defined as $c_{T2} = c_{A2} + c_{B2} + c_{I2}$ is neither a function of time or position (constant pressure during the adsorption step, and negligible pressure drop in the bed)

$$c_{T2} \frac{\partial u}{\partial z} + (\frac{1-\varepsilon}{\varepsilon}) \rho_s \frac{\partial \langle q_A \rangle}{\partial t} = 0 \tag{2.16}$$

The mass transfer rate is represented by the LDF expression

$$\rho_s \frac{\partial \langle q_A \rangle}{\partial t} = a_p k_{gl} (c_{A2} - \langle c_{A2} \rangle) \tag{2.17}$$

The adsorption equilibrium isotherm is

$$\langle c_{A2} \rangle RT = \frac{1}{K_{ads}} \frac{\theta_A}{(1-\theta_A)^n} \tag{2.18}$$

The boundary conditions are (Danckwert's boundary conditions)

$$-D_L \frac{\partial c_{A2}}{\partial z}\Big|_{z=0} = u\Big|_{z=0}(c_{A2,f} - c_{A2}\Big|_{z=0}) \tag{2.19a}$$

$$\frac{\partial c_{A2}}{\partial z}\Big|_{z=L} = 0 \tag{2.19b}$$

Similar boundary conditions apply to component B.

Boundary condition for velocity

$$u\Big|_{z=0} = u_f \tag{2.20}$$

Step 3 (Counter-current Blowdown)

Fluid phase mass balances are

$$-D_L \frac{\partial^2 c_{A2}}{\partial z^2} + \frac{\partial (u c_{A2})}{\partial z} + \frac{\partial c_{A2}}{\partial t} + (\frac{1-\varepsilon}{\varepsilon})\rho_s \frac{\partial \langle q_A \rangle}{\partial t} = 0 \tag{2.21}$$

$$-D_L \frac{\partial^2 c_{B2}}{\partial z^2} + \frac{\partial (u c_{B2})}{\partial z} + \frac{\partial c_{B2}}{\partial t} = 0 \tag{2.22}$$

$$-D_L \frac{\partial^2 c_{I2}}{\partial z^2} + \frac{\partial (u c_{I2})}{\partial z} + \frac{\partial c_{I2}}{\partial t} = 0 \tag{2.23}$$

The overall material balance is obtained by adding equations (2.21), (2.22) and (2.23), recognizing that the total concentration $c_{T2}$ defined as $c_{T2} = c_{A2} + c_{B2} + c_{I2}$ is a function of time and but not position (due to negligible pressure drop in the bed)

$$c_{T2} \frac{\partial u}{\partial z} + \frac{\partial c_{T2}}{\partial t} + (\frac{1-\varepsilon}{\varepsilon})\rho_s \frac{\partial \langle q_A \rangle}{\partial t} = 0 \tag{2.24}$$

The mass transfer rate is represented by the LDF expression

$$\rho_s \frac{\partial \langle q_A \rangle}{\partial t} = a_p k_{gl} (c_{A2} - \langle c_{A2} \rangle) \tag{2.25}$$

The adsorption equilibrium isotherm is

$$\langle c_{A2} \rangle RT = \frac{1}{K_{ads}} \frac{\theta_A}{(1-\theta_A)^n} \tag{2.26}$$

The boundary conditions are (Danckwert's boundary conditions)

$$-D_L \frac{\partial c_{A2}}{\partial z}\Big|_{z=0} = u\Big|_{z=0} (c_{A2,f} - c_{A2}\Big|_{z=0}) \tag{2.27}$$

But since $u = 0$ at the inlet of the column, $z = 0$, we have

$$\frac{\partial c_{A2}}{\partial z}\Big|_{z=0} = 0 \tag{2.28a}$$

$$\frac{\partial c_{A2}}{\partial z}\Big|_{z=L} = 0 \tag{2.28b}$$

Similar boundary conditions apply to component B.

Boundary condition for velocity

$$u\Big|_{z=0} = 0 \tag{2.29}$$

Step 4 (Counter-current Desorption)

Fluid phase mass balances are

$$-D_L \frac{\partial^2 c_{A2}}{\partial z^2} + \frac{\partial (u c_{A2})}{\partial z} + \frac{\partial c_{A2}}{\partial t} + (\frac{1-\varepsilon}{\varepsilon}) \rho_s \frac{\partial \langle q_A \rangle}{\partial t} = 0 \tag{2.30}$$

$$-D_L \frac{\partial^2 c_{B2}}{\partial z^2} + \frac{\partial (u c_{B2})}{\partial z} + \frac{\partial c_{B2}}{\partial t} = 0 \tag{2.31}$$

$$-D_L \frac{\partial^2 c_{I2}}{\partial z^2} + \frac{\partial (u c_{I2})}{\partial z} + \frac{\partial c_{I2}}{\partial t} = 0 \tag{2.32}$$

The overall material balance is obtained by adding equations (2.30), (2.31) and (2.32), recognizing that the total concentration $c_{T2}$ defined as $c_{T2} = c_{A2} + c_{B2} + c_{I2}$ is neither a function of time or position (constant pressure during the desorption step, and negligible pressure drop in the bed)

$$c_{T2}\frac{\partial u}{\partial z} + (\frac{1-\varepsilon}{\varepsilon})\rho_s \frac{\partial \langle q_A \rangle}{\partial t} = 0 \tag{2.33}$$

The mass transfer rate is represented by the LDF expression

$$\rho_s \frac{\partial \langle q_A \rangle}{\partial t} = a_p k_{gl}(c_{A2} - \langle c_{A2} \rangle) \tag{2.34}$$

The adsorption equilibrium isotherm is

$$\langle c_{A2} \rangle RT = \frac{1}{K_{ads}} \frac{\theta_A}{(1-\theta_A)^n} \tag{2.35}$$

The boundary conditions are (Danckwert's boundary conditions)

$$-D_L \frac{\partial c_{A2}}{\partial z}\Big|_{z=0} = u\Big|_{z=0}(c_{A2,f} - c_{A2}\Big|_{z=0}) \tag{2.36}$$

since a pure inert purge stream is being employed, giving

$$D_L \frac{\partial c_{A2}}{\partial z}\Big|_{z=0} = u\Big|_{z=0}(c_{A2}\Big|_{z=0}) \tag{2.37a}$$

$$\frac{\partial c_{A2}}{\partial z}\Big|_{z=0} = 0 \tag{2.37b}$$

Similar boundary conditions apply to component B.

Boundary condition for velocity

$$u\Big|_{z=0} = u_P \tag{2.38}$$

In the PSA simulations the initial conditions are taken to be clean adsorbent and gas phases

$$c_{A2}(z,t=0)=0 \tag{2.39a}$$

$$c_{B2}(z,t=0)=0 \tag{2.39b}$$

$$\langle q_A \rangle(z,t=0)=0 \tag{2.39c}$$

The above set of equations is written in normalized form using the following dimensionless variables:

$$y_{Ai}=\frac{c_{Ai}}{c_{Ti}} \qquad y_{Bi}=\frac{c_{Bi}}{c_{Ti}} \qquad x=\frac{z}{L} \qquad \tau=\frac{tu_f}{L}$$

$$Q_A=\frac{\langle q_A \rangle}{q_{A.ref}} \qquad C_{Ti}=\frac{c_{Ti}}{c_{Tf}} \qquad U=\frac{u}{u_f} \tag{2.40}$$

where $q_{A.ref}$ represents the solid phase concentration of component A in equilibrium with $y_{A2.f}$ at $P_H$ and $T_f$, calculated by

$$y_{A2.f}P_H=\frac{1}{K_{ads}}\frac{(q_{A.ref}/q_{\max})}{[1-(q_{A.ref}/q_{\max})]^n} \tag{2.41}$$

Thus, the model equations become

(Reactor Section):

$$-\frac{1}{Pe}\frac{d^2y_{A1}}{dx^2}+\frac{dy_{A1}}{dx}+Da[y_{A1}(1+\frac{1}{K_C})-(\frac{y_{Af}+y_{Bf}}{K_C})]=0 \tag{2.42}$$

$$y_{B1}=y_{Af}+y_{Bf}-y_{A1} \tag{2.43}$$

$$-\frac{1}{Pe}\frac{dy_{A1}}{dx}\Big|_{x=0}=(y_{Af}-y_{A1}\big|_{x=0}) \tag{2.44a}$$

$$\frac{dy_{A1}}{dx}\Big|_{x=1} = 0 \tag{2.44b}$$

(PSA Section):

Step 1 (Pressurization)

$$\frac{\partial y_{A2}}{\partial \tau} = \frac{1}{Pe}\frac{\partial^2 y_{A2}}{\partial x^2} - \frac{\partial (U y_{A2})}{\partial x} - \frac{y_{A2}}{C_{T2}}\frac{\partial C_{T2}}{\partial \tau} - \frac{1}{C_{T2}}\zeta_m \frac{\partial Q_A}{\partial \tau} \tag{2.45}$$

$$\frac{\partial y_{B2}}{\partial \tau} = \frac{1}{Pe}\frac{\partial^2 y_{B2}}{\partial x^2} - \frac{\partial (U y_{B2})}{\partial x} - \frac{y_{B2}}{C_{T2}}\frac{\partial C_{T2}}{\partial \tau} \tag{2.46}$$

$$\frac{\partial U}{\partial x} = -\frac{1}{C_{T2}}\frac{\partial C_{T2}}{\partial \tau} - \frac{1}{C_{T2}}\zeta_m \frac{\partial Q_A}{\partial \tau} \tag{2.46}$$

$$-\frac{1}{Pe}\frac{\partial y_{A2}}{\partial x}\Big|_{x=0} = U\Big|_{x=0}(y_{A2,f} - y_{A2}\big|_{x=0}) \tag{2.47a}$$

$$\frac{\partial y_{A2}}{\partial x}\Big|_{x=1} = 0 \tag{2.47b}$$

$$U\Big|_{x=1} = 0 \tag{2.48}$$

Step 2 (Adsorption)

$$\frac{\partial y_{A2}}{\partial \tau} = \frac{1}{Pe}\frac{\partial^2 y_{A2}}{\partial x^2} - \frac{\partial (U y_{A2})}{\partial x} - \zeta_m \frac{\partial Q_A}{\partial \tau} \tag{2.49}$$

$$\frac{\partial y_{B2}}{\partial \tau} = \frac{1}{Pe}\frac{\partial^2 y_{B2}}{\partial x^2} - \frac{\partial (U y_{B2})}{\partial x} \tag{2.50}$$

$$\frac{\partial U}{\partial x} = -\zeta_m \frac{\partial Q_A}{\partial \tau} \tag{2.51}$$

$$-\frac{1}{Pe}\frac{\partial y_{A2}}{\partial x}\Big|_{x=0} = (y_{A2,f} - y_{A2}\big|_{x=0}) \tag{2.52a}$$

$$\frac{\partial y_{A2}}{\partial x}\Big|_{x=1} = 0 \tag{2.52b}$$

$$U\Big|_{x=0} = 1 \tag{2.53}$$

Step 3 (Counter-Current Blowdown)

$$\frac{\partial y_{A2}}{\partial \tau} = \frac{1}{Pe}\frac{\partial^2 y_{A2}}{\partial x^2} - \frac{\partial (U y_{A2})}{\partial x} - \frac{y_{A2}}{C_{T2}}\frac{\partial C_{T2}}{\partial \tau} - \frac{1}{C_{T2}}\zeta_m \frac{\partial Q_A}{\partial \tau} \tag{2.54}$$

$$\frac{\partial y_{B2}}{\partial \tau} = \frac{1}{Pe}\frac{\partial^2 y_{B2}}{\partial x^2} - \frac{\partial (U y_{B2})}{\partial x} - \frac{y_{B2}}{C_{T2}}\frac{\partial C_{T2}}{\partial \tau} \tag{2.55}$$

$$\frac{\partial U}{\partial x} = -\frac{1}{C_{T2}}\frac{\partial C_{T2}}{\partial \tau} - \frac{1}{C_{T2}}\zeta_m \frac{\partial Q_A}{\partial \tau} \tag{2.56}$$

$$\frac{\partial y_{A2}}{\partial x}\Big|_{x=0} = 0 \tag{2.57a}$$

$$\frac{\partial y_{A2}}{\partial x}\Big|_{x=1} = 0 \tag{2.57b}$$

$$U\Big|_{x=0} = 0 \tag{2.58}$$

Step 4 (Desorption)

$$\frac{\partial y_{A2}}{\partial \tau} = \frac{1}{Pe}\frac{\partial^2 y_{A2}}{\partial x^2} - \frac{\partial (U y_{A2})}{\partial x} - \frac{1}{C_{T2}}\zeta_m \frac{\partial Q_A}{\partial \tau} \tag{2.59}$$

$$\frac{\partial y_{B2}}{\partial \tau} = \frac{1}{Pe}\frac{\partial^2 y_{B2}}{\partial x^2} - \frac{\partial (U y_{B2})}{\partial x} \tag{2.60}$$

$$\frac{\partial U}{\partial x} = -\frac{1}{C_{T2}}\zeta_m \frac{\partial Q_A}{\partial \tau} \tag{2.61}$$

$$\frac{1}{Pe}\frac{\partial y_{A2}}{\partial x}\Big|_{x=0} = U\Big|_{x=0}\left(y_{A2}\Big|_{x=0}\right) \tag{2.62a}$$

$$\frac{\partial y_{A2}}{\partial x}\Big|_{x=1} = 0 \tag{2.62b}$$

$$U\big|_{x=0} = u_p / u_f \tag{2.63}$$

In all the four steps, the normalized forms of the mass transfer rate and the adsorption equilibrium isotherm are

$$\zeta_m \frac{\partial Q_A}{\partial \tau} = N_f C_{T2}(y_{A2} - \langle y_{A2} \rangle) \tag{2.64}$$

$$\langle y_{A2} \rangle P_2 = \frac{1}{K_{ads}} \frac{\theta_{ref} Q_A}{(1-\theta_{ref} Q_A)^n} \tag{2.65}$$

The initial conditions are

$$y_{A2}(x, \tau = 0) = 0 \tag{2.66a}$$

$$y_{B2}(x, \tau = 0) = 0 \tag{2.66b}$$

$$Q_A(x, \tau = 0) = 0 \tag{2.66c}$$

In the above dimensionless equations, model parameters are defined as follows:

Damköhler number: $Da = \dfrac{k_1 L}{u_f}$

Mass Peclet number: $Pe = \dfrac{u_f L}{D_L}$

Mass capacity factor: $\zeta_m = \dfrac{1-\varepsilon}{\varepsilon} \dfrac{\rho_s q_{A.ref}}{c_{Tf}}$

Number of film mass-transfer units: $N_f = \dfrac{1-\varepsilon}{\varepsilon} \dfrac{a_p k_{gl} L}{u_f}$

Nonlinearity parameter of isotherm: $\theta_{ref} = \dfrac{q_{A.ref}}{q_{max}}$

There are two advantages for normalizing the equations. First, a better understanding of the parametric effects on the process can be gained. Second, by expressing all variables in the same scale of 0-1, the compounded truncation error caused in numerical computation is minimized [64].

The equations to be solved to produce the breakthrough curves of the fixed-bed adsorber are exactly the same as those of step 2 in PSA section (equation 2.49 to 2.53), with initial conditions the same as equation 2.66.

## 2.3 NUMERICAL METHODS

The equation that describes the reactor dynamic is of a type of a second order ordinary differential equation / boundary value problem. This is transformed into a set of simultaneous linear algebraic equations by the orthogonal collocation method. The linear algebraic equations are solved by the gaussian elimination method. Sixteen collocation points are used.

For the model equations that describe the PSA unit, the partial differential equations are reduced to ordinary differential equations by the method of orthogonal collocation. The total mass balance equation reduces to a set of simultaneous algebraic linear equations. Simultaneous ordinary differential equations are solved using the fourth order Rung-Kutta method. Gaussian elimination method is used to solve simultaneous algebraic

equations. Twenty internal collocation points are used. For the blowdown and desorption steps, the numbering system of the collocation points is reversed in order to take into account the change of the direction of flow. The solution-flow diagram for a step in the PSA unit (adsorption step) is as shown in Figure 2.1

## 2.4 PARAMETERS ESTIMATIONS

Model parameters were estimated from independent experiments and correlations available in the literature. Table 2.1 summarizes the column characteristics, adsorbent properties, and adsorption equilibrium isotherm and reaction parameters. In this table, data for reaction section are experimental data extracted from the work by Bryant and Spivey [9]. The data for the adsorption section are experimental data published by Silva and Rodrigues [53].

The axial mass dispersion coefficient ($D_L$) is calculated approximately by:

$$D_L = 0.7D_m + 0.5ud_p \tag{2.67}$$

At low Reynolds number the second term in the above equation may be neglected [49,50]. This approximation is validated in the next section.

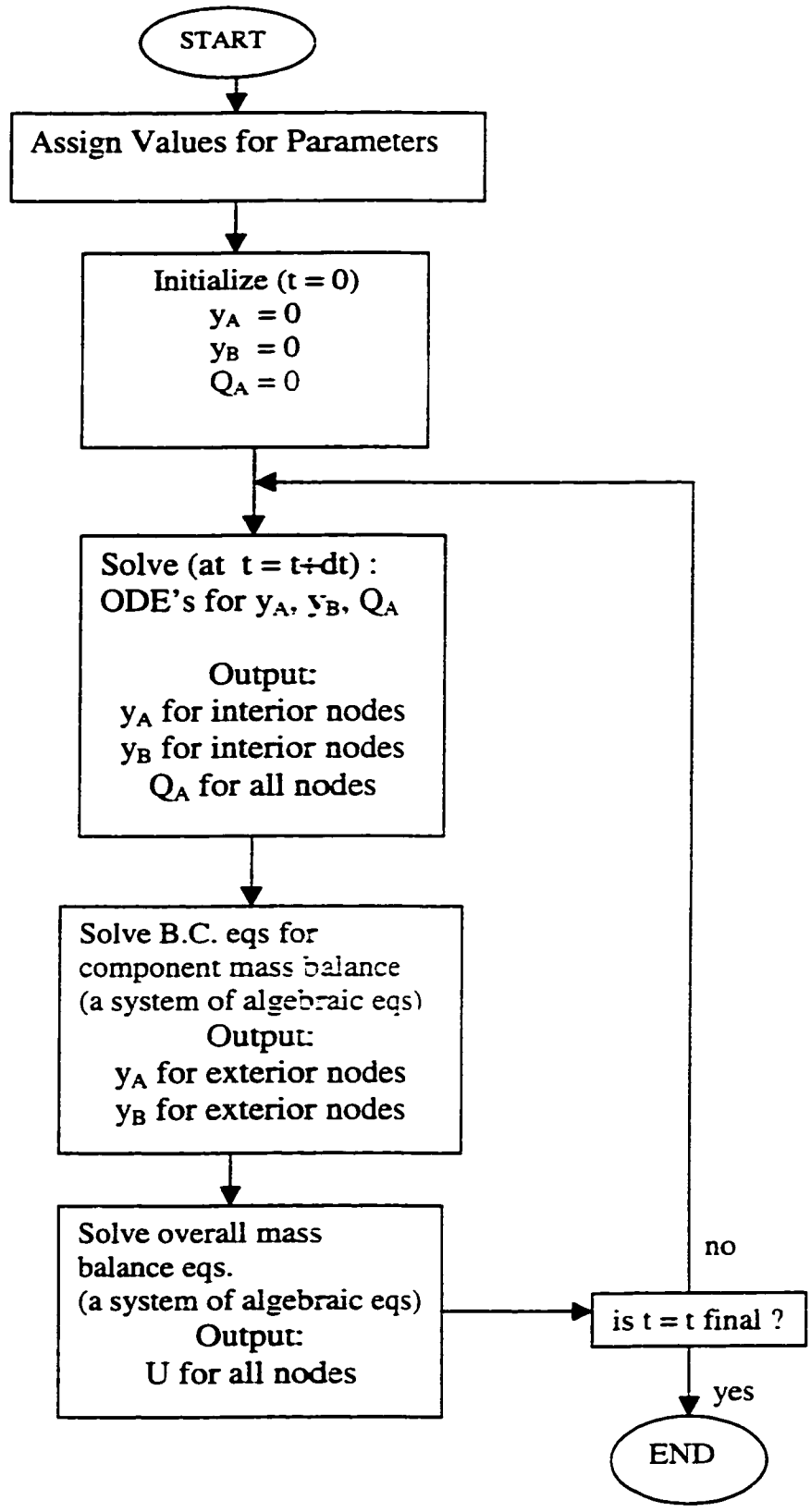


Figure 2.1 Solution-Flow Diagram for Adsorption Step

Table 2.1. Data for the base-case system

| System: n- $C_5$/ i-$C_5$/$H_2$ |
|---|
| Reactor Characteristics: |
| • L = 20 cm |
| • $2R_C$ = 3.35 cm |
| Adsorption Column Characteristics: |
| • L = 20 cm |
| • $2R_C$ = 3.35 cm |
| Adsorbent Properties: |
| • $\rho_b$ = 0.77 g/cm$^3$ |
| • $\rho_s$ = 1.13 g/cm$^3$ |
| • $\varepsilon$ = 0.32 |
| • $\varepsilon_p$ = 0.35 |
| • $d_p$ = 1.6 mm |
| • $a_p$ = 25 cm$^{-1}$ |
| Adsorption Equilibrium Isotherm Parameters: |
| • $-\Delta H_{ads}$ = 13.2 kcal/mol |
| • n = 5 |
| • $q_{max}$ = 13.0 g/100g |
| • $K_O$ = 2.013 * 10$^{-5}$ bar$^{-1}$ |
| Chemical Reaction Parameters: |
| • $k_1$ = 0.034 s$^{-1}$ @ 506 K |
| • $k_1$ = 0.090 s$^{-1}$ @ 533 K |

The reaction equilibrium constants ($K_C$) were estimated from the correlation obtained by Pines and co-workers [37]:

$$R \ln K_C = (1861/T) - 1.299 \tag{2.68}$$

According to a lumped model proposed by Glueckauf [21], the overall mass transfer coefficient ($k_{gl}$) can be calculated by:

$$\frac{1}{k_{gl}} = \frac{1}{k_e} + \frac{1}{\varepsilon_p k_i} \tag{2.69}$$

where the intraparticle mass transfer coefficient ($k_i$) can be calculated by :

$$k_i = \frac{5 D_p}{R_p} \tag{2.70}$$

The external mass transfer coefficients ($k_e$) were estimated from the correlation obtained by Wakao and S. Kaguei [62]:

$$Sh = 2.0 + 1.1(\mathrm{Re})^{0.6} (Sc)^{0.33} \tag{2.71}$$

The parameter values and operating conditions used in the simulations are listed in Tables 2.2 to 2.5.

## 2.5 MODEL SENSITIVITY ANALYSIS

As part of the parameter estimation process, it is important to identify the parameters to which the model is most sensitive. Therefore, work began using nominal parameter values to calculate adsorption breakthrough curves. The nominal parameters used are listed in Table 2.2.

Table 2.2. Parametric values used for the model sensitivity analysis

| Parameter | Figure 2.2* | Figure 2.3* | Figure 2.4* |
|---|---|---|---|
| Varying parameter | no. of nodes | $D_L$ | $k_{gl}$ |
| $y_{Af} = y_{Bf}$ | 0.17 | 0.17 | 0.17 |
| $F_f$ (mol/m$^2$/s) | 0.15 | 0.15 | 0.15 |
| P (bar) | 15 | 15 | 15 |
| T (K) | 498 | 498 | 498 |
| $u_f$ (cm/s) | 0.129 | 0.129 | 0.129 |
| $D_L$ (cm$^2$/s) | 0.072 | 0.086, 0.043 | 0.072 |
| $k_{gl}$ (cm/s) | 0.61 | 0.61 | 0.12, 1.2 |
| $K_{ads}$ (1/bar) | 12.51 | 12.51 | 12.51 |
| $Pe$ | 35.9 | 30, 60 | 35.9 |
| $\zeta_m$ | 6.66 | 6.66 | 6.66 |
| $\theta_{ref}$ | 0.555 | 0.555 | 0.555 |
| $N_f$ | 5024 | 5024 | 1000, 10000 |

*Note: if a parameter in any column has more than one value, the first value corresponds to the first number of the varying parameter.

## 2.5a SENSITIVITY TO NUMBER OF NODES

In general, the quality of the solution improves with a higher numbers of nodes, at the expense of increasing the execution time. Figure 2.2 indicates that there is considerable oscillation in the solution at high pressure with 8 nodes, while the solution is stable at 20 nodes. Therefore, 20 nodes were used for all the results throughout the thesis (unless otherwise specified).

## 2.5b SENSITIVITY TO DISPERSION COEFFICIENT

Figure 2.3 indicates that the breakthrough curves are not that sensitive to the value of the dispersion coefficient The curves are nearly coincident, indicating that the approximation "$D_L = 0.7D_m$" is quite acceptable for the range of flow rates used.

## 2.5c SENSITIVITY TO MASS TRANSFER COEFFICIENT

Figure 2.4 demonstrates breakthrough curve simulation sensitivity to the overall mass transfer coefficient. The curves are nearly coincident for the $k_{gl}$ range of 0.1-1.0 cm/s. The calculated value by equation (2.68) is 0.61 cm/s.

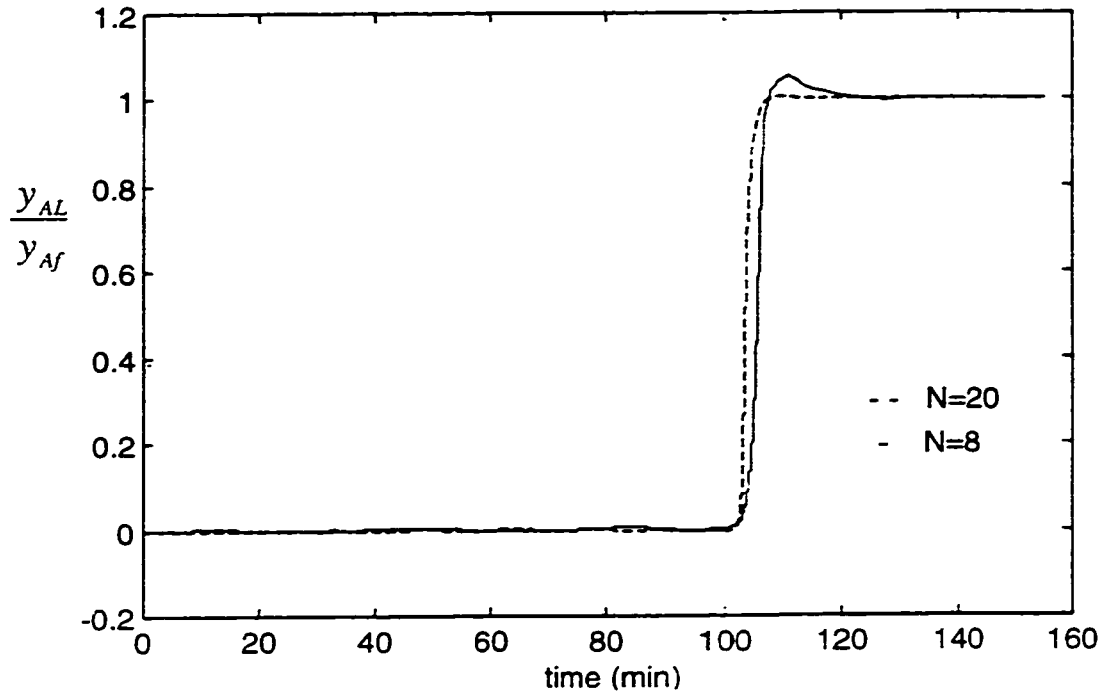


Figure 2.2. Effect of number of nodes on breakthrough curve. Parametric values are in Table 2.2

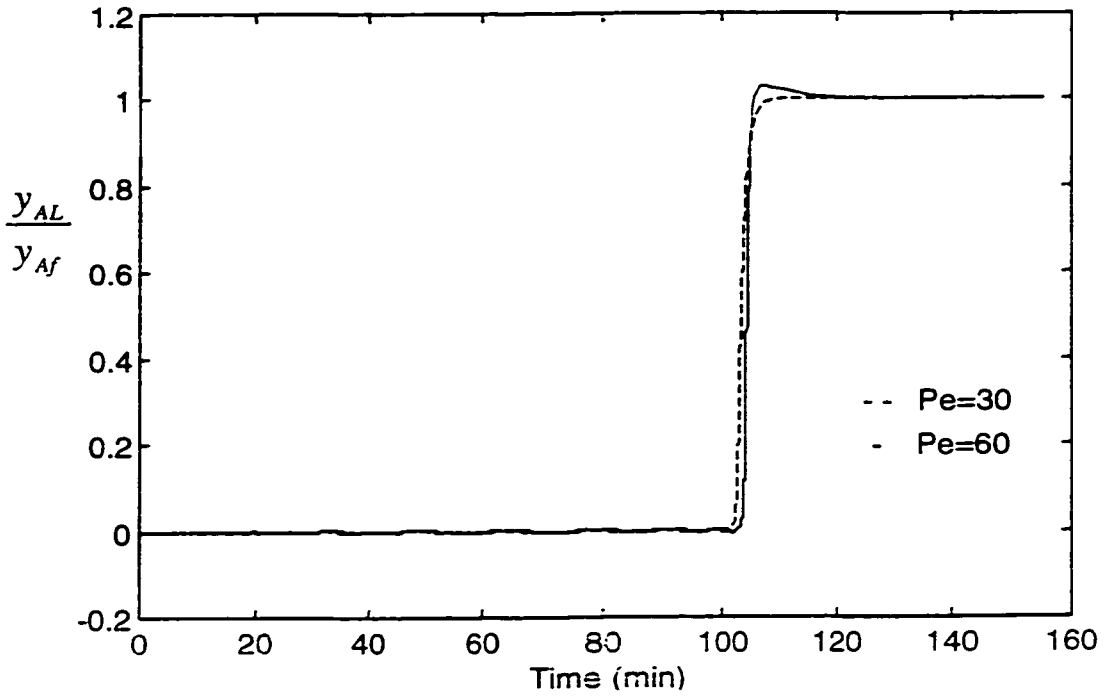


Figure 2.3. Effect of dispersion coefficient on breakthrough curve. Parametric values are in Table 2.2

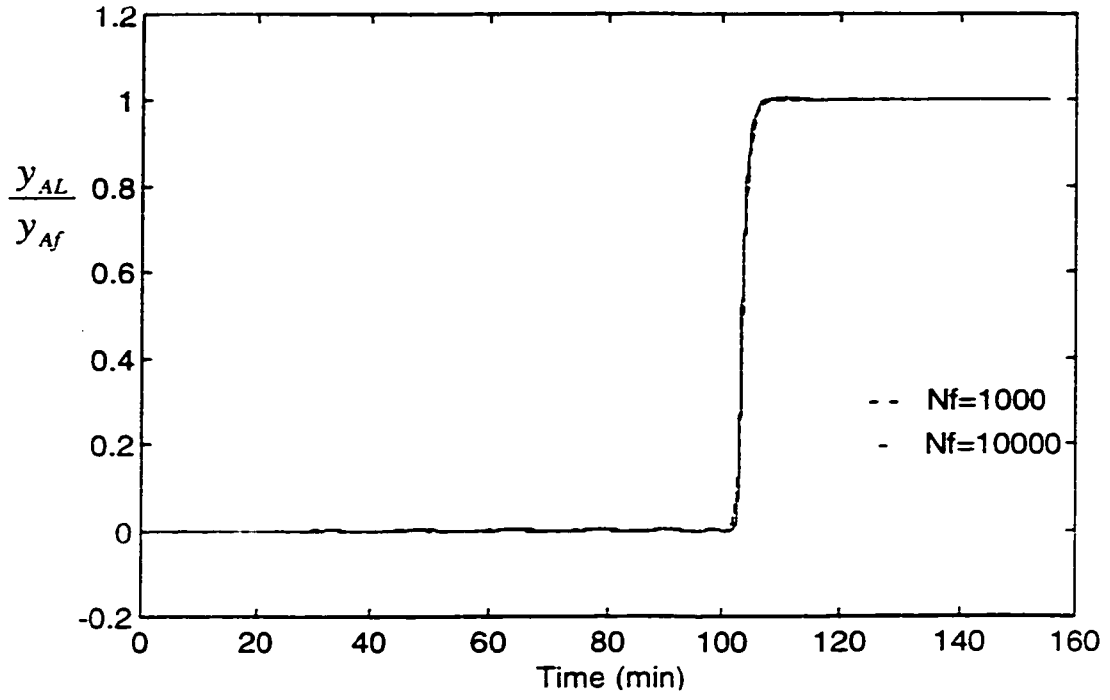


Figure 2.4. Effect of mass transfer coefficient on breakthrough curve. Parametric values are in Table 2.2

## 2.6 RESULTS AND DISCUSSION

### 2.6a REACTION UNIT

The objective of this section is to give qualitative analysis of the reaction unit by considering three basic parameters: the Peclet number, the Damköhler number, and the temperature. By this technique, varying the temperature will affect only the reaction equilibrium constant, with the functionality given by equation 2.68, while holding the other parameters constant. Although the results obtained by this technique are not exact, the method is useful in the sense that it gives a quick way for visualizing the concentration profiles in the reactor at different conditions. Parametric values used for simulation of the reaction unit are summarized in Table 2.3.

Figure 2.5 demonstrates the effect of dispersion on the concentration profile in the reactor. A low Peclet number indicates high dispersion, which lowers conversion. However, it is shown that the effect is not so great. The effect of dispersion can be minimized by increasing the length/diameter ratio and the feed flow rate.

Figure 2.6 demonstrates the effect of the kinetic parameter (the Damköhler number). Conversion increases with increasing the Damköhler number until it gets close to the equilibrium value. Further increase of the Damköhler number does not affect the outlet concentration. To attain the

Table 2.3. Parametric values used for simulation of the reaction unit

| **Parameter** | **Figure 2.5*** | **Figure 2.6*** | **Figure 2.7*** |
|---|---|---|---|
| varying parameter | *Pe* | Da | T |
| $y_{Af}$ | 0.17 | 0.17 | 0.17 |
| $y_{Bf}$ | 0.17 | 0.17 | 0.17 |
| T (K) | 500 | 500 | 400, 500, 600 |
| $y_{A.eq}$ | 0.077 | 0.077 | 0.053, 0.077, 0.097 |
| $K_C$ (-) | 3.38 | 3.38 | 5.41, 3.38, 2.48 |
| *Pe* (-) | 20, 40, 100, 500 | 100 | 100 |
| Da (-) | 1.0 | 0.5, 1, 3, 10 | 1.0 |

***Note**: if a parameter in any column has more than one value, the first value corresponds to the first number of the varying parameter.

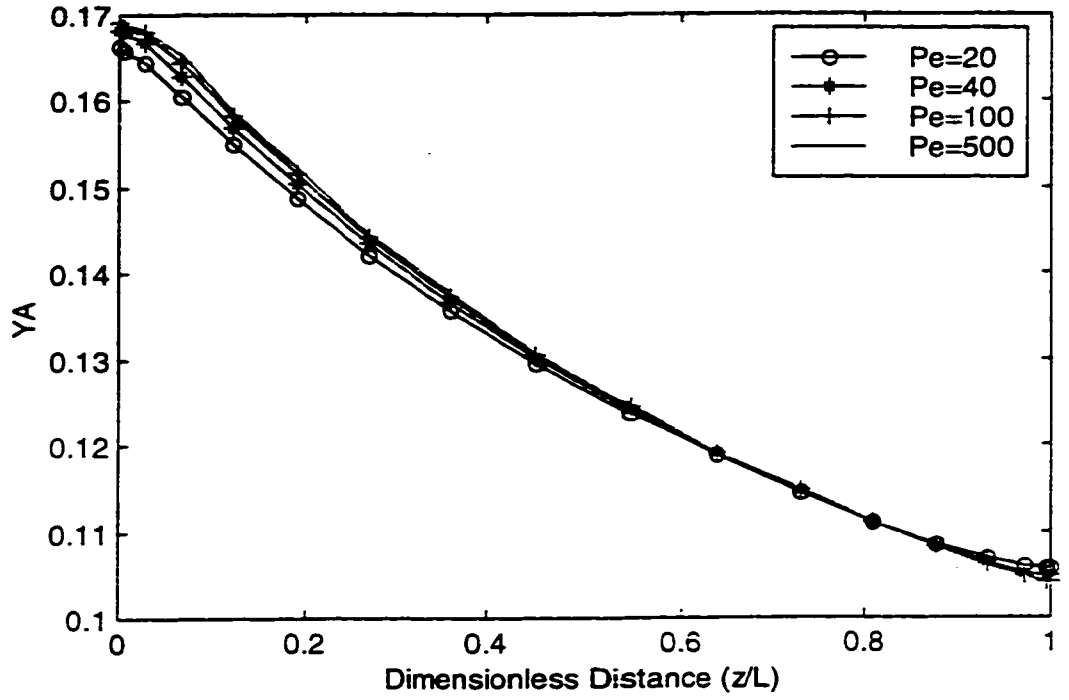


Figure 2.5. Concentration profile in the reactor (effect of dispersion). Parametric values are in Table 2.3.

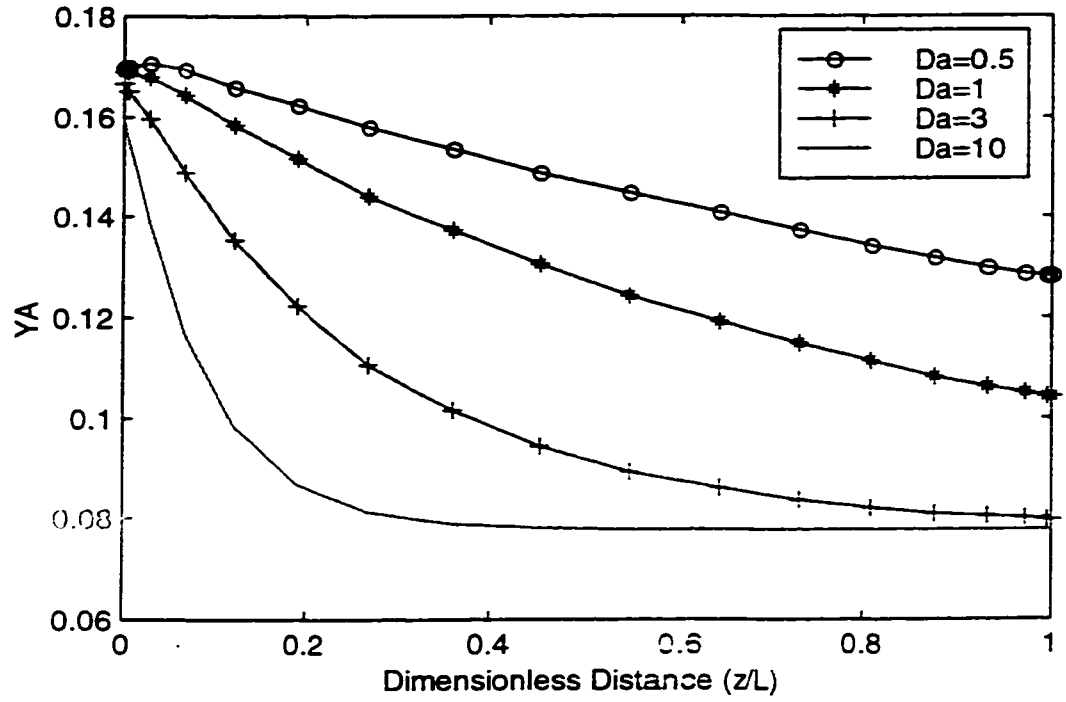


Figure 2.6. Concentration profile in the reactor (effect of Da number). Parametric values are in Table 2.3.

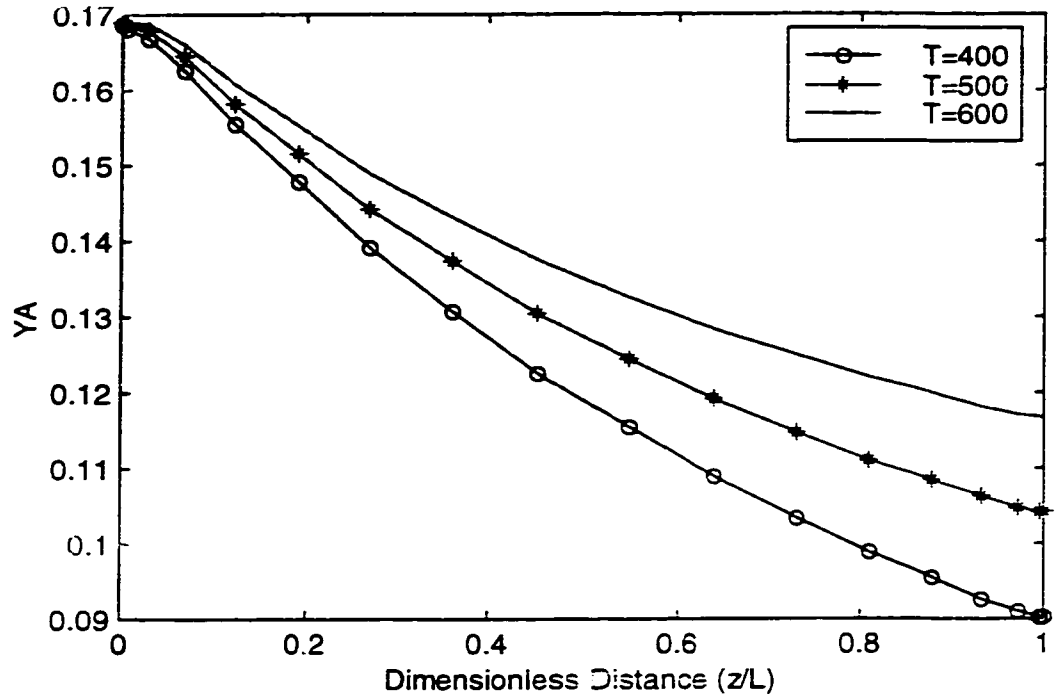


Figure 2.7. Concentration profile in the reactor (effect of temperature at low Da number). Parametric values are in Table 2.3.

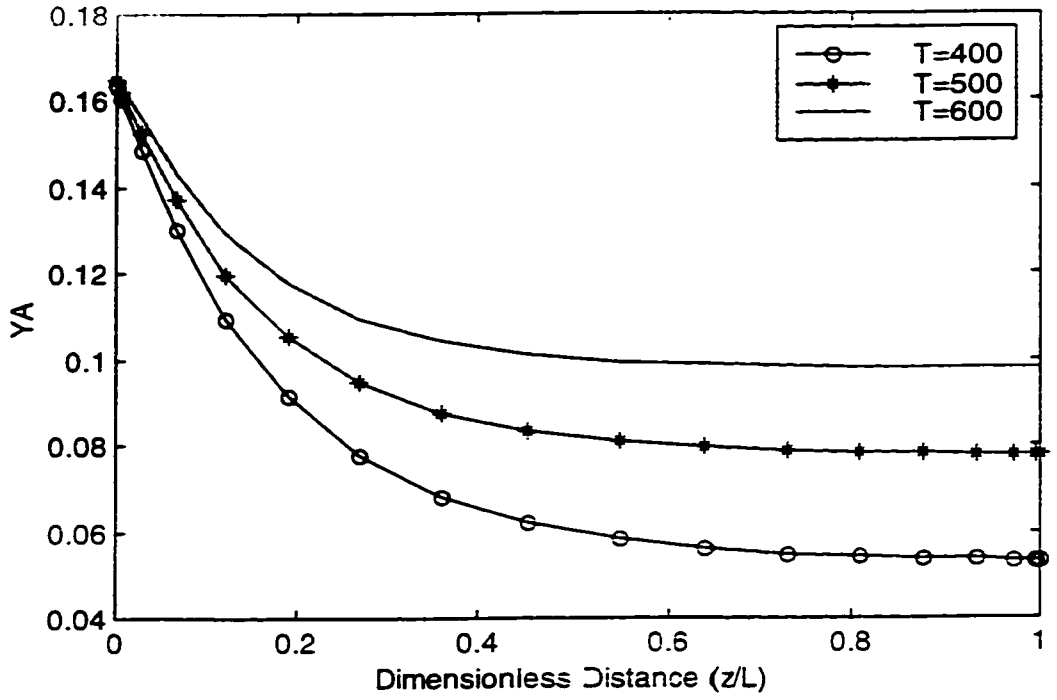


Figure 2.8. Concentration profile in the reactor (effect of temperature at high Da number). Damköhler number is 5. Other parametric values are the same as for Figure 2.7.

desired conversion near to the equilibrium value, a minimum Damköhler number of approximately 3 is required as may be observed from Figure 2.6. The Damköhler number can be increased by increasing the reactor length or by decreasing the feed flow rate. Therefore, an optimum value for the feed velocity is needed to get the desired values for the Peclet and the Damköhler numbers.

The effect of reaction temperature is shown in Figure 2.7. Conversion is favorable at low temperatures. This is expected since the reaction is exothermic, where the reaction equilibrium constant is inversely proportional to temperature. The equilibrium values presented in Table 2.3 are calculated by the relation $(y_{Af} + y_{Bf})/(K_C + 1)$, which is derived from reaction stoichiometry. From the relation, it is clear that for a fixed feed concentration the equilibrium conversion increases as the temperature decreases. It is noticed in Figure 2.7 that none of the three temperature runs reaches its equilibrium value. This is because the three runs are at low Damköhler number of 1. When increasing the Damköhler number to 5, all the three temperature runs reach their equilibrium values, as shown in Figure 2.8.

## 2.6b FIXED-BED ADSORPTION

In simulation of any adsorption processes the usual way to start is to predict the adsorption breakthrough curve by the model. This is because the qualitative shapes of breakthrough curves at different operating parameters are well established. Thus, it serves as a test for the program before going to the complex cyclic process. In addition, knowledge of breakthrough curves is essential for designing the cyclic process. In this section breakthrough curves of the n-pentane/5A-zeolite system in a fixed bed adsorber are predicted. The effect of temperature, sorbate concentration in the feed, and total pressure is studied. Parametric values used for the solution of the breakthrough curves are summarized in Table 2.4.

Figure 2.9 demonstrates the effect of temperature in adsorption breakthrough curves for bed temperatures of 498 and 548 K. The other parameters are kept constant during the simulation. The sharp nature of breakthrough curves is due to the fact that the isotherm of n-pentane is highly favorable at the partial pressure studied (17 mol % of n-$C_5$ in the feed). The adsorbed concentration increases when the temperature decreases due to exothermic nature of adsorbate-adsorbent system. Earlier breakthrough is achieved at higher temperature.

Table 2.4. Parametric values used for the solution of the breakthrough curves of the n,i-$C_5/H_2$ system

| Parameter | Figure 2.9* | Figure 2.10* | Figure 2.11* |
|---|---|---|---|
| Varying parameter | T | $y_{Af}$ | P |
| $y_{Af} = y_{Bf}$ | 0.17 | 0.17, 0.05 | 0.17 |
| $F_f$ (mol/ $m^2$/s) | 0.15 | 0.15 | 0.15 |
| P (bar) | 15 | 15 | 15, 20 |
| T (K) | 498, 548 | 498 | 498 |
| $u_f$ (cm/s) | 0.129, 0.142 | 0.129 | 0.129, 0.097 |
| $D_L$ ($cm^2$/s) | 0.072, 0.085 | 0.072 | 0.072, 0.054 |
| $k_{gl}$ (cm/s) | 0.61, 0.69 | 0.61 | 0.61, 0.48 |
| $K_{ads}$ (1/bar) | 12.51, 3.7 | 12.51 | 12.51 |
| *Pe* | 36, 33.7 | 36 | 36 |
| $\zeta_m$ | 6.63, 5.98 | 6.63, 6.13 | 6.63, 5.17 |
| $\theta_{ref}$ | 0.555, 0.455 | 0.555, 0.454 | 0.555, 0.577 |
| $N_f$ | 5002, 5184 | 5002 | 5002, 5143 |

*Note: if a parameter in any column has more than one value, the first value corresponds to the first number of the varying parameter.

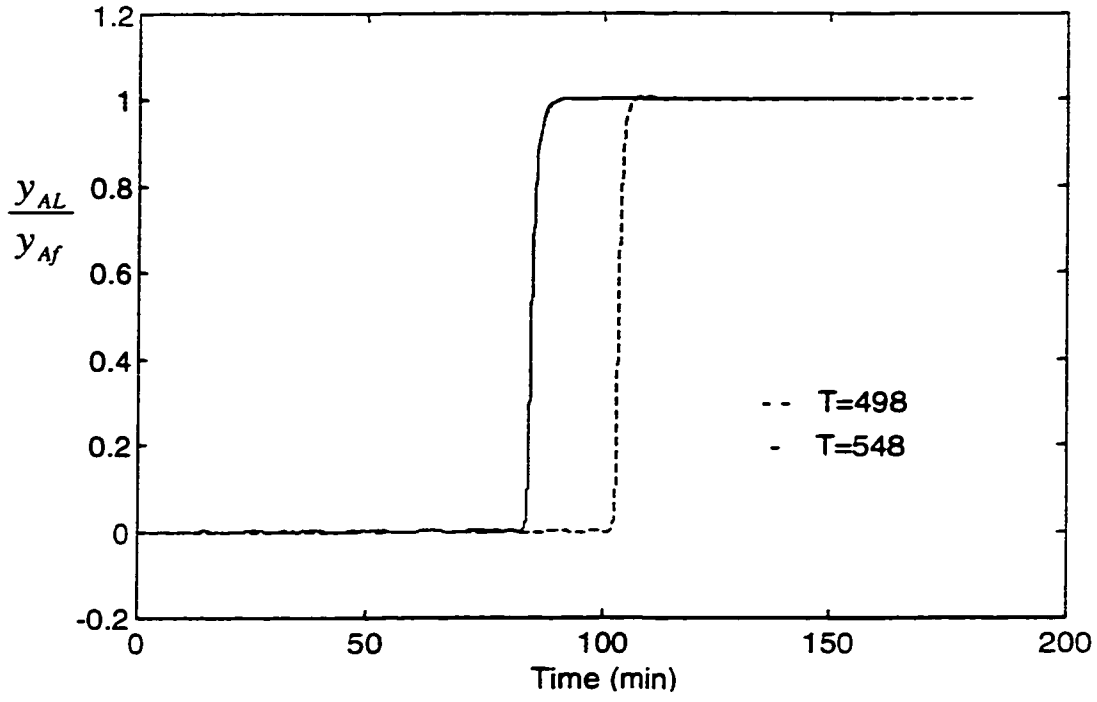


Figure 2.9. Breakthrough curve of the n,i-$C_5/H_2$ system (effect of temperature). Parametric values are in Table 2.4.

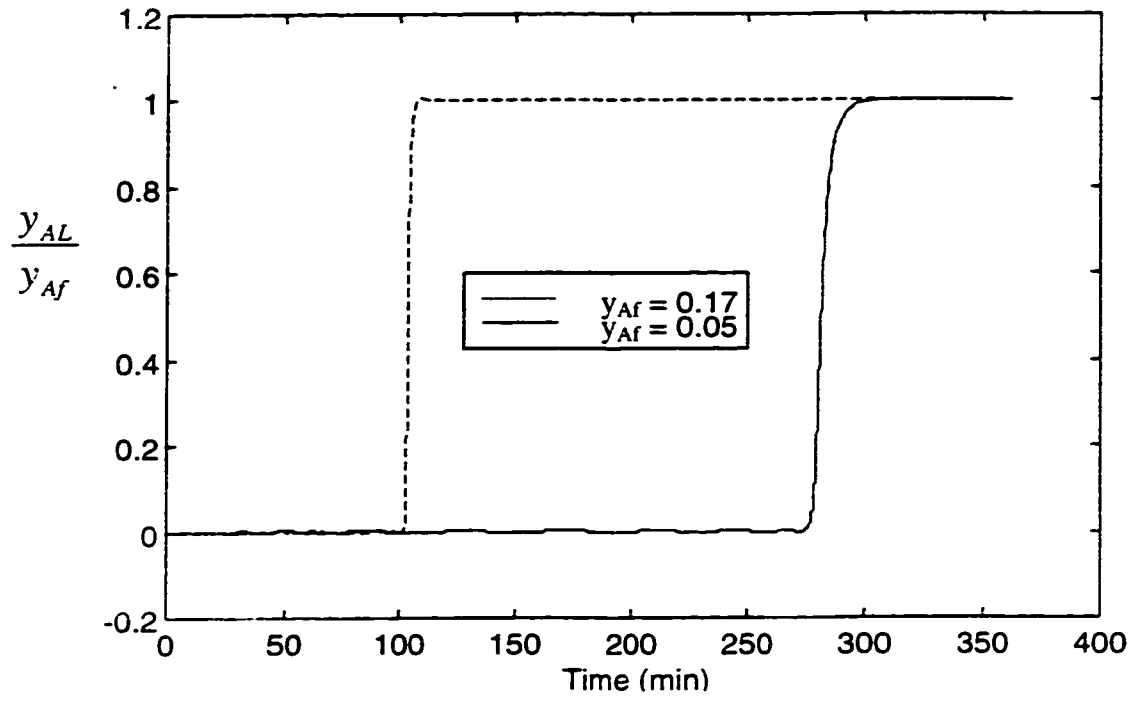


Figure 2.10. Breakthrough curve of the n,i-$C_5/H_2$ system (effect of sorbate mole fraction). Parametric values are in Table 2.4.

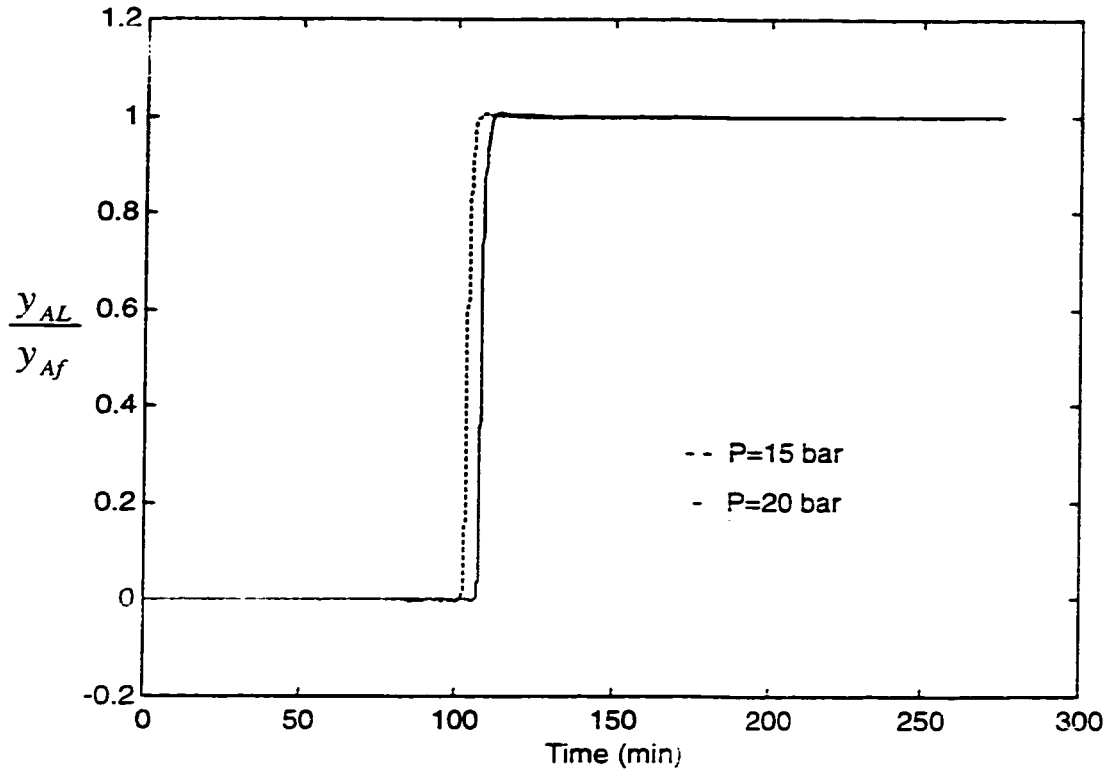


Figure 2.11. Breakthrough curve of the n,i-$C_5/H_2$ system (effect of total pressure ). Parametric values are in Table 2.4.

The effect of n-pentane mole fraction in the feed at 498 K and constant feed flow rate is shown in Figure 2.10 for two cases ($y_{Af}$ = 0.17 and $y_{Af}$ = 0.05). The adsorbent capacity decreases at lower n-$C_5$ mole fraction, and the curves are sharper when the mole fraction of n-$C_5$ increases. This is because of the favorable nature of the adsorption equilibrium isotherm. A sharper breakthrough curve is also the consequence of velocity change due to adsorption as pointed out by Yang [64]. The column takes a long time to breakthrough for low sorbate concentration.

Figure 2.11 demonstrates the influence of total pressure on breakthrough curves at 498 K, for total pressures of 15 and 20 bars. The breakthrough point is later at higher pressure.

### 2.6c PSA Separation

Figures 2.12 and 2.13 demonstrate bed profiles of concentration in the gas phase of n-$C_5$ and i-$C_5$ respectively. The profiles presented are at the cyclic steady state and at the end of the four basic steps. The simulation is done at a temperature of 506 K. Other parameters used in the simulations are summarized in Table 2.5.

As shown in Figures 2.12 and 2.13, during pressurization the initial gas concentration in the bed is pushed toward the closed product end, where it

Table 2.5. Parametric values used for PSA simulations of the n,i-$C_5/H_2$ system

| Parameter | Figure 2.12 and 2.13 |
|---|---|
| $y_{Af} = y_{Bf}$ | 0.17 |
| $F_f$ (mol/m$^2$/s) | 0.15 |
| $P_H$ (bar) | 15 |
| $P_L$ (bar) | 2 |
| T (K) | 506 |
| $u_f$ (cm/s) | 0.131 |
| Purge/Feed Volumetric Ratio | 3.0 |
| $D_L$ @ high pressure (cm$^2$/s) | 0.074 |
| $D_L$ @ low pressure (cm$^2$/s) | 0.555 |
| $k_{gl}$ @ high pressure (cm/s) | 0.62 |
| $k_{gl}$ @ low pressure (cm/s) | 2.23 |
| $K_{ads}$ (1/bar) | 10.13 |
| *Pe* @ high pressure | 35.5 |
| *Pe* @ low pressure | 4.7 |
| Pressurization / Blowdown time (min) | 7.69 |
| Adsorption / Desorption time (min) | 15.38 |
| $\zeta_m$ | 6.54 |
| $\theta_{ref}$ | 0.539 |

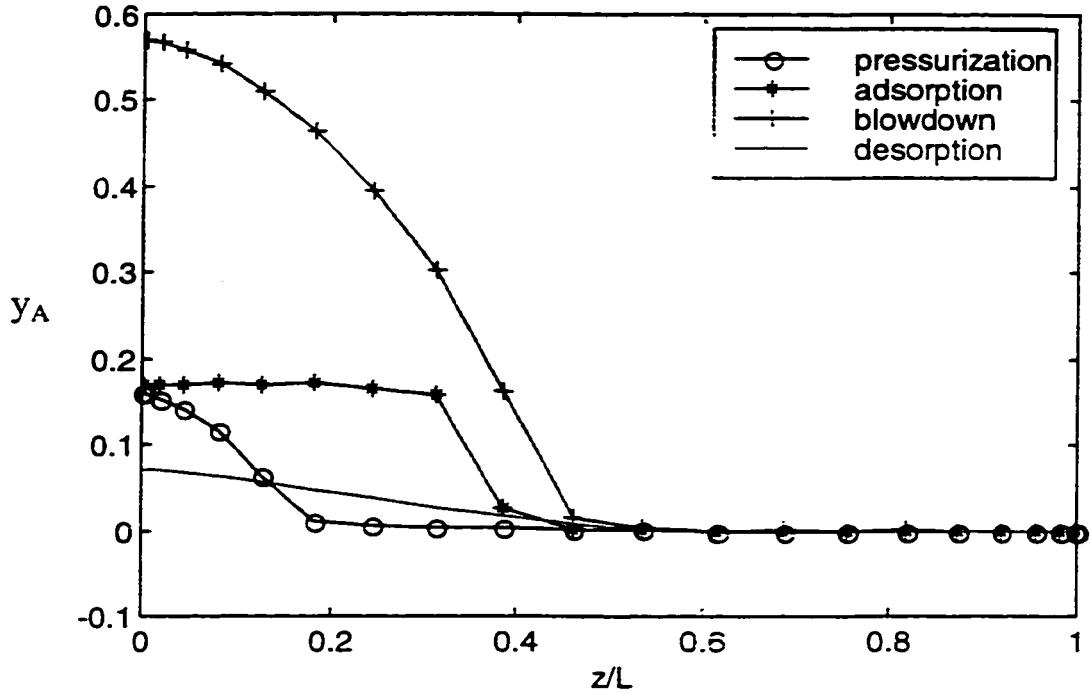


Figure 2.12 Gas phase concentration profiles of n-$C_5$ in the bed at the end of cyclic steady state. Parametric values are in Table 2.5.

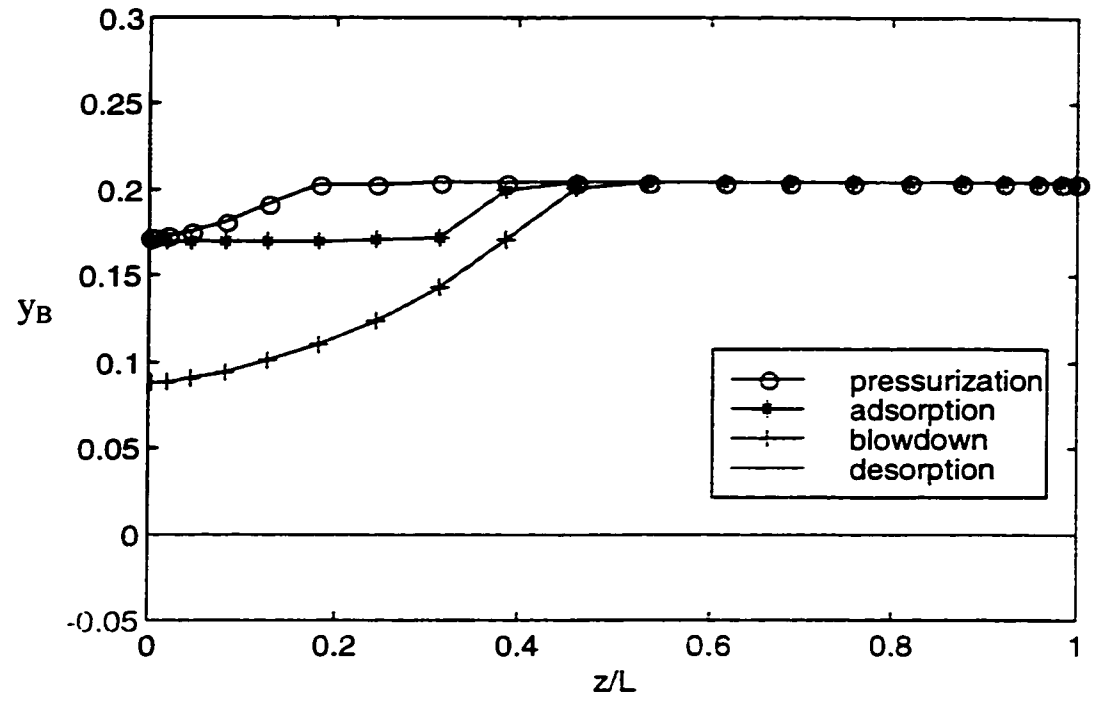


Figure 2.13 Gas phase concentration profiles of i-$C_5$ in the bed at the end of cyclic steady state. Parametric values are in Table 2.5

forms a plateau that is totally enriched in i-$C_5$ and $H_2$. The region before the plateau shows the penetration of the feed gas. In the high-pressure adsorption step the concentration profile moves down the column, and a raffinate product, totally enriched in i-$C_5$ and $H_2$ and free from n-$C_5$, is withdrawn at the product end. In the blowdown and purge steps the concentration profile is pushed back and a relatively clean initial bed condition is established for the next cycle at the end of the purge step.

As shown in Figure 2.12, in the blowdown step increasing concentration of n-$C_5$ in the bed arises due to desorption, where it increases about four times relatively to the feed conditions. At the end of desorption step, the mole fraction of n-$C_5$ is below the feed condition. As demonstrated in Figure 2.13, in the blowdown step decreasing concentration of i-$C_5$ in the bed arises due to desorption of n-$C_5$. At the end of desorption step mole fraction of i-$C_5$ is zero throughout the bed because the purge stream is pure hydrogen gas, and i-$C_5$ does not adsorb on 5A zeolite at all. In other bulk-separation processes such as air separation, where both oxygen and nitrogen adsorb on the adsorbent but at different levels, oxygen and nitrogen always exist in the raffinate and the extract streams.

Figure 2.14 indicates the approach to cyclic steady state, which is here about 10 cycles. It is low because the system considered here is the simplest

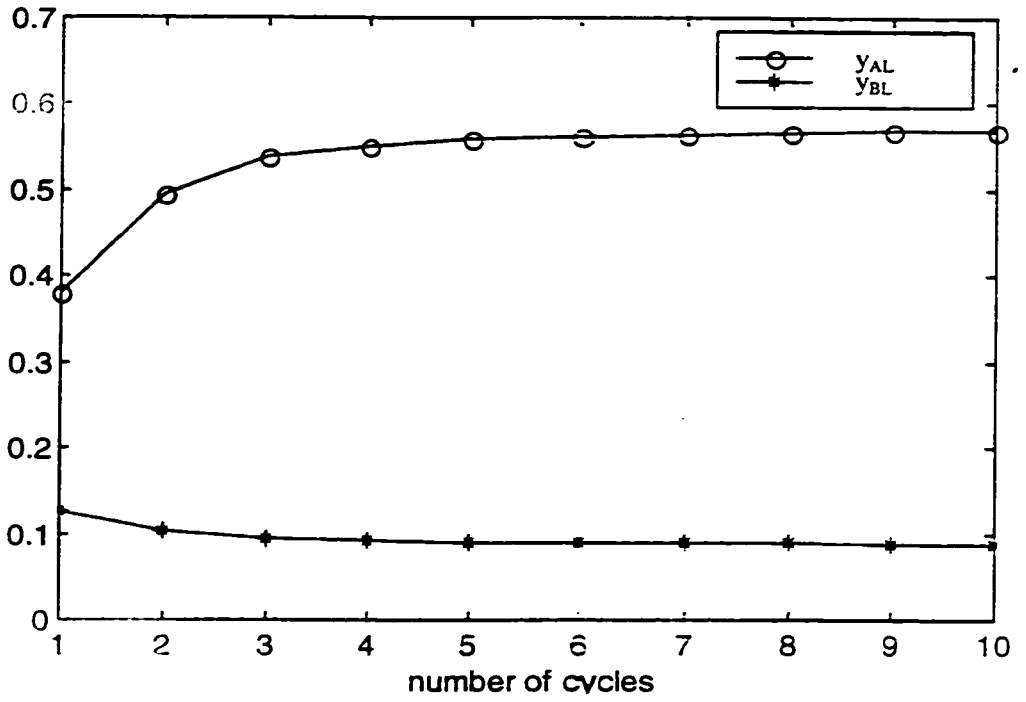


Figure 2.14 Approach to cyclic steady state, showing exit concentration of n-$C_5$ and i-$C_5$ at end of blowdown step. Parametric values are in Table 2.5

case (an isothermal-single adsorbable component system). For the nonisothermal-two adsorbable components system, the number of cycles to reach cyclic steady state is expected to be higher.

In 1998, Silva and Rodrigues studied the binary adsorption of n-pentane/n-hexane mixture on 5A zeolite [56]. They developed a mathematical model and used it for simulating a PSA separation of n,i-$C_5/C_6/H_2$ mixture. Figure 2.15 demonstrates gas phase concentration profiles of $nC_5$ and $nC_6$ at cyclic steady state at end of the four basic steps. Feed concentrations are 13.9 mol% n-$C_5$ and 4.6 mol% n-$C_6$, and feed temperature is 573 K. They used the same pressure ratio as in the present study ($P_H$ is 15 bar and $P_L$ is 2 bar). Although the system considered in the present study (n-pentane) and the system considered by them (n-pentane/hexane) are different, still some comparison could be done. Comparing the concentration profiles for the two systems (Figure 2.12 and Figure 2.15), the qualitative shapes of the profiles are similar, indicating that the present PSA model is adequate. The n-pentane/hexane system will be simulated by the present model in the future.

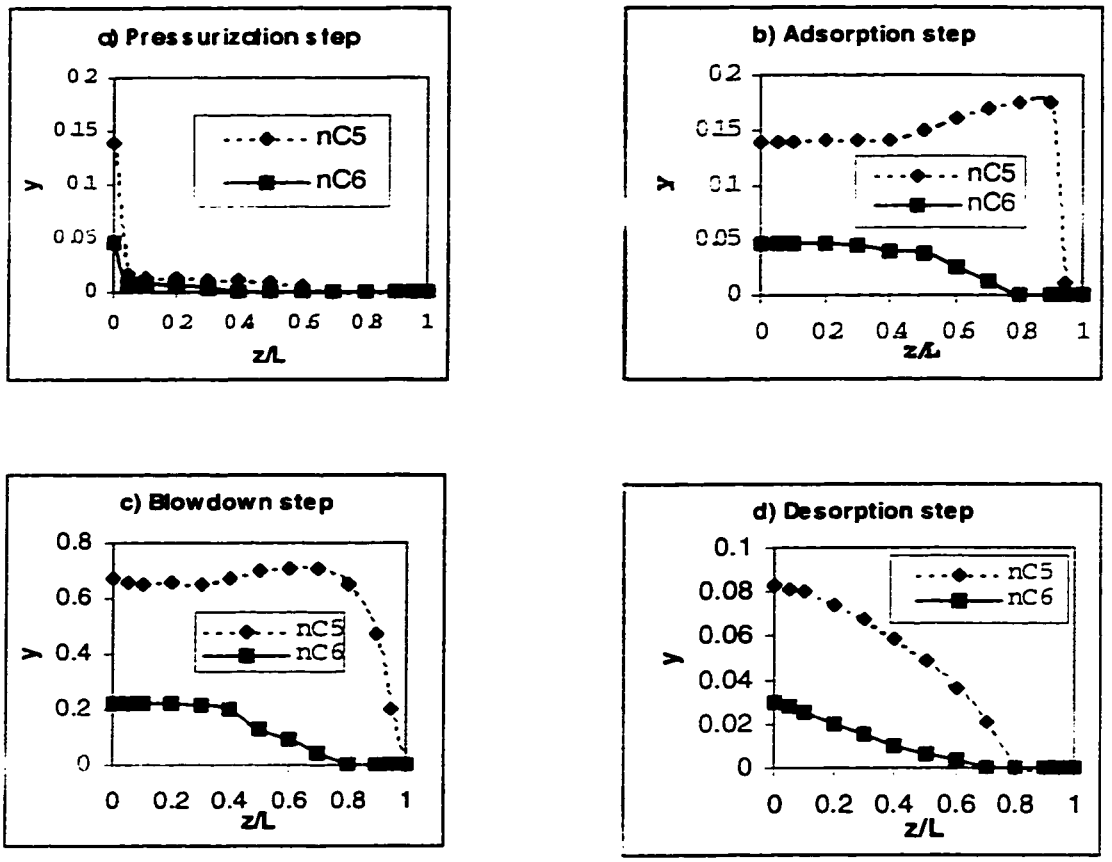


Figure 2.15. Gas phase concentration profiles of $nC_5$ and $nC_6$ at cyclic steady state at end of the four basic steps, for the n,i-$C_5$/$C_6$/$H_2$ system studied by Silva and Rodrigues [figures are taken from reference 56]. Feed compositions are 13.9 mol% $nC_5$ and 4.6 mol% $nC_6$ and feed temperature is 573 K. The purge to feed molar ratio is 0.465. $P_H$ is 15 bar and $P_L$ is 2 bar.

# Nomenclature

| | |
|---|---|
| $a_p$ | specific area of the adsorbent pellet [$cm^{-1}$] |
| $c_{Tj}$ | total gas concentration in column j [$mol/cm^3$] |
| $c_{Tf}$ | total gas concentration of the reactor feed [$mol/cm^3$] |
| $C_{Tj}$ | dimensionless total gas concentration in column j [$mol/cm^3$] |
| $c_{Aj}$ | concentration of component A in the bulk phase in colum j [$mol/cm^3$] |
| $c_{Bj}$ | concentration of component B in the bulk phase in column j [$mol/cm^3$] |
| $c_{Ij}$ | concentration of hydrogen in the bulk phase in column j [$mol/cm^3$] |
| $c_{Af}$ | concentration of component A in the reactor feed [$mol/cm^3$] |
| $c_{Bf}$ | concentration of component B in the reactor feed [$mol/cm^3$] |
| $\langle c_{A2} \rangle$ | average concentration of the sorbate in the pores of the adsorbent pellet in column 2 [$mol/cm^3$] |
| Da | Damköhler number [-] = $k_1 L / u_f$ |
| $D_L$ | axial mass dispersion coefficient [$cm^2/s$] |
| $D_m$ | molecular diffusivity [$cm^2/s$] |
| $D_p$ | macropore diffusivity [$cm^2/s$] |
| $D_c$ | micropore diffusivity [$cm^2/s$] |
| $d_p$ | pellet diameter [cm] |
| $F_0$ | molar feed flux [$mol/m^2/s$] |
| $-\Delta H_{ads}$ | isosteric heat of adsorption [J/mol] |
| $k_1$ | forward reaction rate constant [$cm^3$/g of cat/s] |
| $k_i$ | internal mass transfer coefficient [cm/s] |
| $k_e$ | external mass transfer coefficient [cm/s] |
| $K_{ads}$ | adsorption equilibrium constant [$bar^{-1}$] = $K_o \exp(-\Delta H_{ads} / R / T)$ |
| $K_C$ | equilibrium reaction rate constant [-] |
| $k_{gl}$ | global mass-transfer coefficient [cm/s] |
| $K_o$ | limiting adsorption equilibrium constant [$bar^{-1}$] |
| $L$ | length of column [cm] |
| $n$ | coefficient of Nitta et al. isotherm [-] |

| | |
|---|---|
| $N_f$ | number of film mass-transfer units [-] |
| Pe | mass Peclet number [-] = $u_f L / D_L$ |
| $P_j$ | total pressure in column j [bar] |
| $P_H$ | constant high pressure during adsorption step [bar] |
| $P_L$ | constant low pressure during desorption step [bar] |
| $\langle q_A \rangle$ | average adsorbed-phase concentration [mol/kg] |
| $q_{A.ref}$ | adsorbed-phase concentration at equilibrium with $y_{A2.f}$ at high pressure [mol/kg] |
| $q_{max}$ | maximum adsorbed-phase concentration [mol/kg] |
| $Q_A$ | dimensionless adsorbed-phase concentration [-] |
| R | ideal gas constant [bar.cm$^3$/mol/K] |
| $R_c$ | internal column radius [cm] |
| $R_p$ | pellet radius [cm] |
| $r_c$ | crystal radius [cm] |
| Re | Reynolds number [-] = $\rho u_f d_p / \mu$ |
| Sc | Schmidt number [-] = $\mu / \rho / D_m$ |
| Sh | Sherwood number [-] = $k_c d_p / D_m$ |
| t | time [s] |
| T | gas temperature [K] |
| $T_f$ | feed gas temperature [K] |
| $u$ | interstitial velocity [cm/s] |
| $u_f$ | interstitial feed velocity [cm/s] |
| $U$ | dimensionless interstitial velocity [-] |
| $u_p$ | purge gas velocity [cm/s] |
| $x$ | dimensionless axial coordinate in the column [-] |
| $y_{Af}$ | mole fraction of component A in the reactor feed [-] |
| $y_{A2.f}$ | mole fraction of component A in the adsorber feed [-] |
| $y_{Aj}$ | mole fraction of component A in the bulk phase in column j [-] |
| $y_{Bj}$ | mole fraction of component B in the bulk phase in column j [-] |
| $y_{AL}$ | mole fraction of component A at the exit of the adsorber [-] |
| $y_{A.eq}$ | equilibrium mole fraction of component A for isomerization reaction [-] |
| $\langle y_{A2} \rangle$ | average mole fraction of the sorbate in the pores of the adsorbent pellet in column 2 [-] |
| $z$ | axial coordinate in the column [cm] |

*Greek Letters*

| | |
|---|---|
| $\varepsilon$ | bed porosity [-] |
| $\varepsilon_p$ | solid porosity [-] |
| $\zeta_m$ | mass capacity factor [-] = $(1-\varepsilon)\rho_S q_{A,ref} / \varepsilon / c_{Tf}$ |
| $\rho_b$ | bulk density of the adsorbent pellet [g/cm$^3$] |
| $\rho_s$ | apparent density of the adsorbent pellet [g/cm$^3$] |
| $\rho$ | gas density [g/cm$^3$] |
| $\mu$ | gas viscosity [g/cm/s] |
| $\theta_A$ | coverage of adsorbent [-] |
| $\theta_{ref}$ | coverage of adsorbent at $y_{A2\_f}$ [-] |
| $\tau$ | dimensionless time [-] |

*Subscripts*

| | |
|---|---|
| A | n-pentane |
| B | isopentane |
| I | hydrogen |
| T | total |
| f | feed |
| j | column 1 (reactor) or 2 (adsorber) |

# CHAPTER 3

# PSAR MODELLING FOR n-i/$C_5$ SYSTEM

## 3.1 PSAR PROCESS DESCRIPTION

Figure 1.7 is the proposed process flow diagram for isomerizing of n-alkanes to isoalkanes in the PSAR unit. The unit consists of two columns. Each column consists of a catalyst-packed region followed by an adsorbent-packed region. For simplicity, the system is initially modeled as an isothermal process containing only three components (n-i/$C_5$/$H_2$). The cyclic steps of the PSAR scheme, shown in Figure 3.1, are as follow:

***Step 1: Pressurization/reaction***: The unit is pressurized by feeding a portion of the feedstock (at high pressure) to it, injected into the catalyst bed. In the catalyst bed, partial conversion of n-$C_5$ to i-$C_5$ takes place. There is no effluent from the unit during this step.

***Step 2: Reaction/adsorption***: The feedstock (at high pressure) is fed to the catalyst bed where partial conversion of n-$C_5$ to i-$C_5$ takes place. Then, it enters the adsorbent region where unreacted n-$C_5$ is adsorbed. The effluent from the unit, composed of i-$C_5$ and hydrogen, is fed to a flash drum where i-$C_5$ is separated and taken off as the process product and $H_2$ is recycled to the

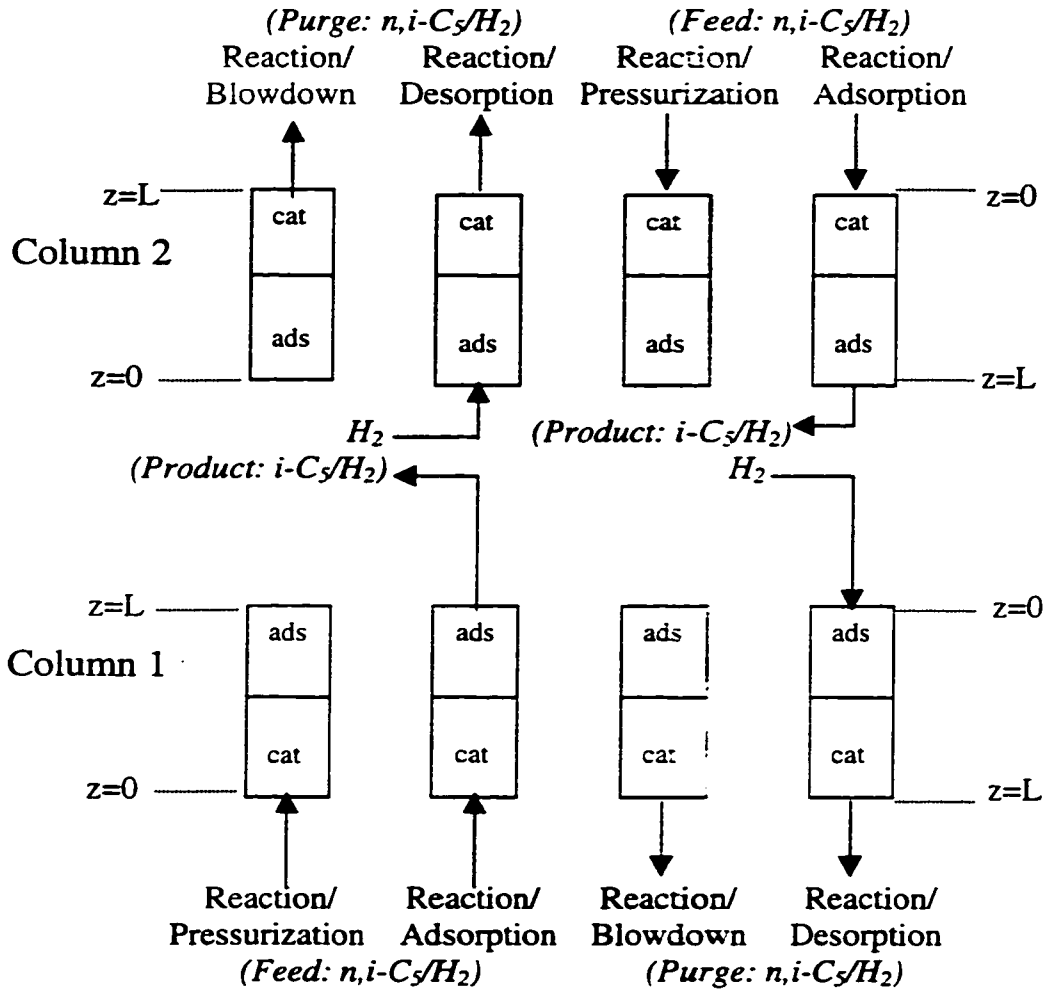


Figure 3.1. Proposed Cyclic Steps for the PSAR Unit

process. This step continues until the adsorbent bed approaches a specified saturation limit. Then, feed is shut off, and step 3 is introduced.

***Step 3: Blowdown/reaction***: The unit is depressurized to a lower pressure level in a direction counter-current to that of the feed gas flow. Desorption of n-$C_5$ takes place in the adsorbent region, followed by partial isomerization in the catalyst region. A gas stream containing all components of the system exits the unit. Usually this stream is considered as a waste stream and discharged off in most conventional PSA processes. In the present case, however, the blowdown stream should be utilized since it contains a considerable portion of i-$C_5$. The utilization of this gas stream will be studied in future planning. In the present case, however, it will be considered as a waste stream to simplify the simulation.

***Step 4: Desorption/reaction***: Hydrogen gas, which is considered as inert, is introduced to the adsorbent bed at low pressure. This step desorbs the remaining n-$C_5$ from the adsorbent bed and forces it to the catalyst bed where partial isomerization takes places. Again the effluent in this step will be considered as a waste stream in the simulation.

## 3.2 MODEL EQUATIONS

A mathematical representation of the problem is as shown in Figure 3.2. The normalized equations developed in Chapter 2 (equations 2.42-2.66) are re-written in terms of two-space variables, defined as follow:

$$v_1 = \frac{x}{\omega} \qquad ; \ 0 < x < \omega \tag{3.1a}$$

$$v_2 = \frac{x-\omega}{1-\omega} \qquad ; \ \omega < x < 1 \tag{3.1b}$$

The model assumptions of chapter 2 are valid here, with the addition that the continuity of concentration, mass flux, and velocity are applicable at the junction of the two subdomains.

Thus, the final form of the model equations becomes

Step 1 (Reaction/Pressurization)

$$\frac{\partial y_{A1}}{\partial \tau} = \frac{1}{\omega^2}\frac{1}{Pe}\frac{\partial^2 y_{A1}}{\partial v_1^{\,2}} - \frac{1}{\omega}\frac{\partial (U_1 y_{A1})}{\partial v_1} - \frac{y_{A1}}{C_T}\frac{\partial C_T}{\partial \tau} - \frac{Da_r}{\omega}\left[y_{A1} - \frac{y_{B1}}{K_C}\right] \tag{3.2}$$

$$\frac{\partial y_{B1}}{\partial \tau} = \frac{1}{\omega^2}\frac{1}{Pe}\frac{\partial^2 y_{B1}}{\partial v_1^{\,2}} - \frac{1}{\omega}\frac{\partial (U_1 y_{B1})}{\partial v_1} - \frac{y_{B1}}{C_T}\frac{\partial C_T}{\partial \tau} + \frac{Da_r}{\omega}\left[y_{A1} - \frac{y_{B1}}{K_C}\right] \tag{3.3}$$

$$\frac{\partial U_1}{\partial v_1} = -\frac{\omega}{C_T}\frac{\partial C_T}{\partial \tau} \tag{3.4}$$

$$\frac{\partial y_{A2}}{\partial \tau} = \frac{1}{(1-\omega)^2}\frac{1}{Pe}\frac{\partial^2 y_{A2}}{\partial v_2^{\,2}} - \frac{1}{(1-\omega)}\frac{\partial (U_2 y_{A2})}{\partial v_2} - \frac{y_{A2}}{C_T}\frac{\partial C_T}{\partial \tau} - \frac{1}{C_T}\zeta_m \frac{\partial Q_A}{\partial \tau} \tag{3.5}$$

$$\frac{\partial y_{B2}}{\partial \tau} = \frac{1}{(1-\omega)^2}\frac{1}{Pe}\frac{\partial^2 y_{B2}}{\partial v_2^{\,2}} - \frac{1}{(1-\omega)}\frac{\partial (U_2 y_{B2})}{\partial v_2} - \frac{y_{B2}}{C_T}\frac{\partial C_T}{\partial \tau} \tag{3.6}$$

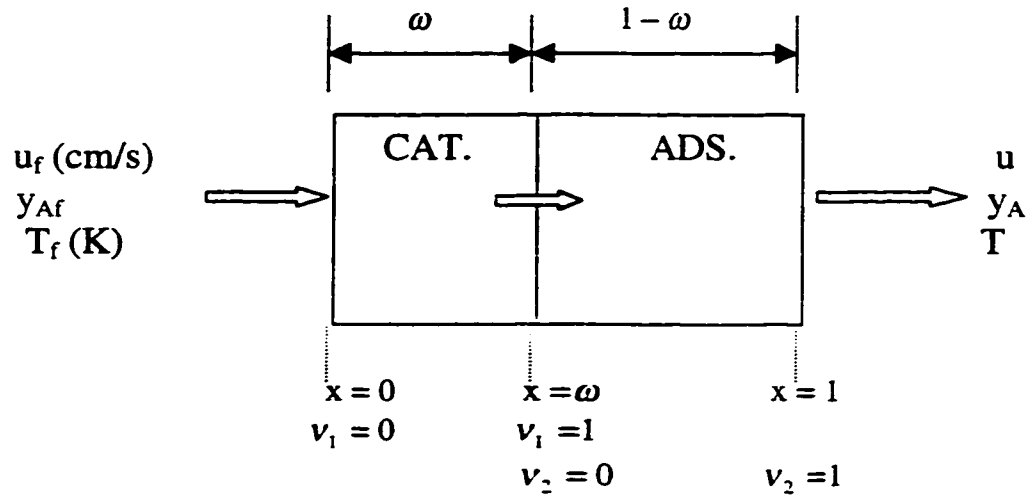


Figure 3.2a Mathematical Representation for the PSAR Unit (steps 1 and 2). Note that for step 1 the product end is closed.

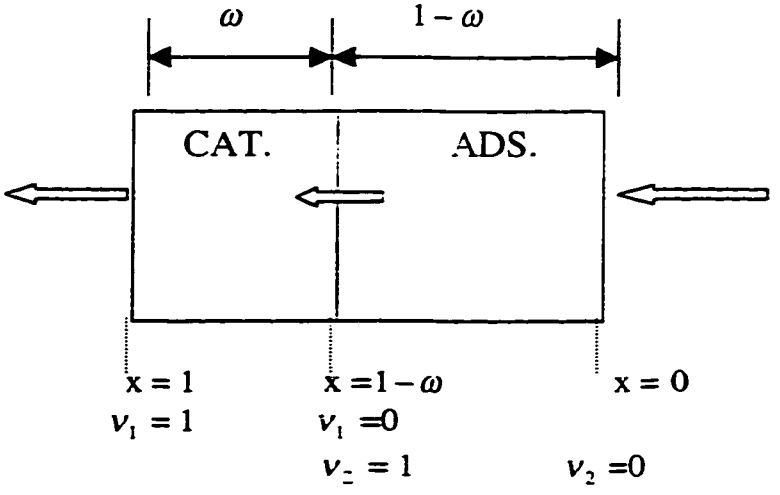


Figure 3.2b Mathematical Representation for the PSAR Unit (steps 3 and 4). Note that for step 3 the feed inlet is closed.

$$\frac{\partial U_2}{\partial v_2} = -\frac{(1-\omega)}{C_T}\frac{\partial C_T}{\partial \tau} - \frac{(1-\omega)}{C_T}\zeta_m \frac{\partial Q_A}{\partial \tau} \tag{3.7}$$

The boundary conditions are

$$x = 1, \tau > 0 \qquad -\frac{1}{Pe}\frac{\partial y_{A1}}{\partial v_1} = U_1\big|_{v_1=0}\,\omega(y_{Af} - y_{A1}) \tag{3.8a}$$

$$v_1 = 1, (v_2 = 0), \tau > 0 \qquad y_{A1} = y_{A2} \tag{3.8b}$$

$$v_1 = 1, (v_2 = 0), \tau > 0 \qquad -(1-\omega)D_A \frac{\partial y_{A1}}{\partial v_1} = -\omega D_A \frac{\partial y_{A2}}{\partial v_2} \tag{3.8c}$$

$$v_1 = 1, (v_2 = 0), \tau > 0 \qquad U_1 = U_2 \tag{3.8d}$$

$$v_2 = 1, \tau > 0 \qquad \frac{\partial y_{A2}}{\partial v_2} = 0 \tag{3.8e}$$

$$v_2 = 1, \tau > 0 \qquad U_2 = 0 \tag{3.8f}$$

Step 2 (Reaction/Adsorption)

$$\frac{\partial y_{A1}}{\partial \tau} = \frac{1}{\omega^2}\frac{1}{Pe}\frac{\partial^2 y_{A1}}{\partial v_1^{\,2}} - \frac{1}{\omega}\frac{\partial y_{A1}}{\partial v_1} - \frac{Da_I}{\omega}\left[y_{A1} - \frac{y_{B1}}{K_C}\right] \tag{3.9}$$

$$\frac{\partial y_{B1}}{\partial \tau} = \frac{1}{\omega^2}\frac{1}{Pe}\frac{\partial^2 y_{B1}}{\partial v_1^{\,2}} - \frac{1}{\omega}\frac{\partial y_{B1}}{\partial v_1} + \frac{Da_I}{\omega}\left[y_{A1} - \frac{y_{B1}}{K_C}\right] \tag{3.10}$$

$$\frac{\partial y_{A2}}{\partial \tau} = \frac{1}{(1-\omega)^2}\frac{1}{Pe}\frac{\partial^2 y_{A2}}{\partial v_2^{\,2}} - \frac{1}{(1-\omega)}\frac{\partial (U_2 y_{A2})}{\partial v_2} - \zeta_m \frac{\partial Q_A}{\partial \tau} \tag{3.11}$$

$$\frac{\partial y_{B2}}{\partial \tau} = \frac{1}{(1-\omega)^2}\frac{1}{Pe}\frac{\partial^2 y_{B2}}{\partial v_2^{\,2}} - \frac{1}{(1-\omega)}\frac{\partial (U_2 y_{B2})}{\partial v_2} \tag{3.12}$$

$$\frac{\partial U_2}{\partial v_2} = -(1-\omega)\zeta_m \frac{\partial Q_A}{\partial \tau} \tag{3.13}$$

The boundary conditions are

$$v_1 = 0, \tau > 0 \qquad -\frac{1}{Pe}\frac{\partial y_{A1}}{\partial v_1} = \omega(y_{Af} - y_{A1}) \tag{3.14a}$$

$$v_1 = 1, (v_2 = 0), \tau > 0 \qquad y_{A1} = y_{A2} \tag{3.14b}$$

$$v_1 = 1, (v_2 = 0), \tau > 0 \qquad -(1-\omega)D_A\frac{\partial y_{A1}}{\partial v_1} = -\omega D_A\frac{\partial y_{A2}}{\partial v_2} \tag{3.14c}$$

$$v_2 = 0, \tau > 0 \quad U_2 = 1 \tag{3.14d}$$

$$v_2 = 1, \tau > 0 \qquad \frac{\partial y_{A2}}{\partial v_2} = 0 \tag{3.14e}$$

$$v_1 = 1, (v_2 = 0), \tau > 0 \qquad U_1 = U_2 \tag{3.14f}$$

Step 3 (Reaction/Blowdown)

$$\frac{\partial y_{A1}}{\partial \tau} = \frac{1}{\omega^2}\frac{1}{Pe}\frac{\partial^2 y_{A1}}{\partial v_1^2} - \frac{1}{\omega}\frac{\partial (U_1 y_{A1})}{\partial v_1} - \frac{y_{A1}}{C_T}\frac{\partial C_T}{\partial \tau} - \frac{Da_I}{\omega}\left[y_{A1} - \frac{y_{B1}}{K_C}\right] \tag{3.15}$$

$$\frac{\partial y_{B1}}{\partial \tau} = \frac{1}{\omega^2}\frac{1}{Pe}\frac{\partial^2 y_{B1}}{\partial v_1^2} - \frac{1}{\omega}\frac{\partial (U_1 y_{B1})}{\partial v_1} - \frac{y_{B1}}{C_T}\frac{\partial C_T}{\partial \tau} - \frac{Da_I}{\omega}\left[y_{A1} - \frac{y_{B1}}{K_C}\right] \tag{3.16}$$

$$\frac{\partial U_1}{\partial v_1} = -\frac{\omega}{C_T}\frac{\partial C_T}{\partial \tau} \tag{3.17}$$

$$\frac{\partial y_{A2}}{\partial \tau} = \frac{1}{(1-\omega)^2}\frac{1}{Pe}\frac{\partial^2 y_{A2}}{\partial v_2^2} - \frac{1}{(1-\omega)}\frac{\partial (U_2 y_{A2})}{\partial v_2} - \frac{y_{A2}}{C_T}\frac{\partial C_T}{\partial \tau} - \frac{1}{C_T}\zeta_m\frac{\partial Q_A}{\partial \tau} \tag{3.18}$$

$$\frac{\partial y_{B2}}{\partial \tau} = \frac{1}{(1-\omega)^2}\frac{1}{Pe}\frac{\partial^2 y_{B2}}{\partial v_2^2} - \frac{1}{(1-\omega)}\frac{\partial (U_2 y_{B2})}{\partial v_2} - \frac{y_{B2}}{C_T}\frac{\partial C_T}{\partial \tau} \tag{3.19}$$

$$\frac{\partial U_2}{\partial v_2} = -\frac{(1-\omega)}{C_T}\frac{\partial C_T}{\partial \tau} - \frac{(1-\omega)}{C_T}\zeta_m\frac{\partial Q_A}{\partial \tau} \tag{3.20}$$

The boundary conditions are

$$v_2 = 0, \tau > 0 \quad \frac{\partial y_{A2}}{\partial v_2} = 0 \tag{3.21a}$$

$$v_1 = 0, (v_2 = 1), \tau > 0 \qquad y_{A1} = y_{A2} \tag{3.21b}$$

$$v_1 = 0, (v_2 = 1), \tau > 0 \qquad -(1-\omega) D_A \frac{\partial y_{A1}}{\partial v_1} = -\omega D_A \frac{\partial y_{A2}}{\partial v_2} \tag{3.21c}$$

$$v_1 = 0, (v_2 = 1), \tau > 0 \qquad U_1 = U_2 \tag{3.21d}$$

$$v_1 = 1, \tau > 0 \quad \frac{\partial y_{A1}}{\partial v_1} = 0 \tag{3.21e}$$

$$v_2 = 0, \tau > 0 \quad U_2 = 0 \tag{3.21f}$$

Step 4 (Reaction/Desorption)

$$\frac{\partial y_{A1}}{\partial \tau} = \frac{1}{\omega^2} \frac{1}{Pe} \frac{\partial^2 y_{A1}}{\partial v_1^2} - \frac{1}{\omega} \frac{\partial (U_1 y_{A1})}{\partial v_1} - \frac{Da_I}{\omega} [y_{A1} - \frac{y_{B1}}{K_C}] \tag{3.22}$$

$$\frac{\partial y_{B1}}{\partial \tau} = \frac{1}{\omega^2} \frac{1}{Pe} \frac{\partial^2 y_{B1}}{\partial v_1^2} - \frac{1}{\omega} \frac{\partial (U_1 y_{B1})}{\partial v_1} + \frac{Da_I}{\omega} [y_{A1} - \frac{y_{B1}}{K_C}] \tag{3.23}$$

$$\frac{\partial U_1}{\partial v_1} = 0 \tag{3.24}$$

$$\frac{\partial y_{A2}}{\partial \tau} = \frac{1}{(1-\omega)^2} \frac{1}{Pe} \frac{\partial^2 y_{A2}}{\partial v_2^2} - \frac{1}{(1-\omega)} \frac{\partial (U_2 y_{A2})}{\partial v_2} - \frac{1}{C_T} \zeta_m \frac{\partial Q_A}{\partial \tau} \tag{3.25}$$

$$\frac{\partial y_{B2}}{\partial \tau} = \frac{1}{(1-\omega)^2} \frac{1}{Pe} \frac{\partial^2 y_{B2}}{\partial v_2^2} - \frac{1}{(1-\omega)} \frac{\partial (U_2 y_{B2})}{\partial v_2} \tag{3.26}$$

$$\frac{\partial U_2}{\partial v_2} = -\frac{(1-\omega)}{C_T} \zeta_m \frac{\partial Q_A}{\partial \tau} \tag{3.27}$$

The boundary conditions are

$$v_2 = 0, \tau > 0 \qquad \frac{1}{Pe}\frac{\partial y_{A2}}{\partial v_2} = U_2\big|_{v_2=0}(1-\omega)y_{A2} \tag{3.28a}$$

$$v_1 = 0, (v_2 = 1), \tau > 0 \qquad y_{A1} = y_{A2} \tag{3.28b}$$

$$v_1 = 0, (v_2 = 1), \tau > 0 \qquad -(1-\omega)D_A\frac{\partial y_{A1}}{\partial v_1} = -\omega D_A\frac{\partial y_{A2}}{\partial v_2} \tag{3.28c}$$

$$v_1 = 0, (v_2 = 1), \tau > 0 \qquad U_1 = U_2 \tag{3.28d}$$

$$v_1 = 1, \tau > 0 \qquad \frac{\partial y_{A1}}{\partial v_1} = 0 \tag{3.28e}$$

$$v_2 = 0, \tau > 0 \qquad U_2 = u_p / u_f \tag{3.28f}$$

In all the four steps, the mass transfer rate and the adsorption equilibrium isotherm for the adsorbent region are

$$\zeta_m \frac{\partial Q_A}{\partial \tau} = N_f C_T (y_{A2} - \langle y_{A2} \rangle) \tag{3.29}$$

$$\langle y_{A2} \rangle P = \frac{1}{K_{ads}} \frac{\theta_{ref} Q_A}{(1-\theta_{ref} Q_A)^n} \tag{3.30}$$

The initial conditions are

$$y_{A1} = y_{B1} = y_{A2} = y_{B2} = Q_A = 0 \tag{3.31a}$$

$$y_{B1}(v_1, \tau = 0) = 0 \tag{3.31b}$$

$$y_{A2}(v_2, \tau = 0) = 0 \tag{3.31c}$$

$$y_{B2}(v_2, \tau = 0) = 0 \tag{3.31d}$$

$$Q_A(v_2, \tau = 0) = 0 \tag{3.31e}$$

Note that for each step of the PSAR cycle the boundary conditions for fluid flow of component B are similar to that of component A.

## 3.3 NUMERICAL METHODS

The numerical technique used here is basically the same as that for solving the PSA model, which is discussed in Chapter 2. Twenty collocation points are used for each subdomain. Since there are three boundaries (two at the inlet and outlet, and one at the junction point), the entire column length is divided into 43 distance intervals. The simulation program is to calculate the concentration in gas and solid phases and the velocity at all distance intervals at different times. The solution-flow diagram for a step in the PSAR unit (reaction/adsorption step) is as shown in Figure 3.3.

## 3.4 RESULTS AND DISCUSSION

### 3.4a FIXED-BED ADSORPTION/REACTION

In this section simulation of a single PSAR column, which undergoes only step 2 (reaction/adsorption at constant high pressure), is considered. The simulation is achieved by solving the model equations of step 2 (equations 3.9 to 3.14), with equation 3.31 as the initial conditions. The

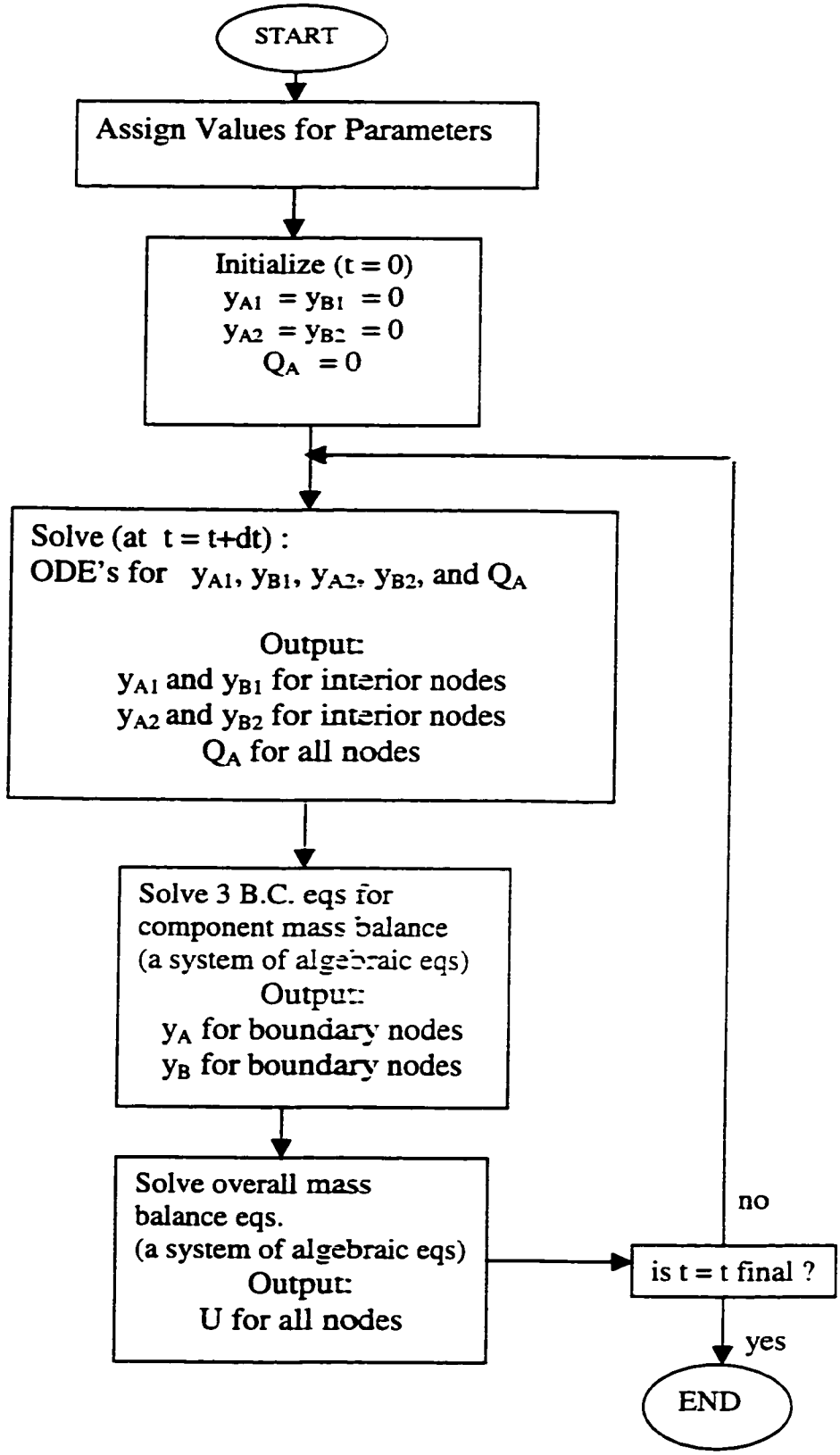


Figure 3.3 Solution-Flow Diagram for Reaction/Adsorption Step

objective is to predict the breakthrough curves for the n-$C_5$/adsorbent system under the new column configuration at different operating conditions. Such predictions will help in designing the cyclic PSAR process. Model parameters used in the simulation are presented in Table 3.1.

Figures 3.4 and 3.5 demonstrate the concentration profiles in the column for n-$C_5$ and i-$C_5$ respectively. The simulation is done at 506 K with $\omega$ equal to 0.5. The total time for this run is about 200 minutes. Figures 3.4 and 3.5 indicate that the concentration profiles in the catalyst region are time-independent after 20 minutes. This is far below the breakthrough point (90 minutes, as shown in Figure 3.6). In the adsorbent region, however, the concentration profiles change with time until reaching the breakthrough point, where the adsorbent bed is totally saturated with n-$C_5$. After that, the concentration profiles are uniform and equal to the exit concentrations from the catalyst bed.

Figure 3.6 demonstrates the effect of temperature in adsorption breakthrough curves for the PSAR bed, at bed temperatures of 506 and 533 K. The other parameters are kept constant during the simulation. The dimensionless equilibrium values for n-pentane ($y_{A,eq}$ / $y_{Af}$ ) are 0.464 and 0.499 at 506 and 533 K, respectively. For a feed mixture of equal concentration of n,i-$C_5$, the ($y_{A,eq}$ / $y_{Af}$) values are calculated by a simple

Table 3.1. Parametric values used for the solution of the breakthrough curves of the n-$C_5$/PSAR system

| Parameter | Figures 3.4 and 3.5 | Figure 3.6* | Figure 3.7* |
|---|---|---|---|
| varying parameter | - | T | $y_{Af}$ and $y_{Bf}$ |
| $y_{Af} = y_{Bf}$ | 0.17 | 0.17 | 0.17, 0.1 |
| $F_f$ (mol/m$^2$/s) | 0.15 | 0.15 | 0.15 |
| P (bar) | 15 | 15 | 15 |
| T (K) | 506 | 506, 533 | 506 |
| $u_f$ (cm/s) | 0.131 | 0.131, 0.138 | 0.131 |
| $D_L$ (cm$^2$/s) | 0.074 | 0.074, 0.081 | 0.074 |
| $k_{gl}$ (cm/s) | 0.62 | 0.62, 0.67 | 0.62 |
| $K_{ads}$ (1/bar) | 10.13 | 10.13, 5.21 | 10.13 |
| $k_1$ (1/s) | 0.034 | 0.034, 0.09 | 0.034 |
| $K_C$ (-) | 3.31 | 3.31, 3.01 | 3.31 |
| $y_{A.eq} / y_{Af}$ | 0.464 | 0.464, 0.499 | 0.464 |
| $Pe$ | 35.5 | 35.5, 34.2 | 35.5 |
| $\zeta_m$ | 6.54 | 6.54, 6.19 | 6.54, 6,02 |
| $v_{ref}$ | 0.539 | 0.539, 0.484 | 0.539, 0.496 |
| $N_f$ | 5039 | 5039, 5150 | 5039 |
| $Da_t$ | 2.59 | 2.59, 6.55 | 2.59 |
| $\omega$ | 0.5 | 0.5 | 0.5 |

*Note: if a parameter in any column has more than one value, the first value corresponds to the first number of the varying parameter

Table 3.1. Parametric values used for the solution of the breakthrough curves of the n-$C_5$/PSAR system (continued)

| Parameter | Figure 3.8* | Figure 3.9* | Figure 3.10* |
|---|---|---|---|
| varying parameter | P | $\omega$ at 506 K | $\omega$ at 533 K |
| $y_{Af} = y_{Bf}$ | 0.17 | 0.17 | 0.17 |
| $F_f$ (mol/m$^2$/s) | 0.15 | 0.15 | 0.15 |
| P (bar) | 15, 20, 2 | 15 | 15 |
| T (K) | 506 | 506 | 533 |
| $u_f$ (cm/s) | 0.131, 0.099, 0.986 | 0.131 | 0.138 |
| $D_L$ (cm$^2$/s) | 0.074, 0.055, 0.55 | 0.074 | 0.081 |
| $k_{gl}$ (cm/s) | 0.62, 0.49, 2.23 | 0.62 | 0.67 |
| $K_{ads}$ (1/bar) | 10.13 | 10.13 | 5.21 |
| $k_1$ (1/s) | 0.034 | 0.034 | 0.09 |
| $K_C$ (-) | 3.31 | 3.31 | 3.01 |
| $y_{A.eq} / y_{Af}$ | 0.464 | 0.464 | 0.499 |
| *Pe* | 35.5 | 35.5 | 34.2 |
| $\zeta_m$ | 6.54, 5.11, 33 | 6.54 | 6.19 |
| $\theta_{ref}$ | 0.539, 0.561, 0.363 | 0.539 | 0.484 |
| $N_f$ | 5039, 5261, 2402 | 5039 | 5150 |
| $Da_t$ | 2.59, 3.42, 0.34 | 1.55, 2.59, 3.63 | 3.93, 9.17 |
| $\omega$ | 0.5 | 0.3, 0.5, 0.7 | 0.3, 0.7 |

*Note: if a parameter in a column has more than one value, the first value corresponds to the first number of the varying parameter.

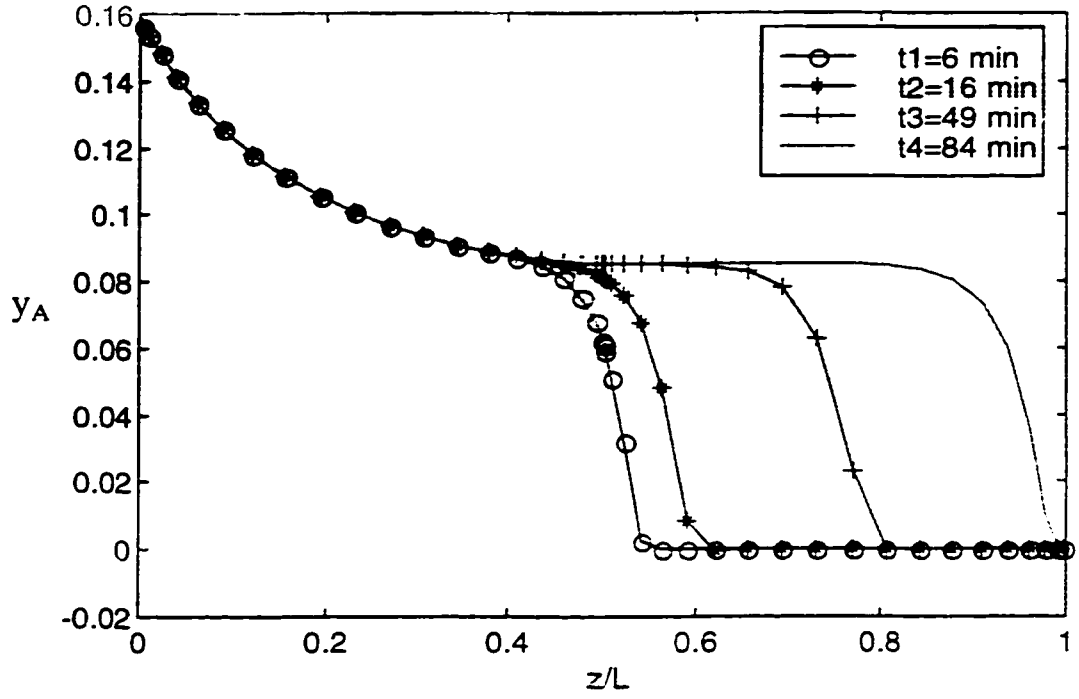


Figure 3.4. Concentration profiles in the fixed-bed PSAR column for n-$C_5$ in the gas phase. Parametric values are in Table 3.1

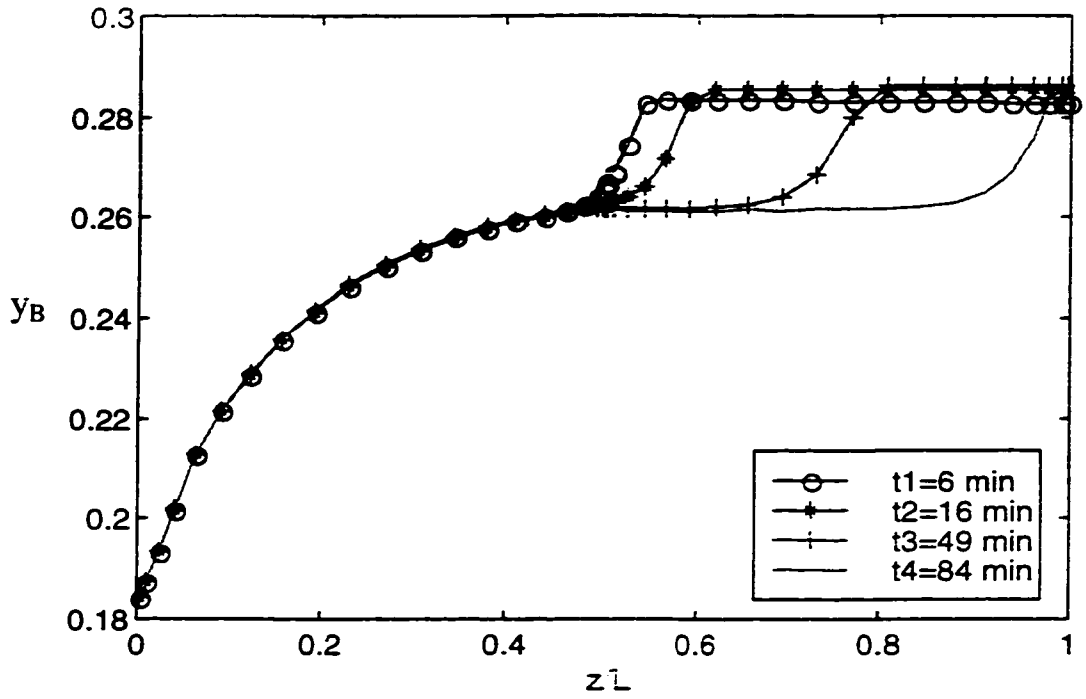


Figure 3.5. Concentration profiles in the fixed-bed PSAR column for i-$C_5$ in the gas phase. Parametric values are in Table 3.1

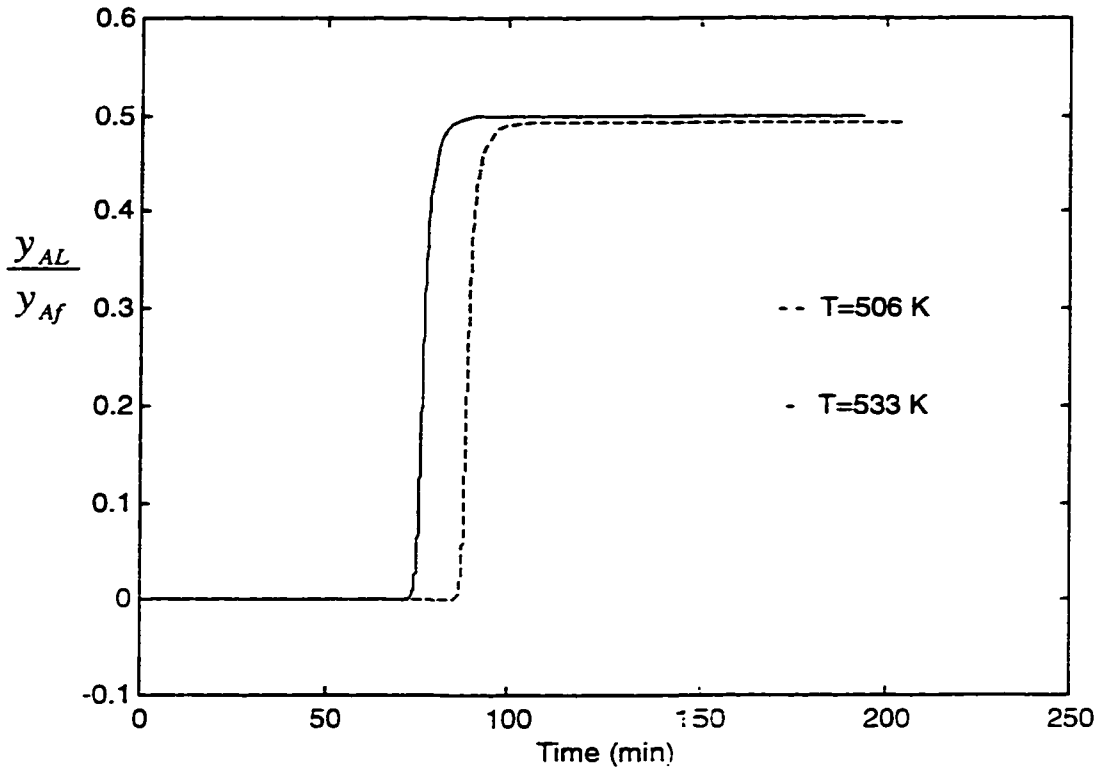


Figure 3.6. Breakthrough curve of the n.i-$C_5$/$H_2$/PSAR system (effect of temperature). Parametric values are in Table 3.1.

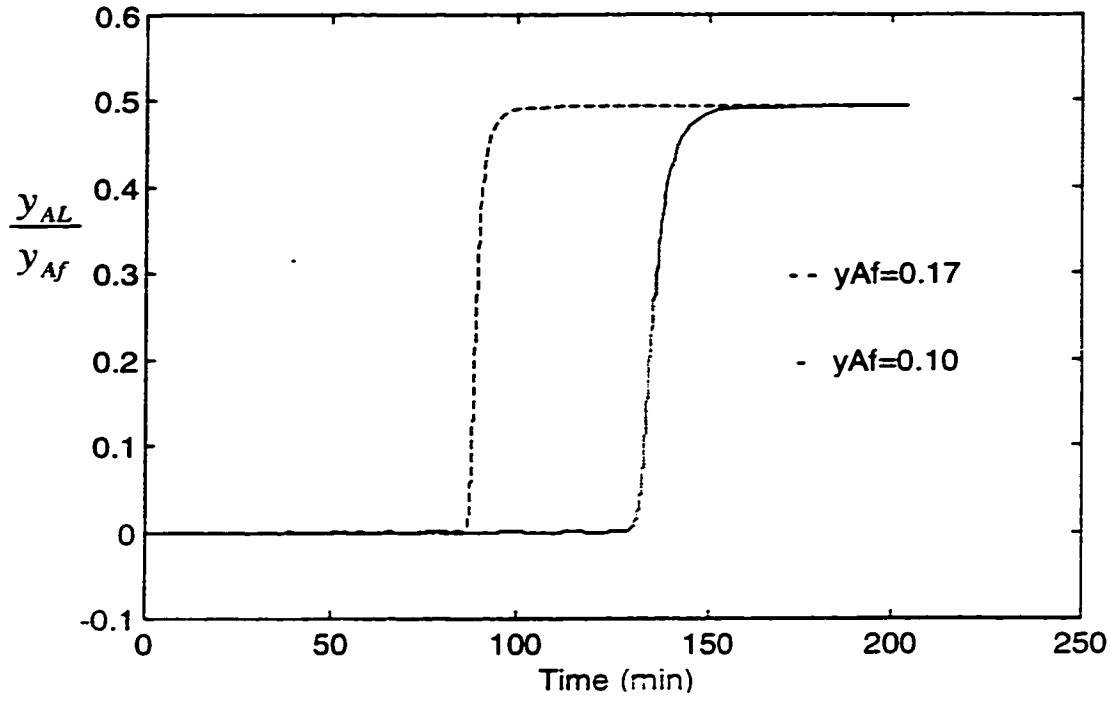


Figure 3.7. Breakthrough curve of the n,i-$C_5$/$H_2$/PSAR system (effect of sorbate mole fraction). Parametric values are in Table 3.1.

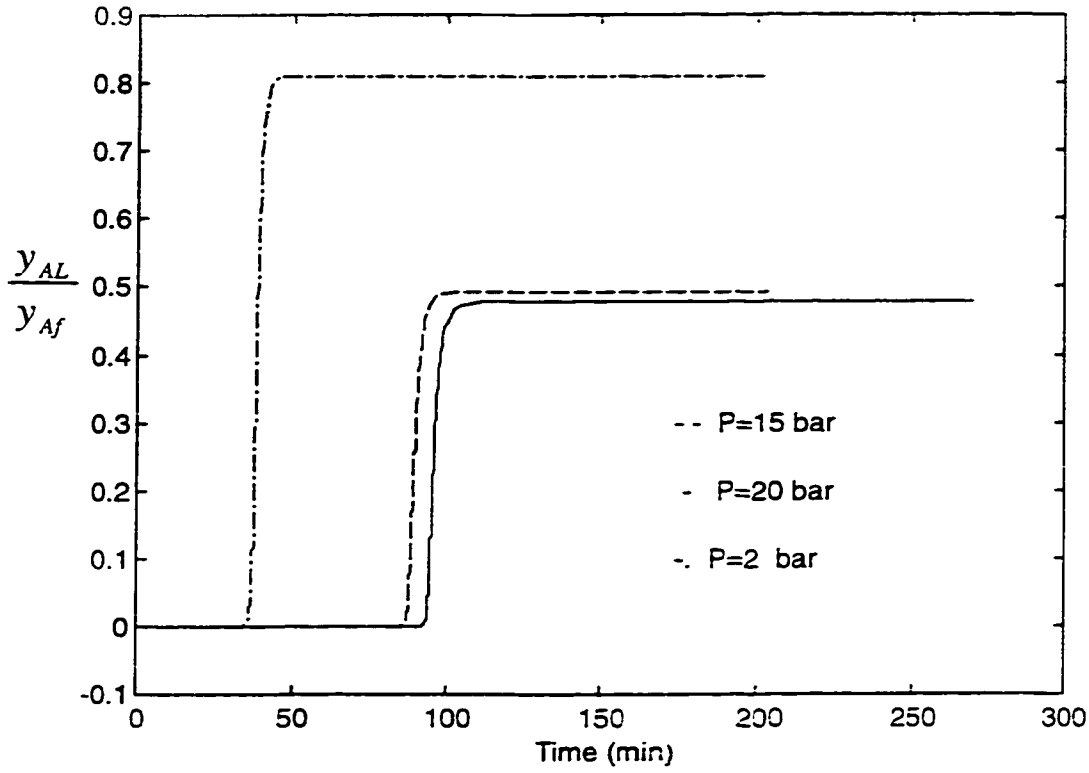


Figure 3.8. Breakthrough curve of the n,i-$C_5$/$H_2$/PSAR system (effect of total pressure). Parametric values are in Table 3.1.

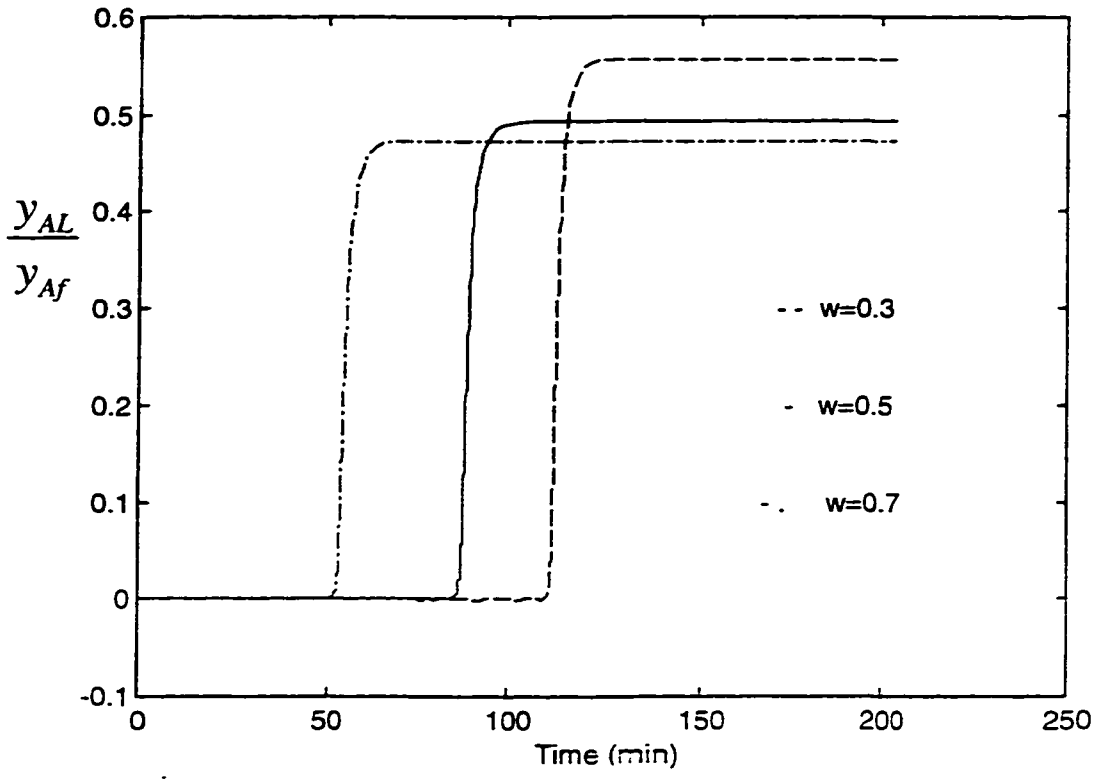


Figure 3.9. Breakthrough curve of the n,i-$C_5$/$H_2$/PSAR system (effect of catalyst/column length ratio at 506 K). Parametric values are in Table 3.1.

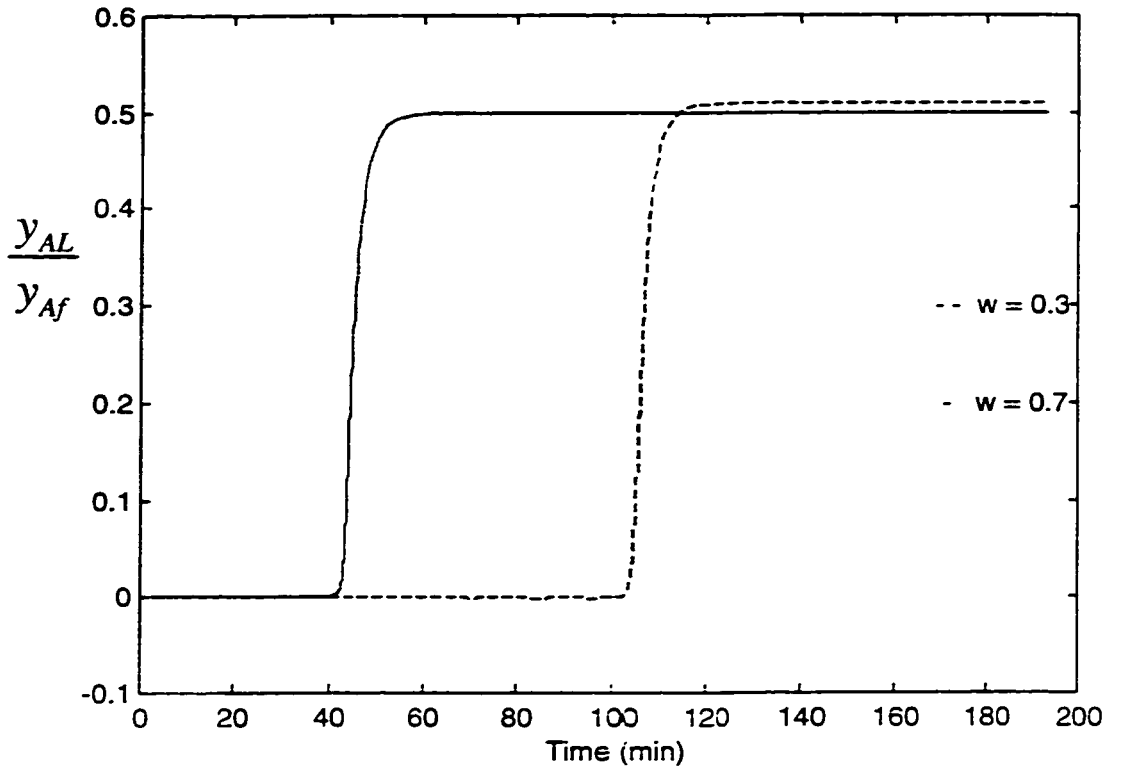


Figure 3.10. Breakthrough curve of the n,i-$C_5$/$H_2$/PSAR system (effect of catalyst/column length ratio at 533 K). Parametric values are in Table 3.1.

relation $2/(K_C+1)$, which is derived from reaction stoichiometry. As shown in the Figures, a better conversion is gained at the lower temperature, although the gain is not so high. On the other hand, the reaction at the higher temperature approached its equilibrium value, due to a higher reaction rate constant, which resulted in a higher Damköhler number. For the adsorbent bed region, higher adsorption is observed at lower temperature.

The effect of feed concentration on the behavior of the breakthrough curve is shown in Figure 3.7. The reactant and the product are assigned the same feed mole fractions of 0.1 and 0.17 at runs 1 and 2, respectively. Here, the dimensionless equilibrium value is the same at both runs because the temperature is fixed. At higher sorbate feed concentration, the curve is sharper and more adsorption takes place resulting in earlier breakthrough.

Figure 3.8 demonstrates the effect of total pressure on breakthrough curves. The simulations are done at 15, 20 and 2 bars, keeping the other parameters unchanged. Although the equilibrium value is not a function of pressure, more conversion is achieved at higher pressures because of lower feed velocity, which resulted in a higher Damköhler number. The conversion at 2 bars is only 20%, due to a low Damköhler number (0.34). For the adsorbent bed, more adsorption takes place at higher pressure.

Figures 3.9 and 3.10 demonstrate the effect of the ratio of catalyst to adsorbent in the column at 506 and 533 K, respectively. The effect is dramatic at the lower temperature, where we need at least 70% of the column to be packed with the catalyst in order to get close to the equilibrium value. At the higher temperature, however, the effect is not so noticeable, where 50% catalyst packing is enough to get close to the equilibrium value. This different behavior is due to the big difference in the reaction rate constants at the two temperature (0.034 and 0.09 $s^{-1}$ at 506 and 533 K, respectively), which resulted in a big difference in Damköhler numbers.

### 3.4b PSAR CYCLIC PROCESS

With basic information obtained from prediction of the breakthrough curves for the fixed-bed PSAR column. the simulation of the four–steps PSAR cycle is now considered. The cycle starts initially with clean adsorbent and clean gas phase. The total length of the column is 20 cm. Parametric values used for simulations of the PSAR cycle are summarized in Table 3.2.

Figures 3.11 and 3.12 demonstrate the concentration profiles of n-$C_5$ and i-$C_5$ in the gas phase at the end of the four basic steps at cyclic steady state, respectively. The simulation is done at 506 K with $\omega$ equal to 0.5. The

simulation is done also at the same conditions of Figure 3.11, but with $\omega$ equal to 0.3 and 0.1, and the results are shown in Figures 3.13 and 3.14.

Several conclusions can be drawn up from the above Figures. At pressurization and adsorption steps, the concentration decreases with position in the catalyst region due to reaction. The concentration of n-pentane at reaction equilibrium state (given by: $y_{A,eq} = (y_{Af} + y_{Bf})/(K_C + 1)$ ) is equal to 0.079 at the given temperature and feed concentrations. How close the concentration of n-pentane at the exit of the catalyst bed approaches to this equilibrium value depends on the catalyst/column length ratio, keeping the other operating conditions unchanged. As indicated in Figure 3.11 and 3.13, the catalyst exit concentrations are 0.08 and 0.09 for $\omega$ values of 0.5 and 0.3, respectively. These results are close to the equilibrium value of 0.079. For $\omega$ equal to 0.1, however, the catalyst exit concentration is 0.12, as shown in Figure 3.14. This is far above the equilibrium value, indicating that the catalyst bed length is not sufficient for the reaction.

At blowdown step increasing concentration of n-pentane is due to desorption, and the rate of increase is higher at a lower value of $\omega$. This is expected since a lower value of $\omega$ means higher adsorbent capacity. When n-pentane exits from the adsorbent region and enters the catalyst region, its concentration decreases with distance due to reaction. Here, the rate of

Table 3.2. Parametric values used for simulations of the n-$C_5$ / PSAR system

| Parameter | Figure 3.11 | Figure 3.13 |
|---|---|---|
| $y_{Af} = y_{Bf}$ | 0.17 | 0.17 |
| $F_f$ (mol/m$^2$/s) | 0.15 | 0.15 |
| $P_H$ (bar) | 15 | 15 |
| $P_L$ (bar) | 2 | 2 |
| T (K) | 506 | 506 |
| $u_f$ (cm/s) | 0.131 | 0.131 |
| Purge/ Feed volumetric ratio | 3.0 | 3.0 |
| $D_L$ @ high pressure (cm$^2$/s) | 0.074 | 0.074 |
| $D_L$ @ low pressure (cm$^2$/s) | 0.555 | 0.555 |
| $k_{gl}$ @ high pressure (cm/s) | 0.62 | 0.62 |
| $k_{gl}$ @ low pressure (cm/s) | 2.23 | 2.23 |
| $k_l$ (1/s) | 0.034 | 0.034 |
| $K_C$ | 3.31 | 3.31 |
| $K_{ads}$ (1/bar) | 10.13 | 10.13 |
| *Pe* @ high pressure | 35.5 | 35.5 |
| *Pe* @ low pressure | 4.7 | 4.7 |
| Pressurization & Blowdown time (min) | 7.69 | 7.69 |
| Adsorption & Desorption time (min) | 15.38 | 15.38 |
| $y_{A,eq}$ | 0.079 | 0.079 |
| $Da_t$ | 2.59 | 1.55 |
| $\omega$ | 0.5 | 0.3 |
| $\zeta_m$ | 6.54 | 6.54 |
| $\theta_{ref}$ | 0.539 | 0.539 |

Table 3.2. Parametric values used for simulations of the n-$C_5$ / PSAR system (continued)

| Parameter | Figure 3.14 | Figure 3.15 |
|---|---|---|
| $y_{Af} = y_{Bf}$ | 0.17 | 0.17 |
| $F_f$ (mol/m$^2$/s) | 0.15 | 0.15 |
| $P_H$ (bar) | 15 | 15 |
| $P_L$ (bar) | 2 | 2 |
| T (K) | 506 | 533 |
| $u_f$ (cm/s) | 0.131 | 0.138 |
| Purge/Feed volumetric ratio | 3.0 | 3.0 |
| $D_L$ @ high pressure (cm$^2$/s) | 0.074 | 0.081 |
| $D_L$ @ low pressure (cm$^2$/s) | 0.555 | 0.608 |
| $k_{gl}$ @ high pressure (cm/s) | 0.62 | 0.67 |
| $k_{gl}$ @ low pressure (cm/s) | 2.23 | 2.31 |
| $k_l$ (1/s) | 0.034 | 0.09 |
| $K_C$ | 3.31 | 3.01 |
| $K_{ads}$ (1/bar) | 10.13 | 5.21 |
| $Pe$ @ high pressure | 35.5 | 34.2 |
| $Pe$ @ low pressure | 4.7 | 4.3 |
| Pressurization & Blowdown time (min) | 7.69 | 7.25 |
| Adsorption & Desorption time (min) | 15.38 | 14.5 |
| $y_{A,eq}$ | 0.079 | 0.084 |
| $Da_t$ | 0.518 | varying |
| $\omega$ | 0.1 | varying |
| $\zeta_m$ | 6.54 | 6.19 |
| $\theta_{ref}$ | 0.539 | 0.484 |

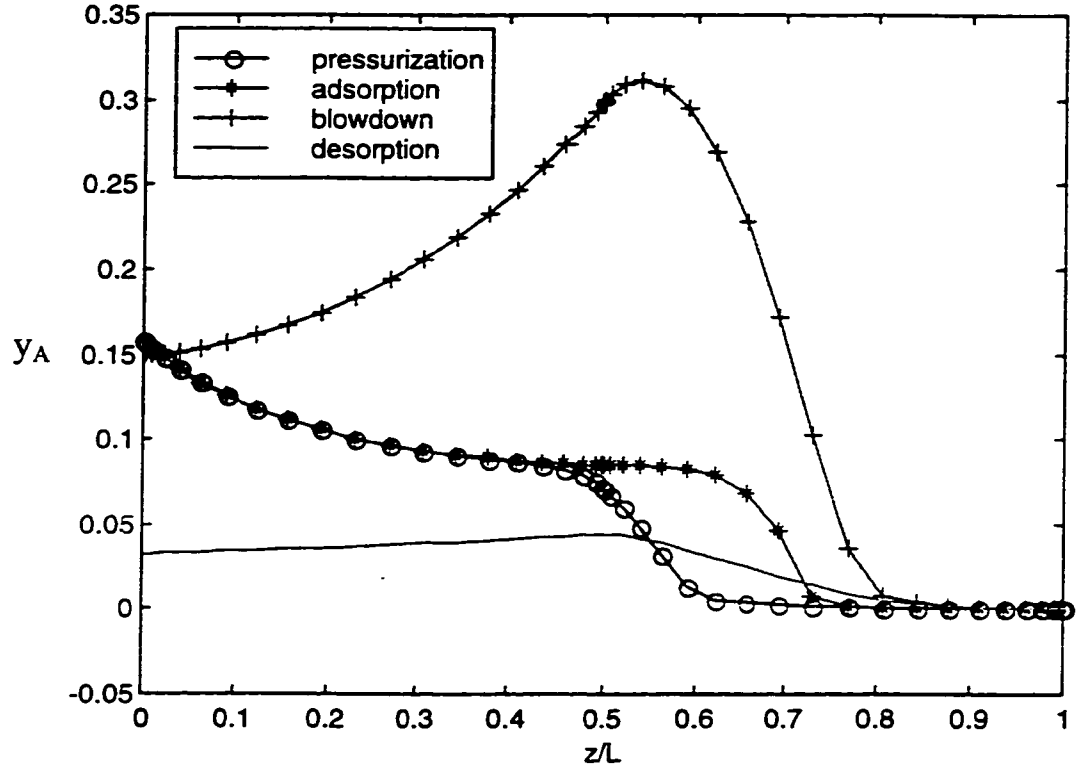


Figure 3.11 Gas phase concentration profiles of n-$C_5$ in the PSAR bed at the end of cyclic steady state ($\omega$ = 0.5). Parametric values are in Table 3.2.

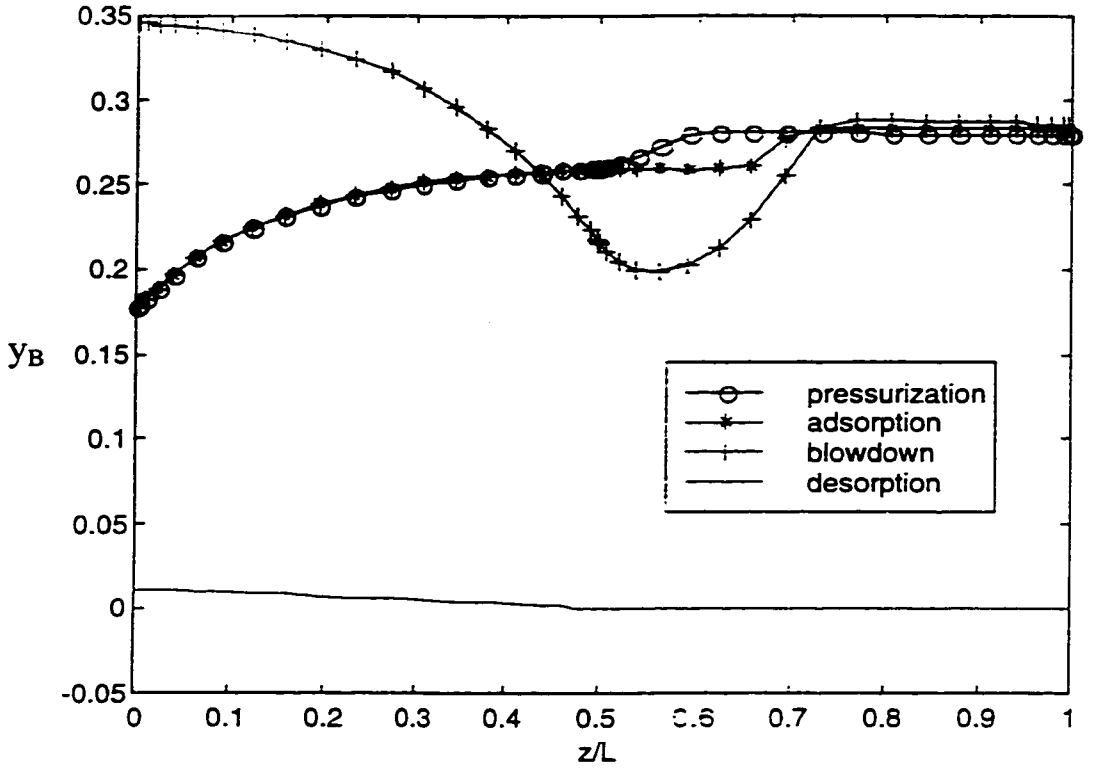


Figure 3.12 Gas phase concentration profiles of i-$C_5$ in the PSAR bed at the end of cyclic steady state ($\omega = 0.5$). Parametric values are the same as for Figure 3.11.

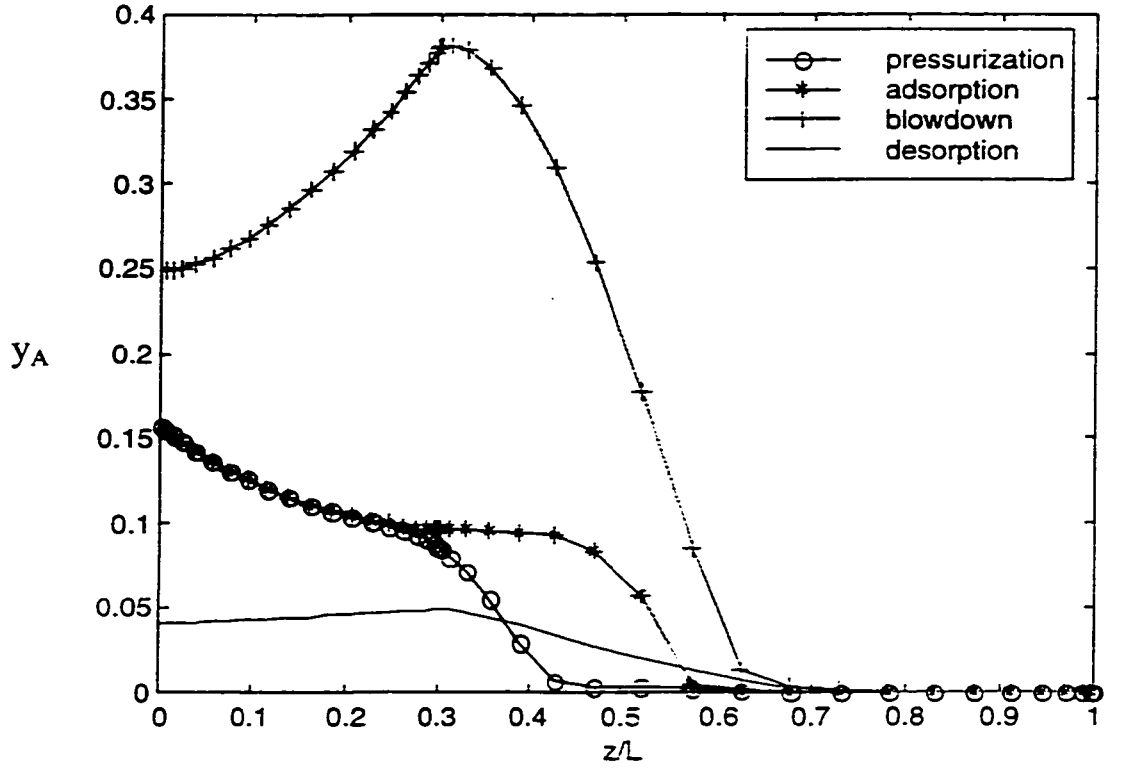


Figure 3.13 Gas phase concentration profiles of n-$C_5$ in the PSAR bed at the end of cyclic steady state ($\omega$ = 0.3). Parametric values are in Table 3.2.

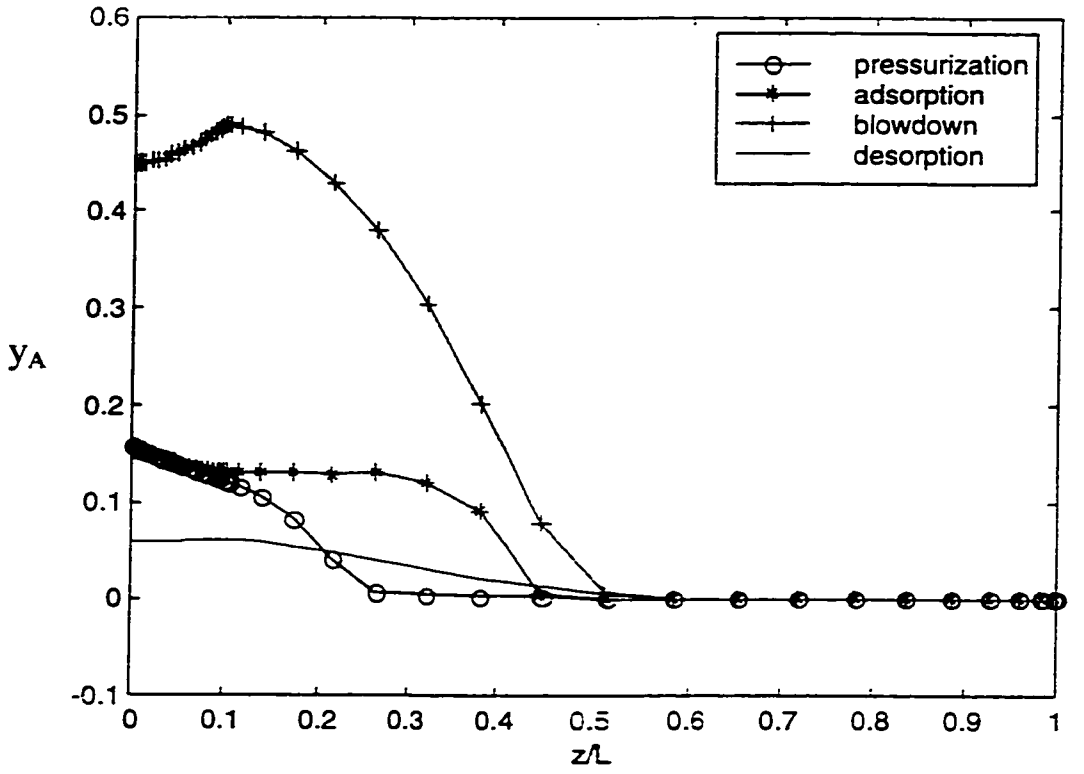


Figure 3.14 Gas phase concentration profiles of n-$C_5$ in the PSAR bed at the end of cyclic steady state ($\omega = 0.1$). Parametric values are in Table 3.2.

decrease is highest at higher value of $\omega$ due to larger Damköhler number. The above observation is emphasized more clearly in Figure 3.15, where the ratio of ($y_B/y_A$) in the column effluent at end of blowdown step is plotted against $\omega$. The (product/reactant) concentration ratio increases as $\omega$ increases, and the relationship is almost linear. Results for another temperature of 533 K are also shown. The two temperatures have the same trend, with 533 K is slightly better than 506 K for $\omega$ below 0.5, and almost have the same performance for $\omega$ above 0.6.

These results indicate that the blowdown effluent is valuable at moderate to higher catalyst/column length ratio, and should be utilized rather than discharged. One way to utilize the blowdown effluent is to feed it directly to the adsorbent region of the second column. This alternative is represented as the dash line in the block-flow diagram of the PSAR system (Figure 1.7 in Chapter 1). This alternative suggests that there is perhaps a need to increase the diameter of the adsorbent region in order to take into account the increase in flow rate capacity.

As shown in Figure 3.16, 10 cycles are needed in the simulations in order to reach cyclic steady state conditions. The number of cycles here is not high because the system is isothermal and contains one adsorbable component.

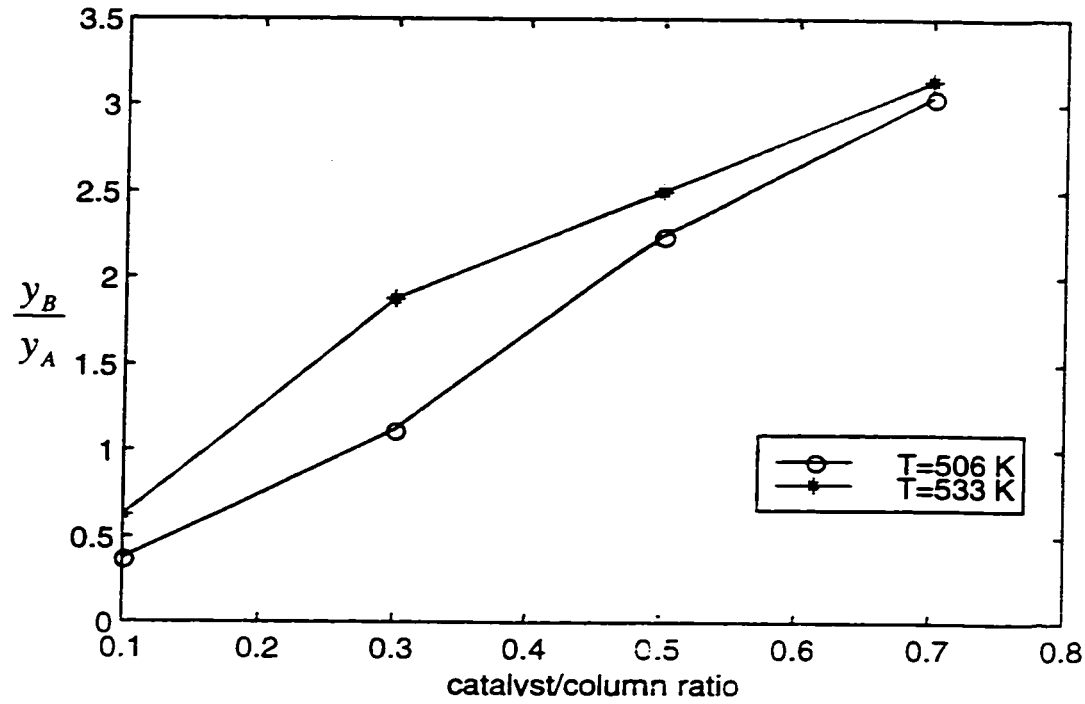


Figure 3.15 Effect of catalyst/adsorbent ratio on the exit concentration of n,i-$C_5$ in the gas phase at the end of blowdown step at cyclic steady state. Parametric values are in Table 3.2.

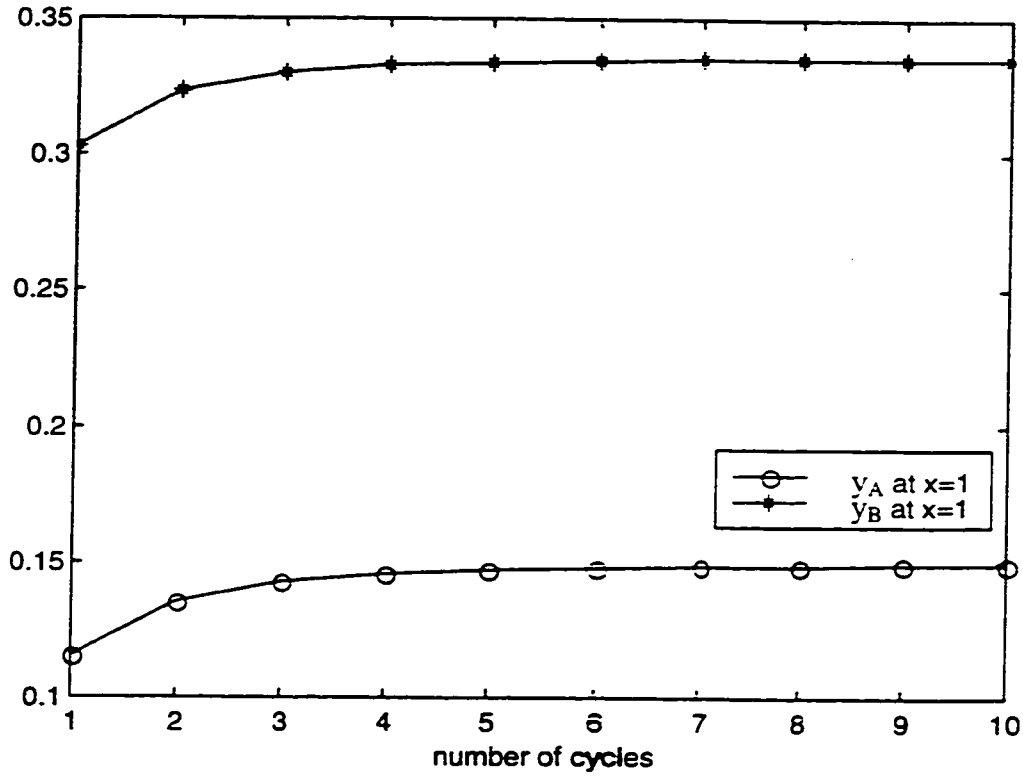


Figure 3.16 Approach to cyclic steady state, showing exit concentration of n-$C_5$ and i-$C_5$ at end of blowdown step. Parametric values are the same as that for Figure 3.11.

Another interesting conclusion can be observed from Figure 3.14. At $\omega$ equals to 0.1, the concentration profiles of the PSAR system are similar to that of the PSA system (Figure 2.12 in chapter 2). Thus, as $\omega$ approaches zero the PSAR model reduces to the PSA model. This indicates that the equations and computer simulation code developed in this chapter are general in the sense that they can be used to solve the PSAR model as will as the base-case PSA model.

### 3.4c COMPARISON WITH THE CONVENTIONAL PROCESS

To compare between the performance of the new PSAR process to that of the conventional process, a set of common parameters are given to both processes. Simulation of the conventional process is carried out by the base-case model, and simulation of the new process is carried out by the PSAR model. The conventional process consists of two columns connected in series (the reactor and the adsorber). For simulations of the conventional process, the effluent concentrations of the packed-bed reactor are determined by solving the steady state reactor model. These effluent concentrations are considered as the feed concentrations for the base-case PSA model. The reactor, the adsorber, and the PSAR unit are all common in length of 1 m. The feed to the reactor and the PSAR unit is fixed at 506 K, with

compositions fixed at 30 mol% n-$C_5$ and 5 mol% i-$C_5$. The reactor pressure is fixed at 15 bar, the high-pressure adsorption step is fixed at 15 bar, and the low-pressure desorption step is fixed at 2 bar. All other physical/chemical properties and parameters that are needed in the simulations are presented in Table 3.1.

A summary of simulation results of the above conventional and PSAR systems is summarized in Table 3.3, showing the effect of the purge/feed velocity ratio on the performance of the two systems. Here, the catalyst/column length ratio is fixed at 0.5 for the PSAR process, while the purge/feed velocity ratio is varied from 5 to 0.5 for both processes. The product purity, which is defined here as the $y_B/(y_A+y_B)$ exit composition ratio at end of step 2, increases as the purge/feed velocity ratio increases until the purge/feed velocity ratio reaches a value of about 3. Further increase of the purge/feed ratio does not affect the purity, where it is almost 100% after that.

A comparison based on the effect of the catalyst/column length ratio, which is denoted as $\omega$, is summarized in Table 3.4. Here, $\omega$ is varied between 0.3 to 0.7 for the PSAR process, while the purge/feed volumetric ratio is fixed at 3 for both processes. The purity is almost 100% for all cases because the purge/feed ratio is high. The yields of i-$C_5$ by both processes are comparable at various values of $\omega$. The concentration of i-$C_5$ in

Table 3.3 Performance comparison between the conventional and PSAR isomerization Processes. [Effect of purge/feed volumetric ratio]. Feed conditions are: T = 506 K, $y_{Af}$ = 0.3, and $y_{Bf}$ = 0.05. Other conditions are: L = 1 m, $P_H$ = 15 bar, and $P_L$ = 2 bar. Dimensionless cycle time is 3 for all steps

| $U_{PF}$ | **PSA** Concentration of high-pressure product stream | | **PSAR** [w = 0.5] Concentration of high-pressure product stream | |
|---|---|---|---|---|
| | mol % n-$C_5$ | mol % i-$C_5$ | mol % n-$C_5$ | mol % i-$C_5$ |
| 5 | 0.00042 | 29.23 | 0.0039 | 28.78 |
| 4 | 0.00045 | 29.22 | 0.0041 | 28.80 |
| 3 | 0.00058 | 29.22 | 0.0046 | 28.79 |
| 2 | 0.120 | 29.23 | 0.251 | 28.78 |
| 1 | 0.863 | 29.20 | 1.07 | 28.68 |
| 0.5 | 2.51 | 29.12 | 2.89 | 28.27 |

Table 3.4 Performance comparison between the conventional and PSAR isomerization Processes. [Effect of catalyst/column length ratio]. All conditions are the same as written above in Table 3.3, except that the purge/feed volumetric ratio is fixed at 3.

| Process | Concentration of high-pressure product stream | |
|---|---|---|
| | mol % n-$C_5$ | mol % i-$C_5$ |
| PSA | 0.00058 | 29.22 |
| PSAR [w=0.3] | 0.0051 | 26.93 |
| PSAR [w=0.5] | 0.0046 | 28.79 |
| PSAR [w=0.7] | 0.0042 | 29.07 |

the product is 29.07 mol% by the PSAR process with $\omega$ equal to 0.7, a value very close to a value of 29.22 mol% obtained by the conventional process.

The above example demonstrated that the new compact PSAR process is effective for total isomerization of n-pentane. Despite the fact that one column and all its auxiliary equipment such as valves and piping are reduced from the conventional process, The technical specifications of the product are still satisfied. The product yield and purity are comparable to that of the conventional process.

For the conventional process, the purge stream contains a high content of n-$C_5$. It is usually compressed and recycled back to the reactor, as shown in Figure 1.2. However, this point was not considered in the above example to simplify the simulations. On the other hand, the purge stream for the PSAR process contains a high content of i-$C_5$. Thus, it is better not to recycle and combine it with the fresh feed. Alternatively, the purge stream from the low-pressure column could be injected directly to the adsorbent bed in the adjacent high-pressure column. By this way the overall yield of the isomers could be increased. This point will be studied in more detail in the future. For the above comparison, however, the purge stream is considered as a waste stream for both processes.

As shown in Tables 3.3 and 3.4, the product contains approximately 29 mol% i-$C_5$ and 71 mol% $H_2$, for a fresh feed consisting of 30% n-$C_5$/5% i-$C_5$/65% $H_2$. As shown in Figures 1.2 and 1.7 in Chapter 1, this product mixture is fed to a flash drum to complete the separation. In order to get a 99 mol% i-$C_5$ product stream and a 95 mol% $H_2$ recycled stream, the flashing temperature should be about 62 $^0$F if the flash drum operates at a high pressure of 15 bar. If it is required not to lower the flashing temperature below 100 $^0$F, the purity of the $H_2$ recycled stream and the i-$C_5$ product stream will be about 90% and 99%, respectively, keeping the other conditions unchanged. These calculations of flashing temperatures are obtained by applying HYSYS, a process simulation software. It is better to keep the pressure of the flash drum the same as that of the high-pressure adsorption column, so that there will be no need to compress the portion of the recycled $H_2$ stream that is combined with the fresh feed, which should be fed at high pressure. Also, it is not desirable to lower the temperature below 100 $^0$F because this will add additional refrigeration cost to the total cost.

# Nomenclature

| | |
|---|---|
| $C_T$ | dimensionless total gas concentration [mol/cm$^3$] |
| $Da_t$ | true Damköhler number [-] = $\omega \frac{k_1 L}{u_f}$ |
| $D_L$ | axial mass dispersion coefficient [cm$^2$/s] |
| $D_A$ | pore diffusivity of component A [cm$^2$/s] |
| $k_1$ | forward reaction rate constant [cm$^3$/g of cat/s] |
| $K_{ads}$ | adsorption equilibrium constant [bar$^{-1}$] |
| $k_{gl}$ | global mass-transfer coefficient [cm/s] |
| $K_C$ | equilibrium reaction rate constant [-] |
| $L$ | length of the PSAR column [cm] |
| $n$ | coefficient of Nitta et al. isotherm [-] |
| $N_f$ | number of film mass-transfer units [-] |
| $Pe$ | mass Peclet number [-] |
| $P$ | total pressure [bar] |
| $P_H$ | constant high pressure during adsorption step [bar] |
| $P_L$ | constant low pressure during desorption step [bar] |
| $Q_A$ | dimensionless adsorbed-phase concentration [-] |
| $t$ | time [s] |
| $T$ | gas temperature [K] |
| $u$ | interstitial velocity [cm/s] |
| $u_f$ | interstitial feed velocity [cm/s] |
| $U_i$ | dimensionless interstitial velocity in bed i [-] |
| $u_p$ | purge gas velocity [cm/s] |
| $x$ | dimensionless axial coordinate in the column [-] |
| $y_{Af}$ | mole fraction of component A in the feed [-] |
| $y_{Aj}$ | mole fraction of component A in the bulk phase in bed i [-] |
| $y_{Bf}$ | mole fraction of component B in the feed [-] |
| $y_{Bj}$ | mole fraction of component B in the bulk phase in bed i [-] |
| $\langle y_{A2} \rangle$ | average mole fraction of the sorbate in the pores of the adsorbent pellet in bed 2 [-] |
| $y_{A,eq}$ | equilibrium mole fraction of component A for isomerization reaction [-] |

| | |
|---|---|
| $y_{AL}$ | mole fraction of component A at the exit of the column [-] |

*Greek Letters*

| | |
|---|---|
| $\nu_1$ | dimensionless axial coordinate in the catalyst-bed region [-] |
| $\nu_2$ | dimensionless axial coordinate in the adsorbent-bed region [-] |
| $\omega$ | fraction of the total length that is catalyst bed [-] |
| $\zeta_m$ | mass capacity factor [-] |
| $\theta_{ref}$ | coverage of adsorbent at $y_{Af}$ and $P_H$ [-] |
| $\tau$ | dimensionless time [-] |

*Subscripts*

| | |
|---|---|
| A | n-pentane |
| B | isopentane |
| I | hydrogen |
| T | total |
| f | feed |
| i | bed 1 (catalyst bed) or 2 (adsorbent bed) |

# CHAPTER 4

# HEAT EFFECT IN PSA SYSTEM & ITS RELEVANCE TO PSAR SIMULATIONS

Local temperature fluctuations in the adsorbent bed due to the exothermic heat of adsorption and the endothermic heat of desorption always exist in the PSA cycle. Depending on the magnitude of the temperature fluctuations, this may significantly reduce the efficiency of separation. The magnitude depends primarily on the heat of adsorption, the throughput, and the heat transfer characteristics of the packed adsorber column. In this chapter simulations of the PSA system are accomplished for the nonisothermal model and the results obtained are compared with those predicted by the isothermal model and presented in chapter 2. The system contains three components (n,i-/$C_5$/$H_2$).

## 4.1 MODEL ASSUMPTIONS AND EQUATIONS

All assumptions stated in Chapter 2 are retained here except that the isothermal condition for the adsorbent bed is relaxed. The additional

assumptions needed to allow for nonisothermal PSA operation are summarized below:

1) The adsorption equilibrium constant is the most sensitive temperature-dependent term, and is assumed to follow the normal exponential temperature dependence ($K_{ads} = K_c \exp[(-\Delta H_{ads})/RT)]$).

2) Effective thermal conductivities of commercial adsorbents are relatively high, and therefore intraparticle temperature gradients can be neglected [47,64].

3) Thermal equilibrium is assumed to exist between the fluid and the adsorbent particles. According to Ruthven and co-workers, this is a very common practical assumption in adsorber calculations [47]. This reduces the computational effort to a large extent since an energy balance for the solid phase is not required.

4) An overall heat transfer coefficient is used to account for heat loss from the system to the surroundings.

5) The temperature of the column wall is taken to be equal to that of the feed temperature.

6) The boundary conditions for the heat balance equation are written assuming the heat-mass transfer analogy for a dispersed plug flow system.

Subject to the above assumptions and following the same nomenclature as in Chapter 2, the additional equations for nonisothermal PSA simulations are:

Fluid phase heat balance is

$$-K_L\frac{\partial^2 T}{\partial z^2}+C_{pg}c_T\frac{\partial}{\partial z}(uT)+[C_{pg}c_T+(\frac{1-\varepsilon}{\varepsilon})C_{ps}\rho_s]\frac{\partial T}{\partial t}$$

$$-(-\Delta H_{ads})(\frac{1-\varepsilon}{\varepsilon})\rho_s\frac{\partial\langle q_A\rangle}{\partial t}+\frac{4h}{d_c\varepsilon}(T-T_w)=0 \qquad (4.1)$$

The boundary conditions for pressurization, adsorption, and desorption steps are

$$-K_L\frac{\partial T}{\partial z}\Big|_{z=0}=u\Big|_{z=0}C_{pg}c_T(T_f-T) \qquad (4.2a)$$

$$\frac{\partial T}{\partial z}\Big|_{z=L}=0 \qquad (4.2b)$$

Boundary conditions for blowdown step are

$$\frac{\partial T}{\partial z}\Big|_{z=0}=0 \qquad (4.3a)$$

$$\frac{\partial T}{\partial z}\Big|_{z=L}=0 \qquad (4.3b)$$

The initial condition is

$$T(z,t=0)=T_f \qquad (4.4)$$

The above set of equations are written in normalized form using the following dimensionless variables and parameters, in addition to those

defined in chapter 2:

Dimensionless gas temperature: $$\overline{T} = \frac{T - T_f}{T_f}$$

Thermal Peclet number: $$Pe_H = \frac{u_f L C_{pg} c_{Tf}}{K_L}$$

Thermal capacity factor: $$\zeta_H = \frac{1-\varepsilon}{\varepsilon}\frac{\rho_s C_{ps}}{C_{pg} c_{Tf}}$$

Number of wall heat-transfer units: $$N_w = \frac{4hL}{d_c u_f C_{pg} c_{Tf} \varepsilon}$$

Adiabatic temperature rise: $$B = \frac{(-\Delta H_{ads}) q_{A.ref}}{C_{ps} T_f}$$

Dimensionless heat of adsorption: $$\gamma_f = \frac{(-\Delta H_{ads})}{RT_f} \qquad (4.5)$$

Thus, the fluid phase heat balance equation become

$$\frac{\partial \overline{T}}{\partial \tau} = \frac{1}{Pe_H (C_T + \zeta_H)}\frac{\partial^2 \overline{T}}{\partial x^2} - \frac{C_T}{(C_T + \zeta_H)}\frac{\partial}{\partial x}[U(\overline{T}+1)] + \frac{B\zeta_H}{(C_T + \zeta_H)}\frac{\partial Q_A}{\partial \tau} - \frac{N_w}{(C_T + \zeta_H)}\overline{T} \qquad (4.6)$$

The boundary conditions for pressurization, adsorption, and desorption steps are

$$-\frac{1}{Pe_H}\frac{\partial \overline{T}}{\partial x}\Big|_{x=0} = U\Big|_{x=0} C_T \overline{T} \qquad (4.7a)$$

$$\frac{\partial \overline{T}}{\partial x}\Big|_{x=1} = 0 \qquad (4.7b)$$

Boundary conditions for blowdown step are

$$\frac{\partial \overline{T}}{\partial x}\Big|_{x=0} = 0 \tag{4.8a}$$

$$\frac{\partial \overline{T}}{\partial x}\Big|_{x=1} = 0 \tag{4.8b}$$

The initial condition is

$$\overline{T}(x, \tau = 0) = 0 \tag{4.9}$$

The numerical solution of the set of coupled equations 4.6-4.9 for this chapter combined with equations 2.42-2.66 in Chapter 2 gives gas and solid concentration and the bed temperature at several locations in the column for various values of time. Twenty internal collocation points are used.

## 4.2 HEAT PARAMETER ESTIMATIONS

The effective axial bed thermal conductivity ($K_L$) and the overall heat transfer coefficient (h) can be estimated from the method suggested by Wakao and Kaguei [62]. Estimation by these methods requires the thermal properties of 5A zeolite. The heat capacity of 5A zeolite is 0.9 J/(g.K) as published by Breck [7]. However, the thermal conductivity of 5A zeolite is not available and may need to be determined experimentally. Thus, for the present situation, the values used by Silva and Rodrigues for a similar system [54] will be used here. Parameter values of the nonisothermal model are summarized in Table 4.1.

## 4.3 RESULTS AND DISCUSSION

In order to investigate the effect of heat on PSA separation, work is first begun by considering a feed with high sorbate concentration. This is because bulk separation is more affected by temperature fluctuation than purification processes, and hence the effect can by visualized more clearly for bulk separation systems. Thus, a feed with 34% n-pentane is first considered. Then, a system with 17% n-pentane feed, which is the system considered in Chapter 2, is simulated.

One advantage of using the one-dimensional heat transfer model presented in equation 4.1, beside its simplicity in numerical formulation, is that the system behavior at the isothermal and adiabatic limits may be very easily investigated by assigning a very large value and zero, respectively, to the overall heat transfer coefficient. Reducing the model to its asymptotes is a common and practical tool to test the logic of the model and the program. This practice is applied here for some simulation runs.

### 4.3a FIXED-BED ADSORPTION

Figure 4.1 demonstrates the breakthrough curves of the n-$C_5$/5A-zeolite system predicted by both the nonadiabatic and adiabatic nonisothermal models. Prediction by the isothermal model is also shown for comparison.

Table 4.1 Parametric values used for predictions of the breakthrough curves of the n,i-$C_5/H_2$ System by the nonisothermal model. All other parameters needed in the simulations are presented in Table 3.1

| Parameter | Figures 4.1 | Figures 4.2 |
|---|---|---|
| $y_{Af} = y_{Bf}$ | 0.34 | 0.17 |
| $T_f$ (K) | 506 | 506 |
| $K_L$ (W/m.K) | 1.0 | 1.0 |
| h ($W/m^2.K$) | 20 | 20 |
| $C_{ps}$ (J/(g.K)) | 0.9 | 0.9 |
| $C_{pg}$ (J/(mol.K)) | 82.06 | 82.06 |
| $Pe_H$ | 7.67 | 7.67 |
| $\zeta_H$ | 74 | 74 |
| $N_w$ | 48.67 | 48.67 |
| $B$ | 0.117 | 0.117 |
| $\theta_{ref}$ | 0.591 | 0.539 |
| $\gamma_f$ | 13.1 | 13.1 |

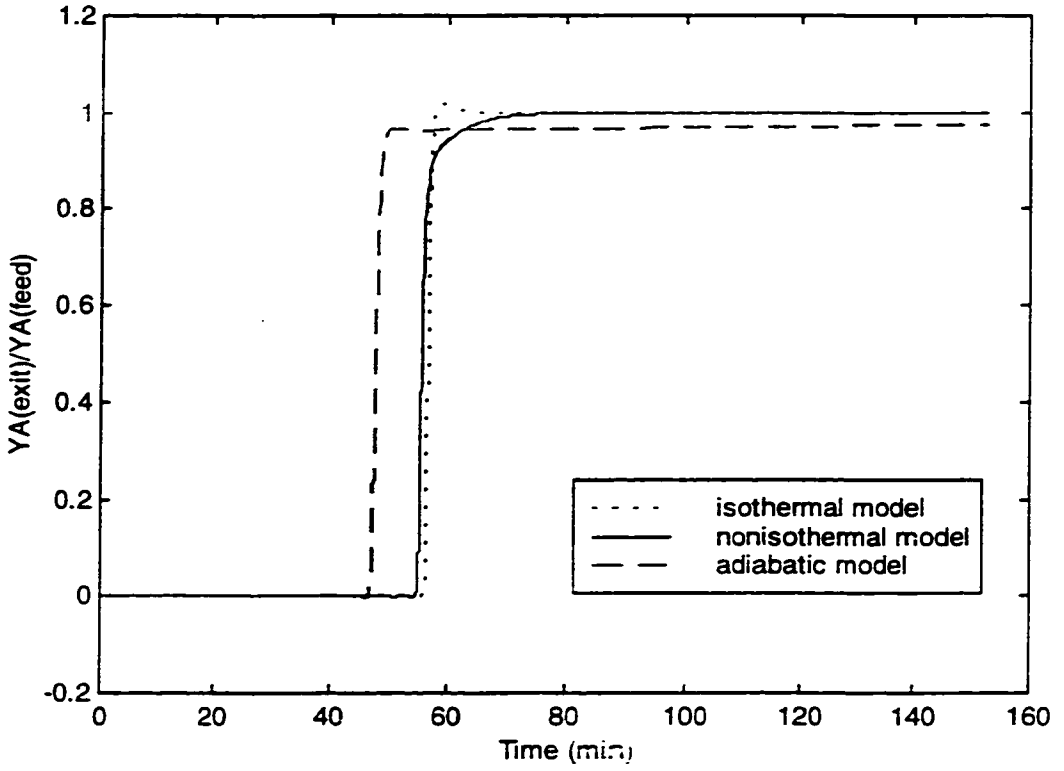


Figure 4.1 Prediction of breakthrough curves for the 34 mol% n-$C_5$ system for different thermal specification. Parametric values are in Table 4.1.

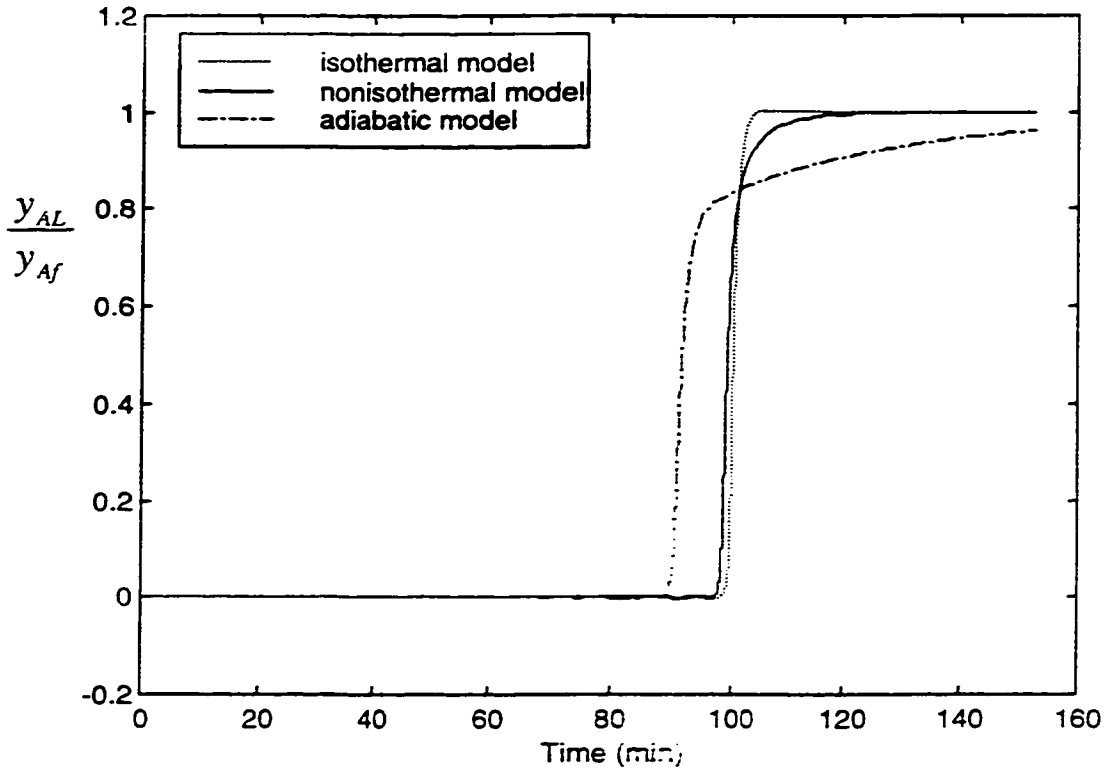


Figure 4.2 Prediction of breakthrough curves for the 17 mol% n-$C_5$ system for different thermal specification. Parametric values are in Table 4.1.

The feed contains 34 mol% n-$C_5$ and is at 506 K. As shown in the Figure, the breakthrough points predicted by the nonisothermal model is earlier than the one predicted by the isothermal model. The difference is not high because a high value of the heat transfer coefficient is used in the simulations (h = 20 $W/m^2$-s). However, the column breakthrough for the adiabatic system is earlier than that for the isothermal system by about 15 minutes. This indicates that operating the PSA system under adiabatic situation should be avoided since it will lead to the worst effect on separation performance.

The above simulation runs are repeated but for a feed containing 17 mol % n-$C_5$, and the results are shown in Figure 4.2. A similar trend is observed as in the previous case, with two differences to be noticed. The relative difference in breakthrough points predicted by the isothermal and adiabatic models, defined as (prediction by the isothermal model-prediction by the adiabatic model)/prediction by the isothermal model, is about 25% for the 34% n-$C_5$ system, while it is about 10% for the 17% n-$C_5$ system. Also, the column for the 34% n-$C_5$ system operating under adiabatic condition breakthroughs after 45 minutes of operation, while for the 17% n-$C_5$ system it breakthroughs after 85 minutes. Usually the cycle time for the PSA process is designed in such a way that it is much lower than the breakthrough

limit. Thus, it can be stated that heat effect is more important for a system containing 30 mol% of n-$C_5$ or higher.

### 4.3b PSA CYCLIC PROCESS

Figure 4.3 demonstrates bed temperature profiles at the cyclic steady state (~ 15 cycles) and at the end of the four basic steps using the parametric values in Table 4.2. The concentration profiles of n-$C_5$ and i-$C_5$ in the gas phase are shown in Figures 4.4 and 4.5, respectively. The feed contains 34 mol% of n-pentane and is at a temperature of 506 K. All other operating conditions are the same as summarized in Table 2.5 in Chapter 2. For the purpose of comparison, concentration profiles are also generated by the isothermal model developed in Chapter 2, and the results are shown in Figures 4.6.

As shown in Figure 4.3, temperature increases above the feed temperature during the adsorption step and decreases below the feed temperature during the desorption step. This is due to the exothermic nature of adsorption and the endothermic nature of desorption. A temperature wave of about 30 °C exists in the column. The effect of temperature rise during adsorption is to push the concentration profiles further downward in the column relatively to the isothermal case, resulting in breakthrough occurring

Table 4.2 Parametric values used for simulations of the nonisothermal PSA system. All other parameters needed in the simulation are the same as summarized in Table 2.5

| Parameter | Figures 4.3 to 4.5 | Figures 4.7 to 4.9 | Figures 4.10 to 4.12 |
|---|---|---|---|
| $y_{Af} = y_{Bf}$ | 0.34 | 0.34 | 0.34 |
| $T_f$ (K) | 506 | 506 | 506 |
| $K_L$ (W/m.K) | 1.0 | 1.0 | 1.0 |
| h ($W/m^2.K$) | 20 | 0 (adiabatic) | $10^6$ (isothermal) |
| $C_{ps}$ (J/(g.K)) | 0.9 | 0.9 | 0.9 |
| $C_{pg}$ (J/(mol.K)) | 82.06 | 82.06 | 82.06 |
| $Pe_H$ | 7.67 | 7.67 | 7.67 |
| $\zeta_H$ | 74 | 74 | 74 |
| $N_w$ | 48.67 | 0 | $2.4 \times 10^6$ |
| $B$ | 0.117 | 0.117 | 0.117 |
| $\theta_{ref}$ | 0.591 | 0.591 | 0.591 |
| $\gamma_f$ | 13.1 | 13.1 | 13.1 |

Table 4.2 Parametric values used for simulations of the nonisothermal PSA system (continued)

| Parameter | Figures 4.13 to 4.14 | Figures 4.15 to 4.16 | Figures 4.17 to 4.18 |
|---|---|---|---|
| $y_{Af} = y_{Bf}$ | 0.17 | 0.17 | 0.17 |
| $T_f$ (K) | 506 | 506 | 506 |
| $K_L$ (W/m.K) | 1.0 | 1.0 | 0.35 |
| h ($W/m^2.K$) | 0 (adiabatic) | 20 | 20 |
| $C_{ps}$ (J/(g.K)) | 0.9 | 0.9 | 0.9 |
| $C_{pg}$ (J/(mol.K)) | 82.06 | 82.06 | 82.06 |
| $Pe_H$ | 7.67 | 7.67 | 21.9 |
| $\zeta_H$ | 74 | 74 | 74 |
| $N_w$ | 0 | 48.67 | 48.67 |
| $B$ | 0.117 | 0.117 | 0.117 |
| $\theta_{ref}$ | 0.539 | 0.539 | 0.539 |
| $\gamma_f$ | 13.1 | 13.1 | 13.1 |

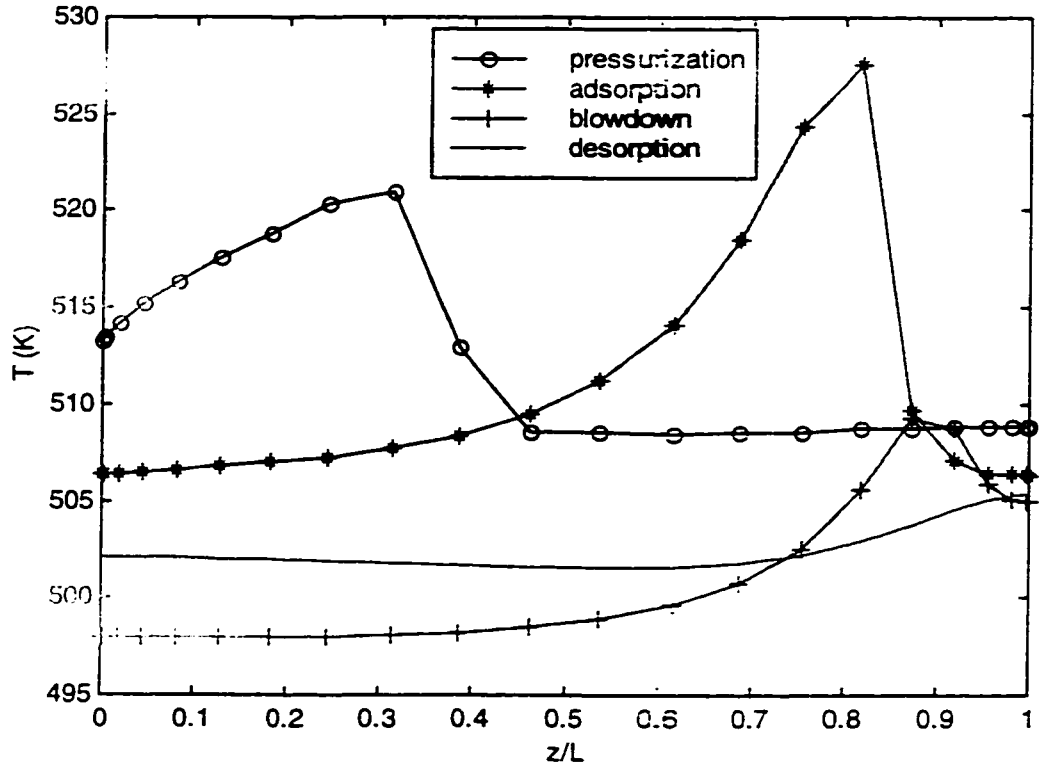


Figure 4.3 Temperature profiles in the bed at the end of cyclic steady state. (h = 20 W/m$^2$.K). Parametric values are in Table 4.2.

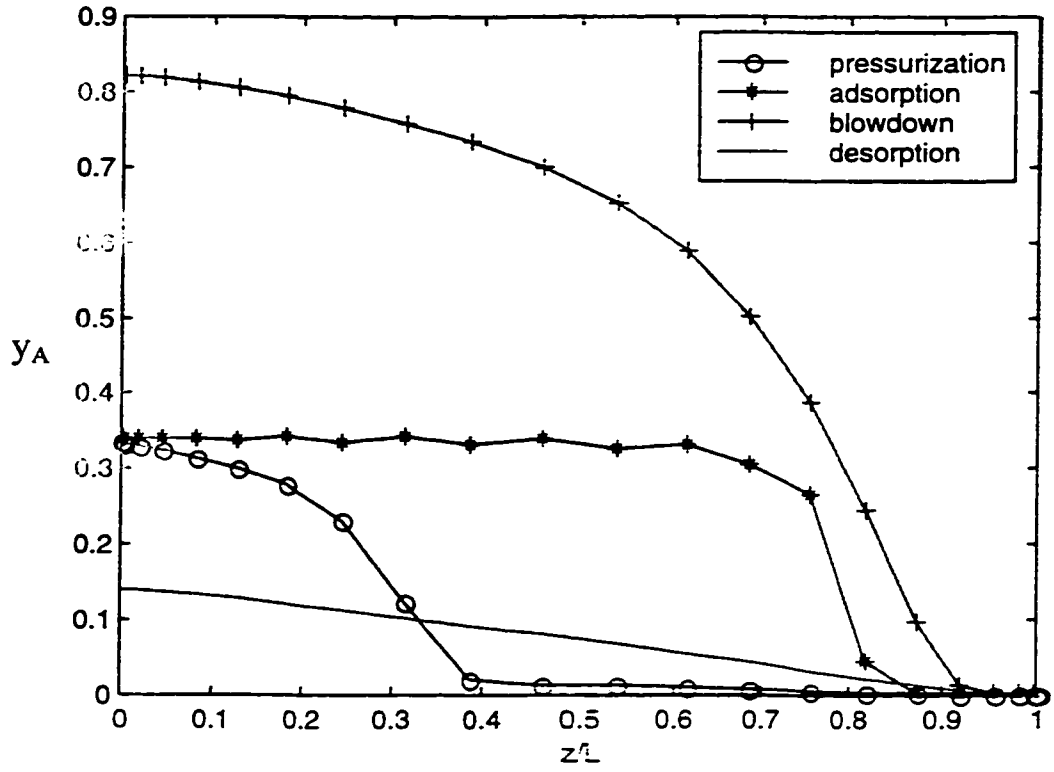


Figure 4.4 Gas phase concentration profiles of n-$C_5$ in the bed at the end of cyclic steady state. (h = 20 W/m$^2$.K). Parametric values are in Table 4.2.

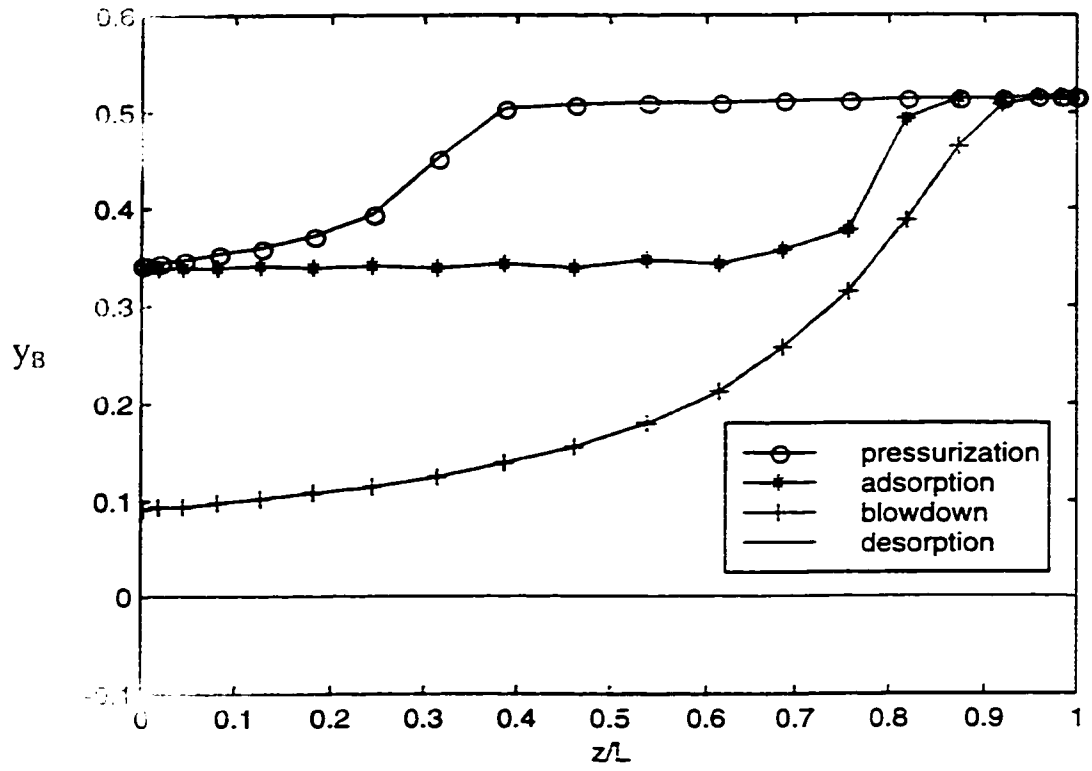


Figure 4.5 Gas phase concentration profiles of i-$C_5$ in the bed at the end of cyclic steady state. (h = 20 W/m$^2$.K). Parametric values are in Table 4.2.

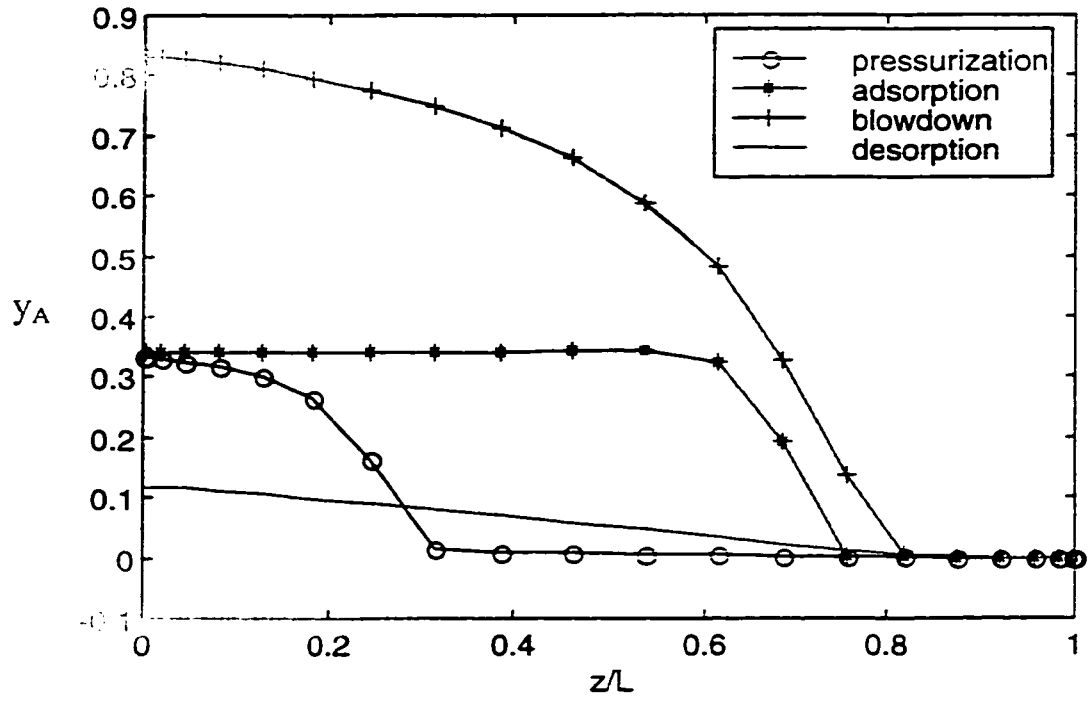


Figure 4.6 Gas phase concentration profiles of n-$C_5$ in the bed at the end of cyclic steady state. (generated by the isothermal model developed in chapter 2). Parametric values are in Table 4.2.

sooner and lowering the PSA performance. This can be seen by comparing Figures 4.6 with 4.4, where the n-$C_5$ concentration wave has moved 14% further down the column.

The largest temperature fluctuation of about 60 $^0$C exists in the column under adiabatic condition, as shown in Figure 4.7. This has the worst effect on separation. To approach the isothermal condition, the simulation is carried out with h equal to $10^6$ W/m$^2$.K, and the results are shown in Figures 4.10 to 4.12. The temperature profiles are constant and equal to the feed temperature of 506 K, as shown in Figure 4.10. The concentration profiles of n-$C_5$ and i-$C_5$ are essentially the same as that generated by the isothermal model developed in Chapter 2, as can be seen by comparing Figure 4.11 with Figure 4.6.

The same simulation runs discussed above are repeated for a feed containing less amount of sorbate (17 mol %), and the results are shown in Figures 4.13 to 4.18. Temperature fluctuations of about 50 and 20 °C exist in the column under adiabatic and nonadiabatic (h=20 W/m$^2$ K) conditions, respectively. However, these temperature fluctuations does not affect the concentration profiles very much as shown in Figures 4.14 and 4.16, which are very similar to those generated by the isothermal model and illustrated in Figure 2.12.

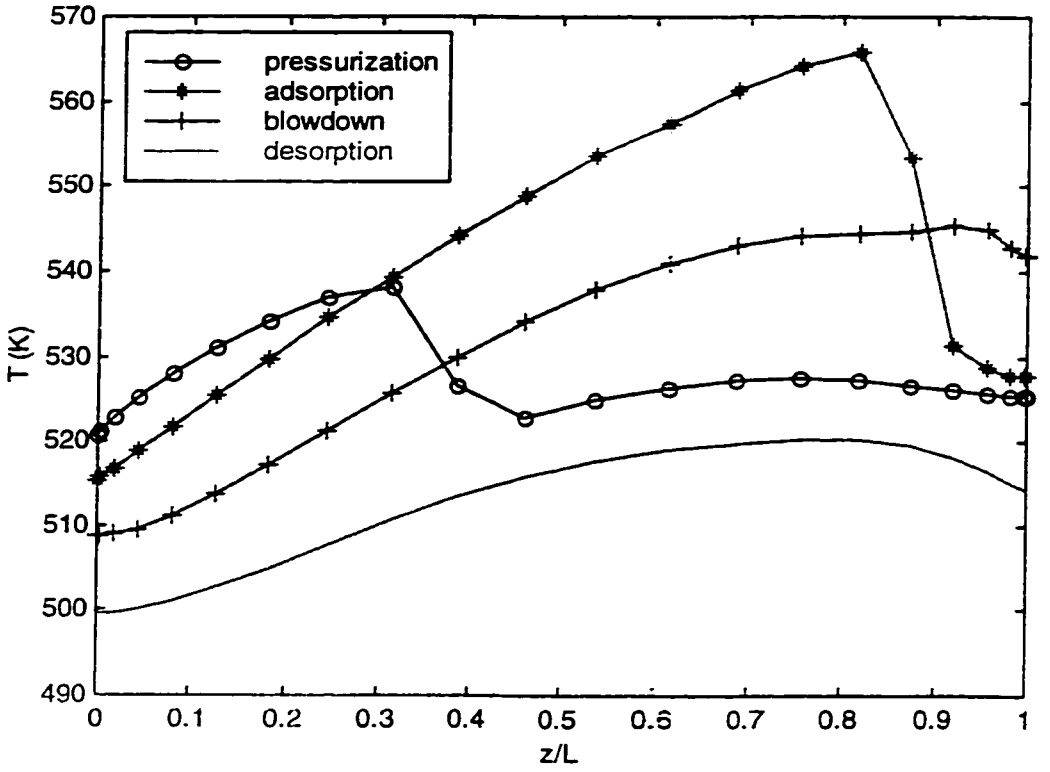


Figure 4.7 Temperature profiles in the bed at the end of cyclic steady state. ($h = 0$ W/m$^2$.K). Parametric values are in Table 4.2.

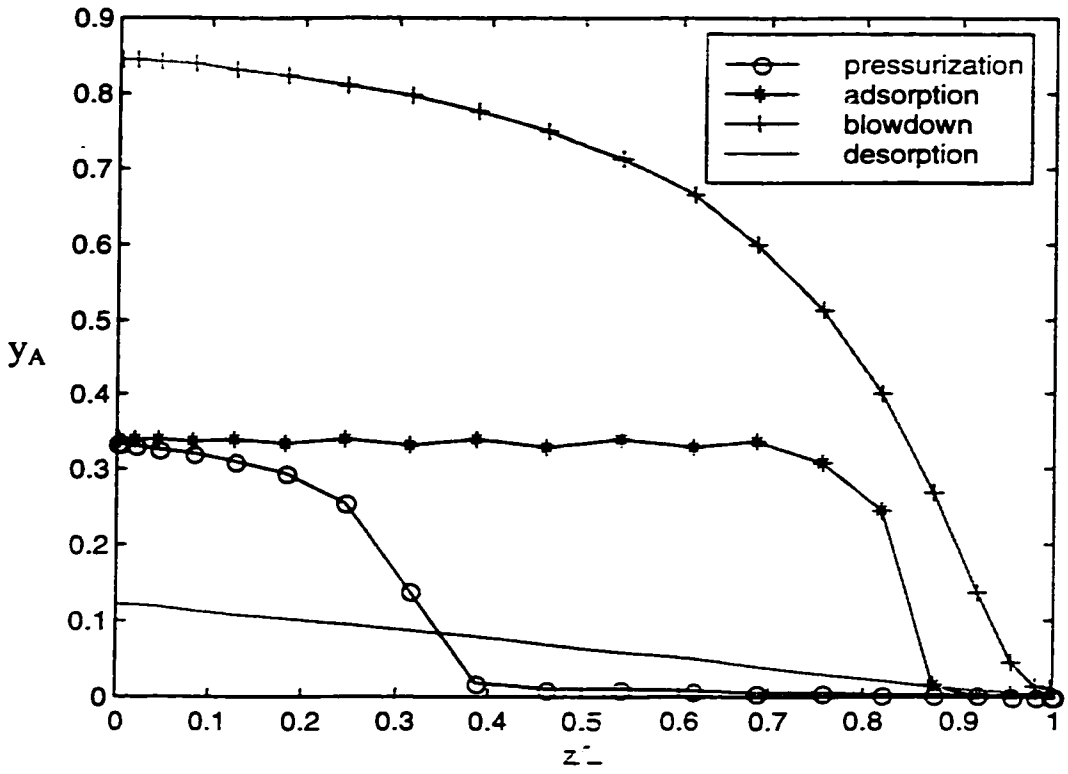


Figure 4.8 Gas phase concentration profiles of n-$C_5$ in the bed at the end of cyclic steady state. (h = 0 W/$m^2$.K). Parametric values are in Table 4.2.

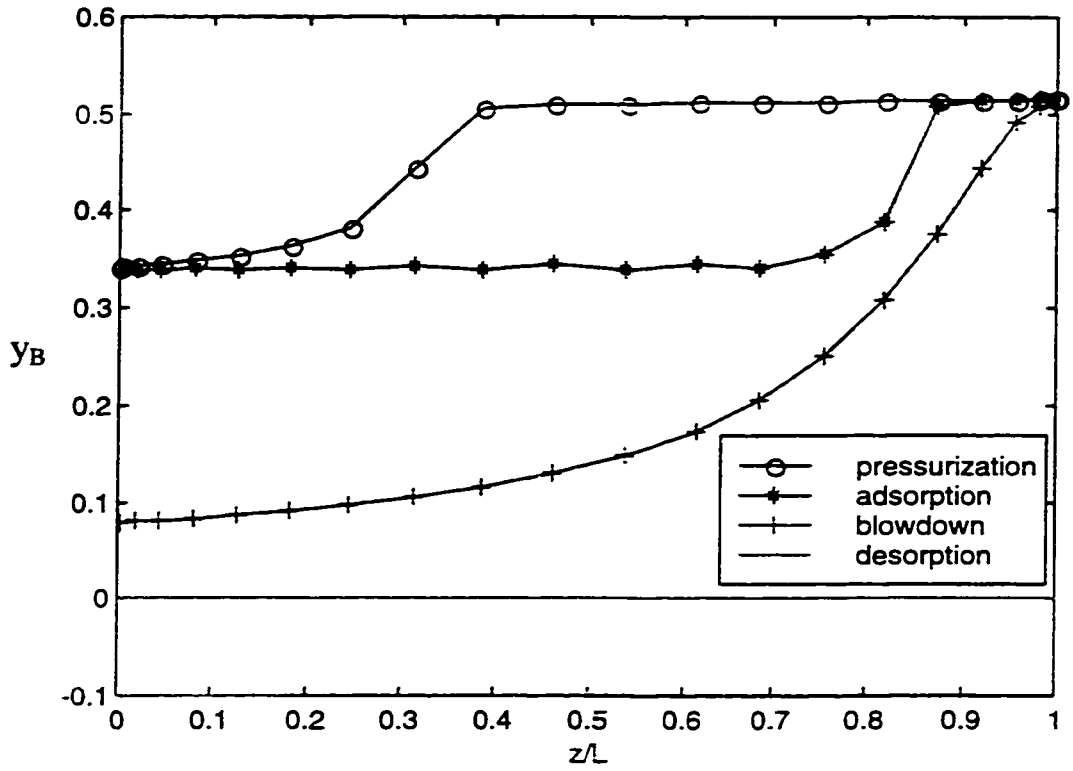


Figure 4.9 Gas phase concentration profiles of i-$C_5$ in the bed at the end of cyclic steady state. (h = 0 W/m$^2$.K). Parametric values are in Table 4.2.

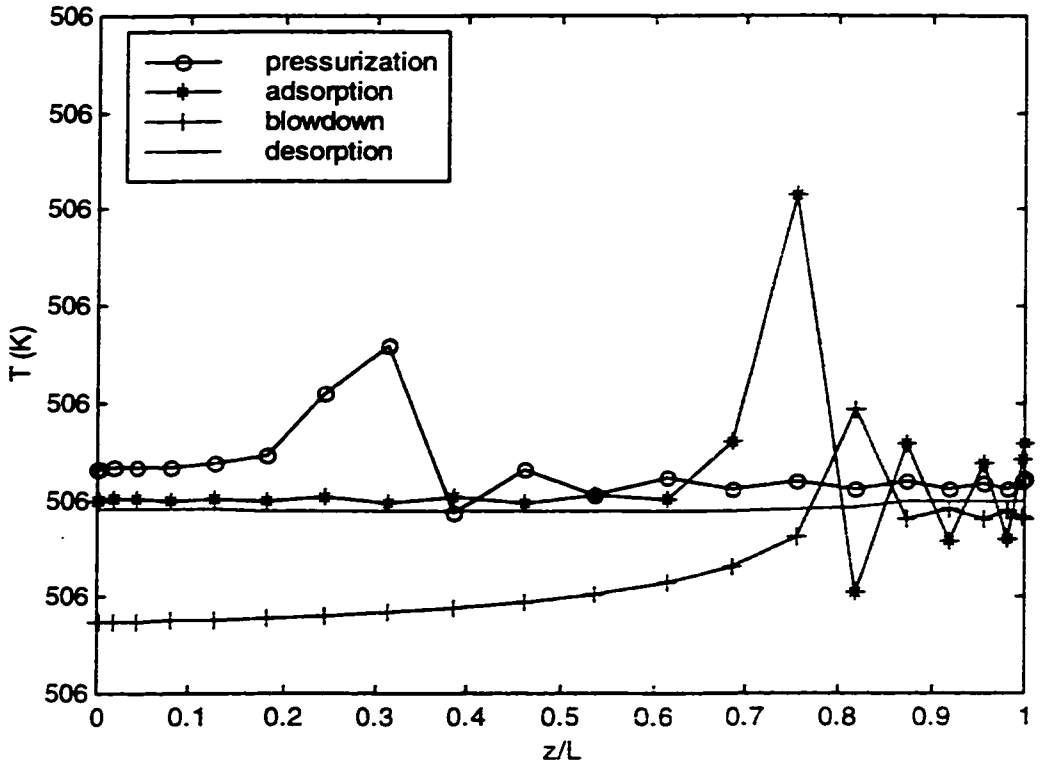


Figure 4.10 Temperature profiles of n-$C_5$ in the bed at the end of cyclic steady state. (h = $10^6$ W/$m^2$.K). Parametric values are in Table 4.2. Note that the y-axis only varies in the $5^{th}$ or $6^{th}$ significant figure.

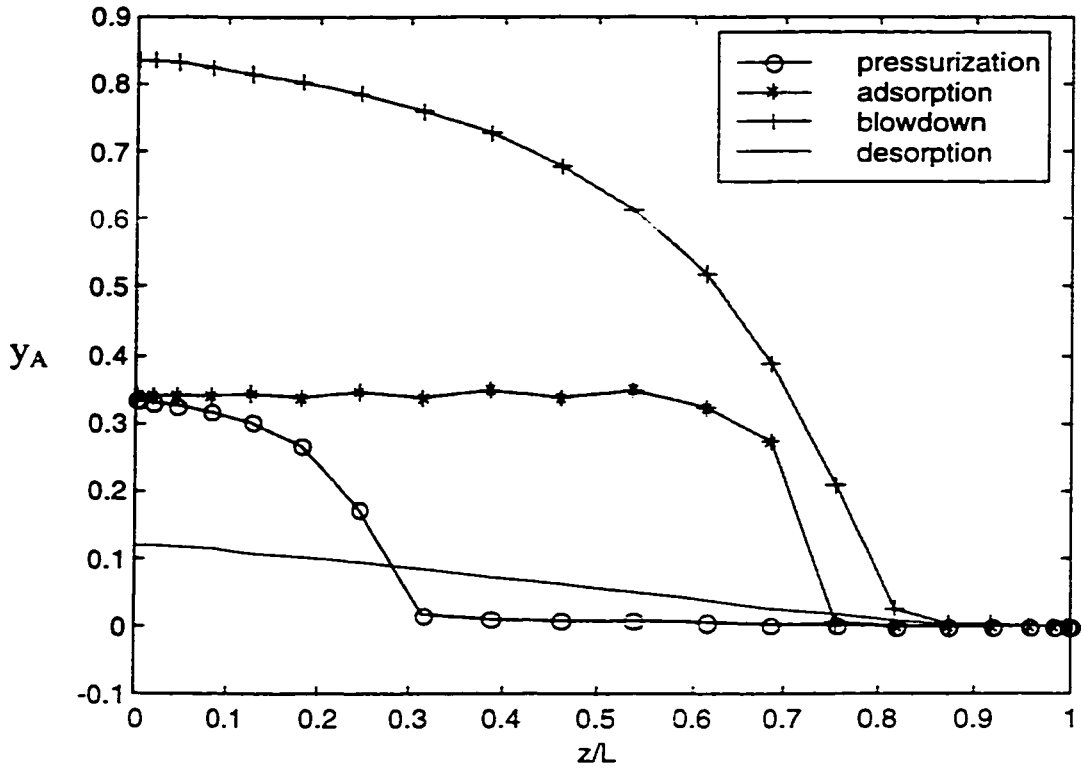


Figure 4.11 Gas phase concentration profiles of n-$C_5$ in the bed at the end of cyclic steady state. (h = $10^6$ W/$m^2$.K). Parametric values are in Table 4.2.

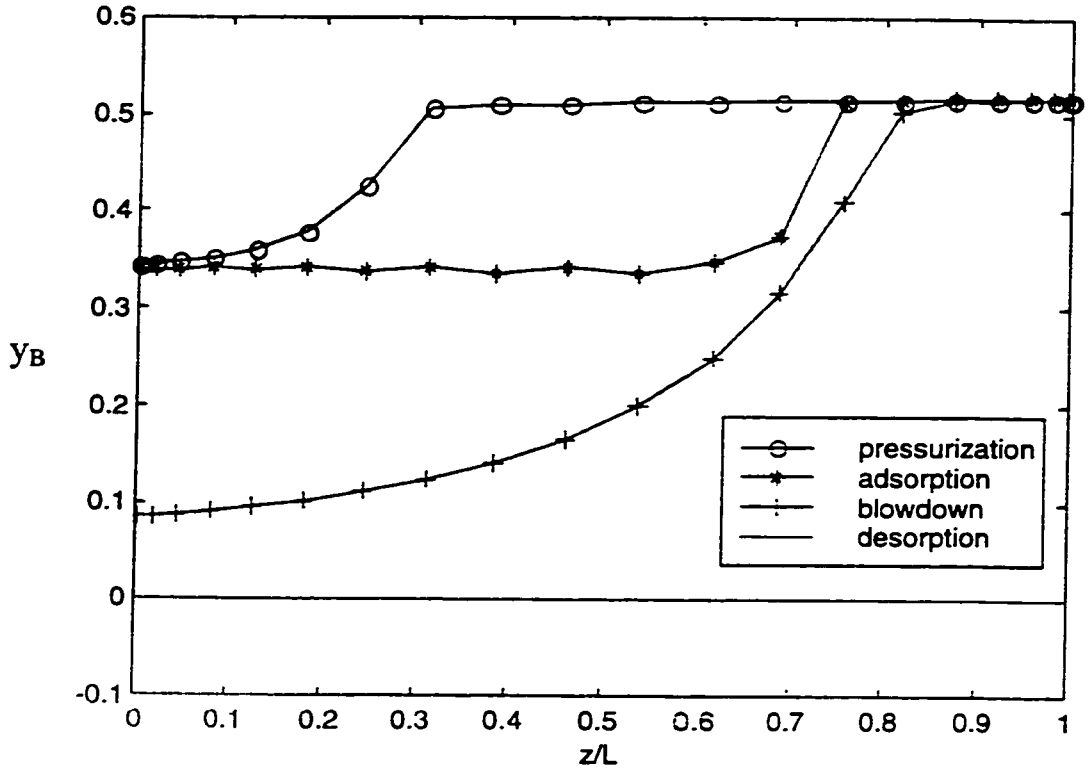


Figure 4.12 Gas phase concentration profiles of i-$C_5$ in the bed at the end of cyclic steady state. (h = $10^6$ W/m$^2$.K). Parametric values are in Table 4.2.

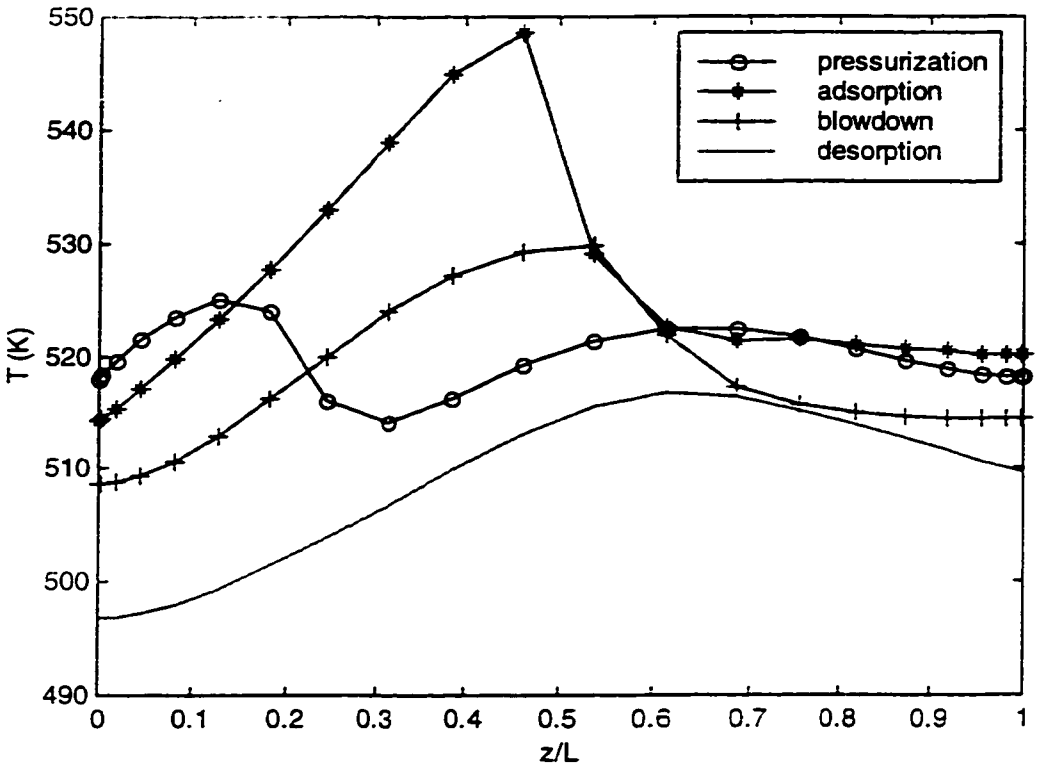


Figure 4.13 Temperature profiles in the bed at the end of cyclic steady state. ($y_{Af} = 0.17$; $h = 0$ W/m$^2$.K). Parametric values are in Table 4.2.

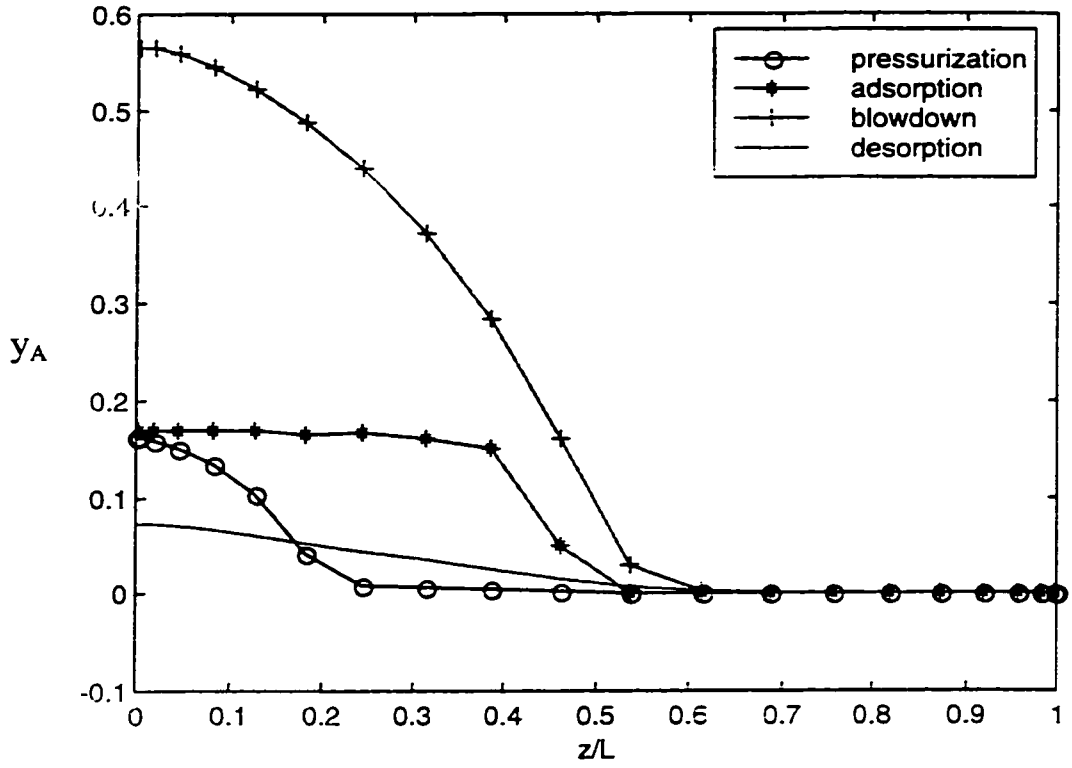


Figure 4.14 Gas phase concentration profiles of n-$C_5$ in the bed at the end of cyclic steady state. ($y_{Af}$ = 0.17; h = 0 W/m$^2$.K). Parametric values are in Table 4.2.

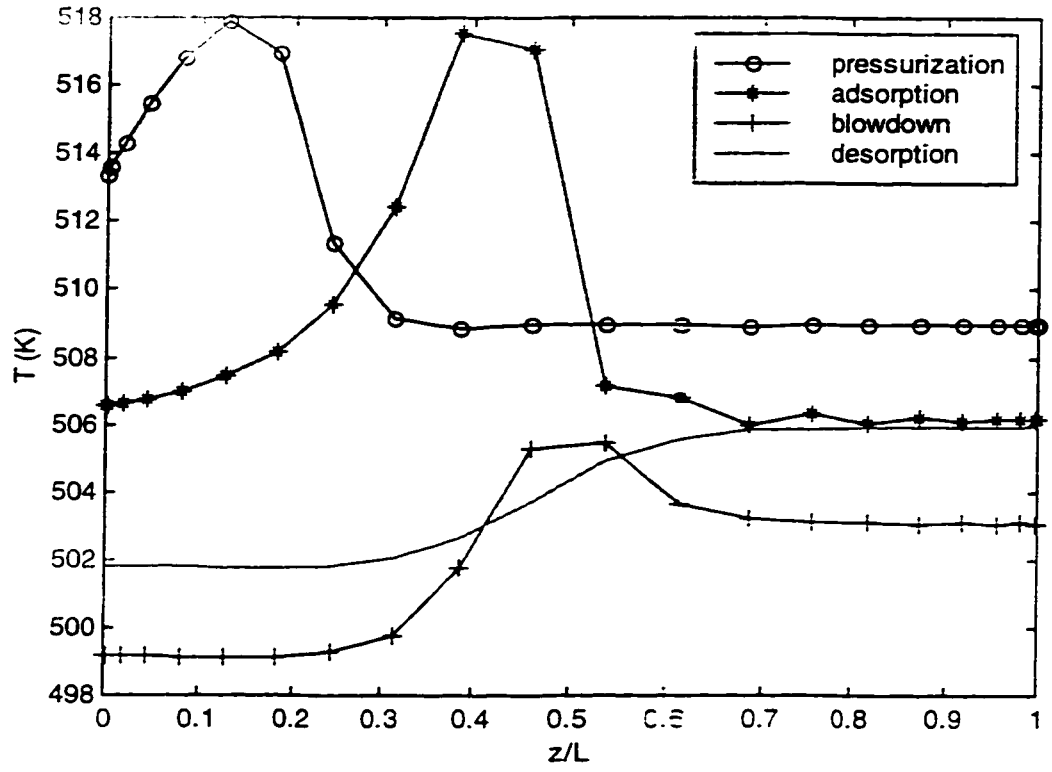


Figure 4.15 Temperature profiles in the bed at the end of cyclic steady state. ($y_{Af}$ = 0.17; h = 20 W/m$^2$.K). Parametric values are in Table 4.2.

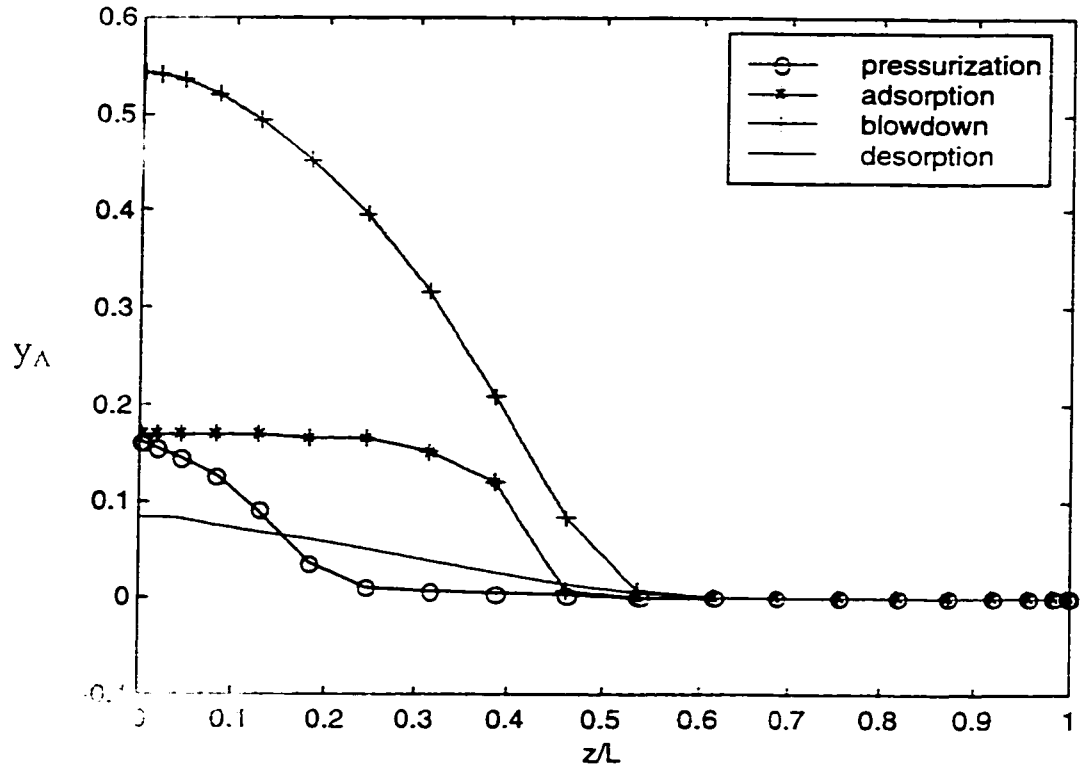


Figure 4.16 Gas phase concentration profiles of n-$C_5$ in the bed at the end of cyclic steady state. ($y_{Af}$ = 0.17; h = 20 W/m$^2$.K). Parametric values are in Table 4.2.

Simulation of the previous system is conducted with $K_L$, the axial thermal conductivity, equal to 1.0 W/m.K. To see the importance of the accuracy of $K_L$ on the accuracy of the results, the simulations are repeated for the same system with $K_L$ equal to 0.35 W/m.K. Practically, there is no effect on the temperature and concentration profiles, as shown in Figures 4.17 and 4.18.

From the above results and discussion, it can be seen that heat effect is important for the n-$C_5$ /PSA system containing above 30 mol% in the feed. In order to simulate the real situation, the nonisothermal model should be used instead of the isothermal model. For a system containing less than 15 mol% of n-$C_5$ in the feed, the isothermal model can be used as an acceptable approximation model.

Several methods have been suggested to achieve a nearly isothermal operation and thereby improve the separation. This can be achieved by working with very short cycles, small throughput ratio and small column diameter [48]. Internal heating of the cold region in the bed by using inserted heaters has been suggested by Collins for air separation [14]. The improvement can be achieved also by allowing heat exchange between adsorbers or by introducing high heat capacity inert additives, as proposed by Yang [64].

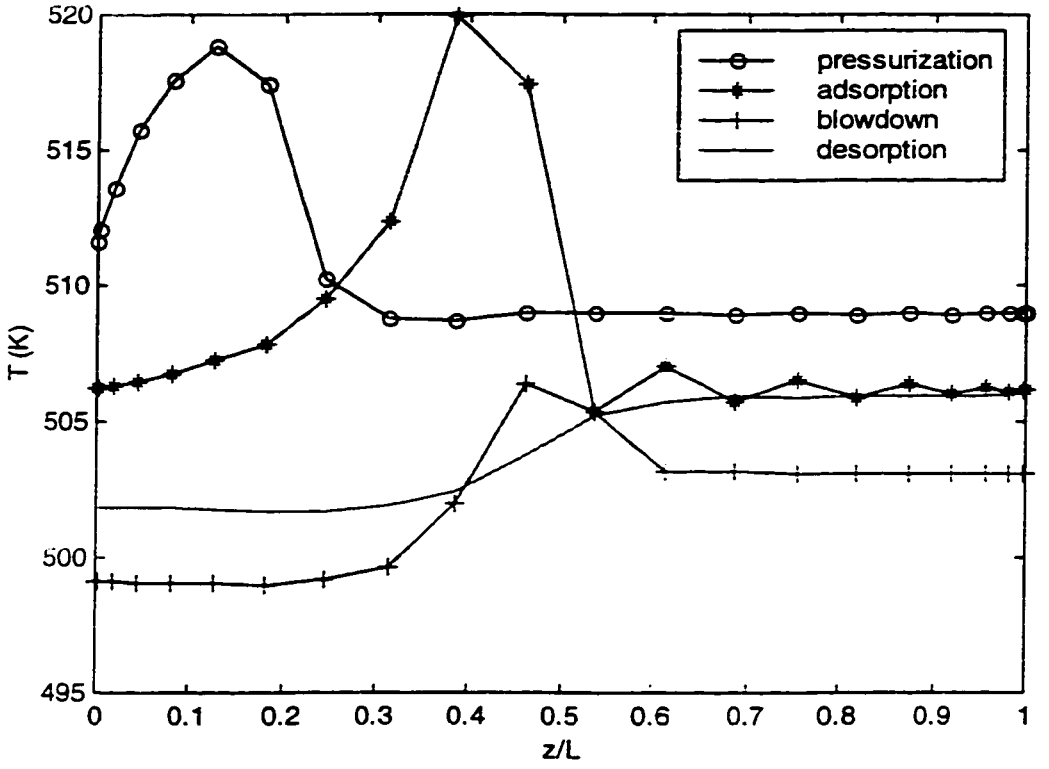


Figure 4.17 Temperature profiles in the bed at the end of cyclic steady state. Parametric values are the same as for Figure 4.15 except that $K_L$ is 0.35 W/m-K.

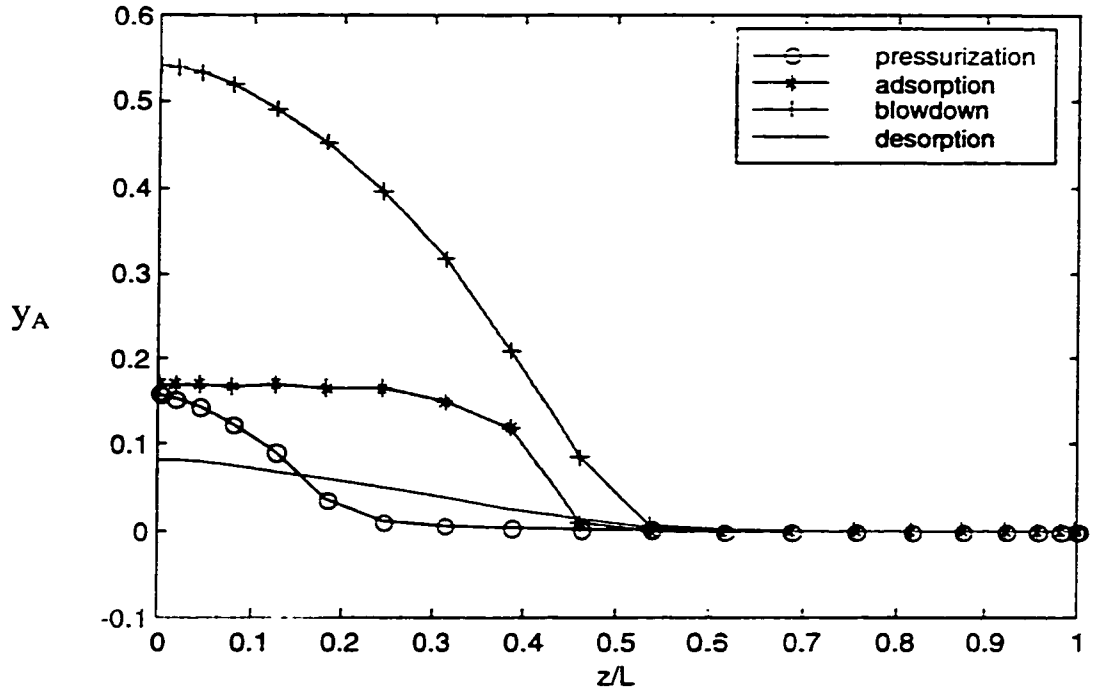


Figure 4.18 Gas phase concentration profiles of n-$C_5$ in the bed at the end of cyclic steady state. Parametric values are the same as for Figure 4.15 except that $K_L$ is 0.35 W/m-K.

## 4.4 RELEVANCE OF HEAT EFFECT TO PSAR SIMULATIONS

For the PSAR system, the feed injected into the catalyst bed contains about 17 mol% of n-$C_5$. After leaving the catalyst bed, it enters the adsorbent bed with a concentration of about 9-12 mol% of n-$C_5$. As mentioned above, it is acceptable to simulate the adsorber by the isothermal model for such a feed condition with low sorbate concentration. For pressurization and adsorption steps of the PSAR cycle, temperature rise in the adsorbent region does not affect the reaction rate constant at all because the feed mixture is first fed to the catalyst region and then to the adsorbent region. Thus, steps 1 and 2 in the PSAR cycle could be considered isothermal. Since the direction of flow is reversed in blowdown and desorption steps of the PSAR cycle, the temperature of the catalyst region will differ from the feed temperature and may need to be adjusted to meet the reaction criteria. As demonstrated in the previous temperature profiles, the exit temperature during the blowdown and desorption steps is lowered than the feed temperature by about 4 to 7 $^0$C. The reaction rate constants are 0.034 and 0.09 $s^{-1}$ at 506 and 533 K, respectively. For a feed temperature of 506 K, the effect of temperature drop during steps 3 and 4 is to reduce the reaction rate constant to a value of approximately 0.02 $s^{-1}$. This will reduce the Damköhler number to a value of about 3. As shown in Chapter 2, the reaction system gets close to its equilibrium value if

the Damköhler number is greater than or equal to 3. Thus, the whole PSAR cycle could be considered isothermal for the present study. In the future, an experimental study for a small PSAR laboratory unit will be conducted, and the results obtained will be compared with predictions by the PSAR isothermal model. If deviations are too much, the PSAR nonisothermal model should be considered.

Table 4.3 summarized the features for the different PSA and PSAR models discussed so far and the performance of the Pentium II computer used in simulations. All the information presented here correspond to a particular system containing three components (n,i-$C_5$/$H_2$). As shown in the table, the simplest case is the isothermal PSA system, which requires about five hours to complete on run. The most difficult case is the nonisothermal PSAR system, where the simulation is not conducted yet but the CPU time for one run is expected to be more than 20 hours. Of course, the CPU time for all cases will be decreased to a large extent if using a more sophisticated computer such as 700 MHz Pentium III. This will be done in the future.

Table 4.3 Summary of computer simulation performance for PSA and PSAR modeling of the n,i-$C_5/H_2$ system on a Pentium II computer. [number of internal collocation points used = 20; ODE solver in MATLAB code: ode23s]

| System | no. of ODE's/step/cycle | CPU time/run (hours) |
|---|---|---|
| Isothermal **PSA** model | 62 | 5 |
| Isothermal **PSAR** model | 102 | 10 |
| Nonisothermal **PSA** model | 82 | 10 |
| Nonisothermal **PSAR** model | 122 | > 20* |

* expected

# Nomenclature

| | |
|---|---|
| $B$ | dimensionless adiabatic temperature rise [-] = $(-\Delta H_{ads})q_{A.ref}/(C_{ps}T_f)$ |
| $c_T$ | total gas concentration in the column [mol/cm$^3$] |
| $c_{Tf}$ | total gas concentration of the feed [mol/cm$^3$] |
| $C_T$ | dimensionless total gas concentration in the column [mol/cm$^3$] |
| $C_{pg}$ | heat capacity of the gas phase [J/(mol.K)] |
| $C_{ps}$ | heat capacity of the adsorbent [J/(g.K)] |
| $d_C$ | column diameter [cm] |
| $h$ | overall heat transfer coefficient [W/(m$^2$.K)] |
| $(-\Delta H_{ads})$ | isosteric heat of adsorption [J/mol] |
| $K_{ads}$ | adsorption equilibrium constant [bar$^{-1}$] = $K_o \exp(-\Delta H_{ads}/R/T)$ |
| $K_O$ | limiting adsorption equilibrium constant [bar$^{-1}$] |
| $K_L$ | axial bed thermal conductivity [W/(m.K)] |
| $L$ | length of column [cm] |
| $N_w$ | number of wall heat-transfer units [-] = $4hL/(d_C u_f C_{pg} c_{Tf} \varepsilon)$ |
| $Pe_H$ | thermal Peclet number [-] = $u_f L C_{pg} c_{Tf}/K_L$ |
| $P$ | total pressure in the column [bar] |
| $P_H$ | constant high pressure during adsorption step [bar] |
| $P_L$ | constant low pressure during desorption step [bar] |
| $\langle q_A \rangle$ | average adsorbed-phase concentration [mol/kg] |
| $q_{A.ref}$ | adsorbed-phase concentration at equilibrium with $y_{Af}$ at $P_H$ and $T_f$ [mol/kg] |
| $q_{max}$ | maximum adsorbed-phase concentration [mol/kg] |
| $Q_A$ | dimensionless adsorbed-phase concentration [-] = $\langle q_A \rangle / q_{max}$ |
| R | ideal gas constant [bar.cm$^3$/mol/K] |
| T | time [s] |
| $T$ | gas temperature in the column [K] |
| $T_f$ | gas temperature in the feed [K] |
| $\overline{T}$ | dimensionless gas temperature in the column [-] = $(T - T_f)/T_f$ |
| $u$ | interstitial velocity [cm/s] |
| $u_f$ | interstitial feed velocity [cm/s] |

| | |
|---|---|
| $U$ | dimensionless interstitial velocity [-] = $u/u_f$ |
| $x$ | dimensionless axial coordinate in the column [-] = $z/L$ |
| $y_{Af}$ | mole fraction of component A in the feed [-] |
| $y_A$ | mole fraction of component A in the bulk phase in the column [-] |
| $z$ | axial coordinate in the column [cm] |

*Greek Letters*

| | |
|---|---|
| $\varepsilon$ | bed porosity [-] |
| $\zeta_H$ | thermal capacity factor [-] = $(1-\varepsilon)\rho_S C_{ps}/(\varepsilon c_{Tf} C_{pg})$ |
| $\rho_s$ | apparent density of the adsorbent [g/cm$^3$] |
| $\tau$ | dimensionless time [-] = $u_f t/L$ |
| $\gamma_f$ | dimensionless heat of adsorption [-] = $(-\Delta H_{ads})/(RT_f)$ |

*Subscripts*

| | |
|---|---|
| A | n-pentane |
| B | isopentane |
| T | total |
| f | feed |

# CHAPTER 5

# CONCLUSIONS AND RECOMMENDATIONS

## 5.1 SUMMARY OF CONCLUSIONS

In conventional chemical reaction processes, the conversion is often limited by chemical equilibrium, and the separation section always follows the reactor section to separate the products from the unconverted reactants.

In certain circumstances, the reaction can be enhanced by the periodic operation or by simultaneous reaction and separation. Another advantage of combining reaction with separation in a single unit is the reduction in unit operation equipment required and hence the reduction in total cost. A new application to this concept is the pressure swing adsorber-reactor (PSAR), a fixed-bed column packed with a mixture of catalyst and adsorbent and operated in pressure swing mode similar to the conventional PSA process.

n-Paraffins isomerization reaction is an important example for the petroleum refining industry. This is because it is one of the best alternatives to increase the octane number of gasoline since environmental restrictions forbid using lead additive compounds.

In the present study, theoretical investigation of n-$C_5$ isomerization

reaction via the PSAR process has been carried out. The unit is packed with two separate layers of a Pd/Y-zeolite catalyst and a 5A zeolite adsorbent. A flowsheet diagram for the isomerization PSAR process is proposed, which consists of two columns with its associated valves and piping system. A cyclic scheme is proposed, which consists of four steps similar to the basic Skarstrom cycle.

A mathematical model describing the dynamics of the PSAR process is developed. It differs from other PSAR models since the previous models are suitable only for a system where the catalyst and the adsorbent are mixed uniformly in the column. Also, the model developed in the present study is very general because it takes into account many factors such as axial dispersion, resistance to mass transfer in the bulk phase, variable velocity along the column length, and mass exchange between bulk and solid phases during pressurization and blowdown steps.

Breakthrough curves for a fixed-bed adsorber/reactor are predicted by the PSAR model. Also, the effect of the operating parameters (temperature, total pressure, and feed concentration) and design parameter (catalyst/column length ratio) on the breakthrough curves are addressed. Faster breakthrough is noticed at higher temperature, higher sorbate concentration, and lower pressure. Better conversions are obtained at higher

catalyst/column length ratio, and the effect is more noticeable at lower temperature.

The PSAR model developed is also used to simulate a four-step PSAR cyclic process. Parametric values used in the simulation are either obtained from experimental data or calculated from empirical correlations available in the literature without any adjustable parameters. The PSAR cycle is simulated at 506 and 533 K, and the catalyst/column length ratio is varied from 0.1 to 0.7. High-pressure feed step is at 15 bar, and low-pressure purge step is at 2 bar.

The catalyst/column length ratio should be greater than 0.3 at both temperatures in order to get close to the equilibrium conversions.

During reaction/blowdown step a high portion of isopentane is formed. During reaction/pressurization step, the equilibrium conversion is exceeded in some combination of conditions due to operating the reactor in an unsteady state mode.

A mathematical model describing a base case, which consists of a steady state packed-bed reactor and a PSA unit, is developed. A test of the PSAR model is made showing that the PSAR model reduces to the base-case PSA model if carrying out the simulation with a very low value of the catalyst/column length ratio.

Based on the two models, a comparison between the conventional process and the PSAR model is made, showing that the new process is effective for n-pentane isomerization. The product yield and purity are satisfied over a wide range of design and operating conditions.

The PSAR model developed is isothermal. To investigate the effect of heat, a nonisothermal PSA model is developed and applied to the base-case system. Both breakthrough curves and concentration and temperature profiles for the cyclic system are obtained by the nonisothermal model. Results demonstrated that significant heat effects arise in the system with a high portion of n-pentane in the feed. This is not the case for the present PSAR system, where n-pentane enters the adsorbent region with a concentration lower than 12%. Thus, the assumption of isothermal condition for the present PSAR system is acceptable.

Four computer simulation codes are developed by MATLAB. The first solves the steady state reactor model. The second and third solve the isothermal and nonisothermal PSA models, and the fourth solves the isothermal PSAR model. MATLAB is shown to be much superior than Fortran in terms of simplicity and visualization of profiles.

## 5.2 RECOMMENDATIONS FOR FUTURE WORK

The simultaneous reaction and separation by pressure swing adsorption is characterized by a large number of design and operating parameters. Only a small number of parameters have been investigated in this work. It is recommended to carry out further simulation runs to investigate optimum conditions for the PSAR process.

The model and cycle configuration have been established theoretically for the n,i-$C_5/H_2$/PSAR system in this study, and the results produced are promising. Thus, it is strongly recommended to carry out experimental work for the above system, and compare the results with simulation results. The set-up for the experiment is recommended to be similar to Figure 1.7.

In addition to n-pentane, gasoline has a high portion of n-hexane. Thus, it is recommended to carry out both simulation and experimental work for the n,i-$C_6/H_2$/PSAR system. The PSAR computer simulation code developed in this study can be used directly with a change in n-$C_6$ physical parameters only.

After that, it is recommended to carry out simulation and experimental work for the n,i- $C_5/C_6/H_2$/PSAR system, which most resemble the real case. For simulation, it is recommend to apply the extended multicomponent isotherm of Nitta *et. al.* [36].

The PSAR simulation code developed in this study is isothermal. If it is found that the agreement between simulation and experimental results is not good, effort should be done to include heat effect in the PSAR simulation code. The equations for the nonisothermal PSAR model are already developed in the present study and presented in the appendix. A summary of steps to complete the PSAR project is presented in Figure 5.1, where step 1 has been completed in the present study.

In the present study, a four step cyclic scheme similar to the basic Skarstrom cycle is used for the PSAR process. It is recommended to investigate other modified cycle configurations. This may include the incorporation of co-current depressurization and pressure equalization steps in the cycle.

In the original patent of the Total Isomerization Process (TIP), four adsorption columns are used [19]. Thus, it is recommended to extend the present work to study such system both experimentally and by simulation.

Also, in actual operation of the TIP process the purge stream is recycled and combined with the fresh feed. However, this point is not considered in comparison between the PSA and PSAR systems for simplicity. More effort should be done to include this point in the simulation.

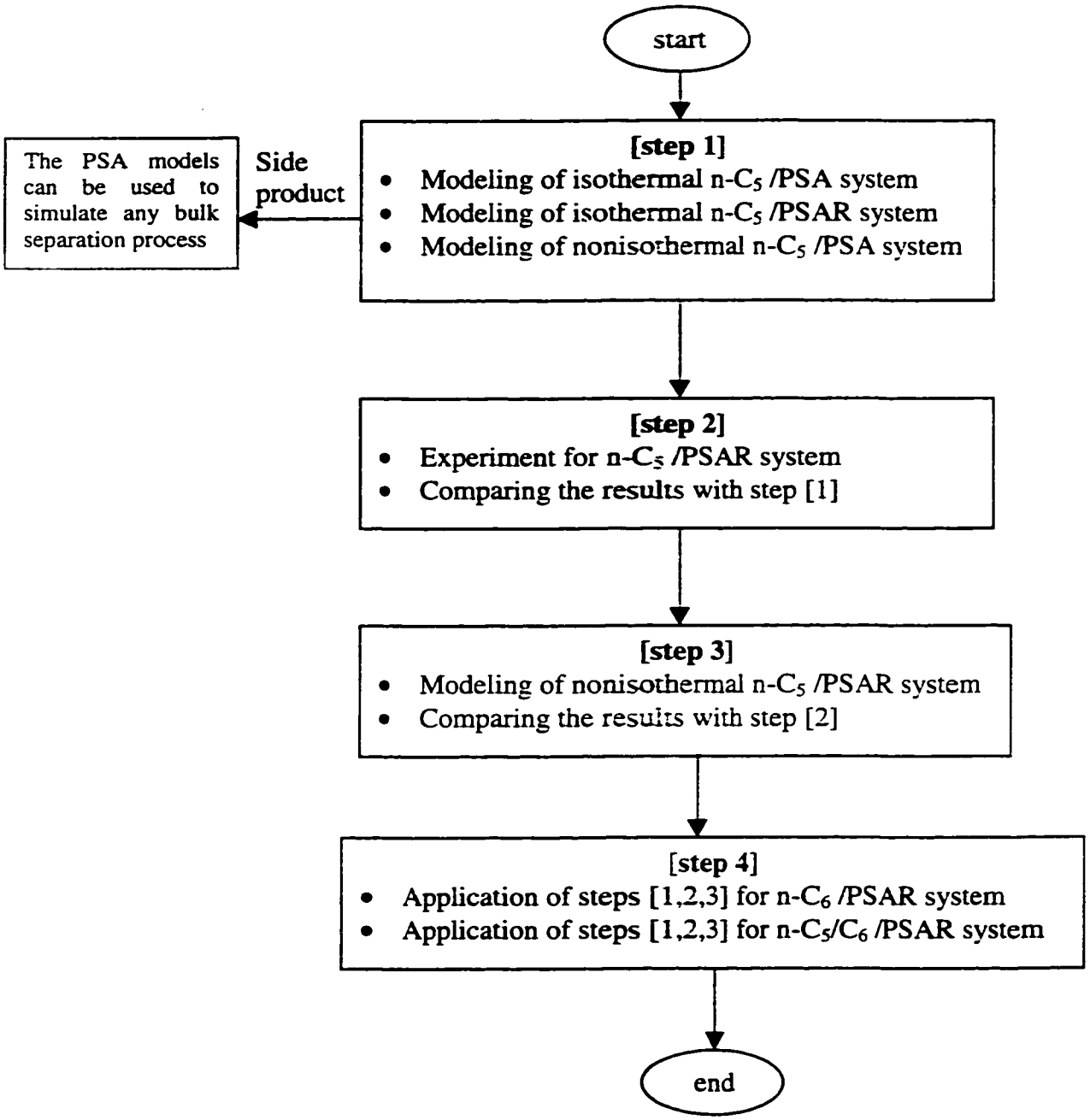


Figure 5.1 Summary of steps to complete the PSAR project

Also, simulation results for the PSAR system demonstrate that the blowdown stream has a considerable amount of isomers. It is not good to recycle this stream to the catalyst region of the adjacent column because the isomer product will be lost by this way. A better alternative is to feed this stream directly to the adsorbent section of the adjacent column. By this way the overall production of the isomers could increase. However, there may be a need to increase the diameter of the adsorbent region in order to take into account the increase in flow rate. Thus, more efforts should be done to investigate this alternative plus others to utilize the blowdown stream efficiently and to consider it in the simulations.

The cyclic steady state (CSS) for all runs in the present study is determined by the common successive substitution method. It is recommended to compare this method with the simultaneous discretisation method, a new method that has been published recently and claimed to be more efficient [3].

The isothermal and nonisothermal PSA computer simulation codes developed in this study are very general and can be applied to any PSA processes. Thus, it is recommended to apply them on different examples of PSA purification and bulk separation processes.

The PSAR model is an example of very stiff problems, and the execution time is found to be very high (in terms of hours) if the runs are carried out on a Pentium II computer. Thus, it is recommended to perform the PSAR runs by the latest and most efficient computer.

# REFERENCES


1. Alpay, E., C. N. Kenney, and D. M. Scott, "Simulation of Rapid Pressure Swing Adsorption and Reaction Process," *Chem. Eng. Sci.*, **48,** 3173 (1993).

2. Alpay, E., D. Chatsiriwech, L. S. Kershenbaum, C. P. Hull, and N. F. Kirkby, "Combined Reaction and Separation by Pressure Swing Adsorption," *Chem. Eng. Sci.*, **49,** 5845-5864 (1995).

3. Alpay, E., Y. S. Cheng, and L. S. Kershenbaum, "Simulation and Optimization of a Rapid Pressure Swing Reactor," Comput. *Chem. Eng.*, **22,** S45-S52 (1998).

4. Barrer, R. M., and D. J. Clarke, "Diffusion of Some n-Paraffins in Zeolite A," *Trans. Faraday Soc.*, **69**, 535-546 (1973).

5. Bhatia, S., and K. Jothimurugesan, "Isomerization of n-Hexane over Nickel-Loaded Zeolite Catalysts," *Can. J. Chem. Eng.*, **62**, 390 (1984).

6. Borse, G. J., *Numerical Methods with MATLAB*, PWS Publishing Company, Boston, (1997).

7. Breck, D. W., *Zeolite Molecular Sieves*. John Wiley & Sons, New York, (1974).

8. Bryant, P., and A. J. Voorhies, "Hydroisomerization of n-Pentane over a Zeolite Catalyst," *AIChE J.*, **14**(6), 852 (1968).

9. Bryant, P., and J. Spivey, "Hydroisomerization of n-$C_5$ and n-$C_6$ Mixtures on Zeolite Catalysts," *Ind. Eng. Chem. Process Des. Dev.*, **21**(4), 750-760 (1982).

10. Cavalcante, C. L., M. Eic, D. M. Ruthven, and M. L. Occeli, "Diffusion of n-Paraffins in Offretite-Erionite Type Zeolite," *Zeolite*, **15**, 293 (1995).

11. Chang, J. R., R. M. Jao, and T. B. Lin, " Light Naphtha Isomerization over Mordenite-Supported Ni-Pt Catalysts: Effect of Ni on the Performance for Pure Feed and Sulfur-Containing Feed," *J. Catal.*, **161**, 222-229 (1996).

12. Chatsiriwech, D., E. Alpay, L. S. Kershenbaum, C. P. Hull, and N. F. Kirkby, "Enhancement of Catalytic Reaction by Pressure Swing Adsorption," *Catal. Today*, **20**, 351 (1994).

13. Chihara, K., and M. Suzuki, "Simulation of Nonisothermal Pressure Swing Adsorption," *J. Chem. Eng. Japan*, 16 (1), 53 (1983).

14. Collins, J. J., "Air Separation by Adsorption," U.S. Patent No. 4,026,680 (1977).

15. Douglas, J. M., "Periodic Reactor Operation," *Ind. Eng. Chem. Proc. Des. Dev.*, **6**(1), 43-48 (1967).

16. Fajula, F., D. McQueen, B. H. Chiche, A. Auroux, C. Guimon, F. Fitoussi, and P. Schulz, "A Multitechnique Characterization of the Acidity of Dealuminated Mazzite," *J. Catal.*, **161**, 587-596 (1996).

17. Fogler, H. S., *Elements of Chemical Reaction Engineering*, Prentice Hall, New York, (1992).

18. Fujimoto, K., A. Zhang, I. Nakamura, and K. Aimoto, "Isomerization of n-Pentane and Other Light Hydrocarbons on Hybrid Catalyst: Effect of Hydrogen Spillover," *Ind. Eng. Chem. Res.*, **34**, 1074-1080 (1995).

19. Gary, J., "Total Isomerization Process," U.S. Patent 4,709,117 (1987).

20. Gates, B., C, and S. G. Ryu, "n-Hexane Conversion Catalyzed by Sulfated Zirconia and by Iron- and Manganese Promoted Sulfated Zirconia: Catalytic Activities and Reaction Network," *Ind. Eng. Chem. Res.*, **37**, 1786-1792 (1998).

21. Glueckauf, E., "Formula for diffusion into spheres and their application to chromatography," *J. Chem. Soc.*, **51**, 1540 (1955).

22. Goto, S., T. Tagawa, and T. Omiya, "Dehydrogenation of Cyclohexane in a PSA Reactor Using Hydrogen Occlusion Alloy," *Chem. Eng Essays (Japan),* **19**(6). 978, (1993).

23. Han, C., and D. P. Harrison, "Simultaneous Shift Reaction and Carbon Dioxide Separation for the Direct Production of Hydrogen," *Chem. Eng. Sci.,* **49,** 5875 (1994).

24. Hufton, R. J., and D. M. Ruthven, "Diffusion of Light Alkanes in Silicalite Studied by the Zero Length Column Method," *Ind. Eng. Chem. Res.*, **32**, 2379 (1993).

25. Kadlec, R. H., and G. G. Vaporciyan, "Periodic Chemical Processing System," U.S. Patent 5,254,368 (1993).

26. Karger, J., and D. M. Ruthven, *Diffusion in Zeolites and other Microporous Solids*, John Wiley, New York, (1992).

27. Kirkby, N. F., and J. E. Morgan, "A Theoretical Investigation of Pressure Swing Reaction," *Trans. Inst. Chem. Eng.,* **72,** 541 (1994).

28. Kouwenhoven, H., and W. C. Langhout, "Shell's Hydroisomerization Process," *Chem. Eng. Prog.*. **67**(4). 65-70 (1971).

29. Kouwenhoven, H. W., *in "Molecular Sieves"*, eds. W. M. Meier and J. B. Uytterhoeven, Adv. Chem. Ser. 121, American Chemical Society, Washington, (1973).

30. Langmuir, I., "The Adsorption of Gases on Plane Surfaces of Glass, Micea, and Platinum," *J. Am. Chem. Soc.*, **40**, 163 (1918).

31. Lee, I. D., and R. H. Kadlec. "Effects of Adsorbent and Catalyst Distributions in Pressure Swing Reactors," *AIChE Symp. Ser.,* **84,** 167 (1989).

32. Lu, Z. P., and A. E. Rodrigues, "Pressure Swing Adsorption Reactors: Simulation of Three-Step One-Bed Process," *AIChE J.,* **40,** 1118 (1994).

33. Minkkinen, A., L. Mank, and S. Jullian, "Process for the Isomerization of of $C_5/C_6$ Normal Paraffins with Recycling of Normal Paraffins," U. S. Patent 5,233,120 (1993).

34. Morbidelli, M., M. Mazzotti, R. Baciochi, and G. Storti, "Vapor-Phase SMB Adsorptive Separation of Linear/Nonlinear Paraffins," *Ind. Eng. Chem. Res.*, **35**, 2313 (1996).

35. Morbidelli, M., A. Servida and G. Storti, "Simulation of Multicomponent Adsorption Bed. Model Analysis and Numerical Solution," *Ind. Eng. Chem. Fundam.*, **21**, 123 (1982).

36. Nitta, T., T. Shigetomi, and T. Katayama, "An Adsorption Isotherm of Multi-site Occupancy Model for Homogeneous Surface," *J. Chem. Eng. Jpn.*, **17**, 39-51 (1984).

37. Pines, H., K. Vetinskas, K. Assel, and I. Patieff, "Determination of Equilibrium Constants for Butanes and Pentanes," *J. Am. Chem. Soc.*, **67**, 631 (1945).

38. Redlich, O., and D. L. Peterson, "Sorption of Normal Paraffins by Molecular Sieves Type 5A," *Chem. Eng. Data*, 7(4), 570 (1962).

39. Ribeiro, F. R., *Nato Advanced Study Institute on Zeolites Science and Technology*, Alcabideche, Portugal, (1983).

40. Ruckenstein, E., A. S. Vaidynathan, and G. R. Youngquist, "Sorption in solids with bidisperse porous structurs," *Chem. Eng. Sci.*, **26**, 1305 (1971).

41. Runstraat, A., J. Grondelle, and R. A. Santen, "On the Temperature Dependence of the Arrhenius Activation Energy for Hydroisomerization Catalyzed by Pt/Mordenite," *J. Catal.*, **167**, 460-463 (1997).

42. Runstraat, A., J. Kamp, P. Stobbelaar, J. Grondelle, S. Krijnen, and R. Santen, "Kinetics of Hydroisomerization of n-Hexane over Platinum Containing Zeolites," *J. Catal.*, **171**, 77-84 (1997).

43. Runstraat, A., J. Grondelle, and R. Santen, "Microkinetics Modeling of the Hydroisomerization of n-Hexane," *Ind. Eng. Chem. Res.*, **36**, 3116-3125 (1997).

44. Ruthven, D. M., and K. F. Loughlin, "The Adsorption and Diffusion of n- Butane in Linede 5A Molecular Sieve," *Chem. Eng. Sci.*, **26**, 1145 (1971).

45. Ruthven, D. M., and K. F. Loughlin, "The Diffusional Resistance of Molecular Sieve Pellets," *Can. J. Chem. Eng.*, **28**, 550 (1972).

46. Ruthven, D. M., and B. K. Kaul, "Adsorption of n-Hexane and Intermediate Molecular Weight Aromatic Hydrocarbons on LaY Zeolite," *Ind. Eng.Chem. Res.*, **35**, 2060 (1996).

47. Ruthven, D. M., *Principles of Adsorption and Adsorption Process*, John Wiley & Sons, New York, (1984).

48. Ruthven, D. M., S. Farooq, and K. S. Knaebel, *Pressure Swing Adsorption*, VCH Publishers, New York, (1994).

49. Ruthven, D. M., M. M. Hassan, and N. S. Raghavan, "Numerical Simulation of a PSA System-Part I," *AIChE J.*, **31**(3), 385-392 (1985).

50. Ruthven, D. M., and N. S. Raghavan, "Numerical Simulation of a PSA System-Part III," *AIChE J.*, **31**(12), 1829 (1985).

51. Shendalman, L. H., and J. E. Mitchell, "A Study of Heatless Adsorption in the Model System CO He," *Chem. Eng. Sci.*, **27**, 1449-58 (1972).

52. Shin, H. S., and K. S. Knaebel, "An Experimental Study of Diffusion-Induced Separation of Gas Mixtures by Pressure Swing Adsorption," *AIChE J.*, **33**, 654 (1987).

53. Silva, J. A., and A. E. Rodrigues, "Sorption and Diffusion of n-Pentane in Pellets of 5A Zeolite," *Ind. Eng. Chem. Res.*, **36**, 493-500 (1997).

54. Silva, J. A., and A. E. Rodrigues, "Fixed-Bed Adsorption of n-Pentane/Isopentane Mixtures in Pellets of 5A Zeolite," *Ind. Eng. Chem. Res.*, **36**, 3769-3777 (1997).

55. Silva, J. A., and A. E. Rodrigues, "Equilibrium and Kinetics of n-Hexane Sorption in Pellets of 5A Zeolite," *AIChE J.*, **43**, 2524-2534 (1997).

56. Silva, J. A., and A. E. Rodrigues, "PSA Separation of n/iso-Paraffins Mixtures," presented at FOA6, (1998).

57. Sircar, S., B. T. Carvill, J. R. Hufton, and M. Anand, "Sorption-Enhanced Reaction Process," *AIChE J.*, **42**(10), 2765-2772 (1996).

58. Skarstrom, C. W., "Method and Apparatus for Fractionating Gaseous Mixtures by Adsorption," U.S. Patent No. 2,944,627 (1960).

59. Vaporciyan, G. G., and R. H. Kadlec, "Equilibrium Limited Periodic Separating Reactors," *AIChE J.*, **33**, 1334 (1987).

60. Vaporciyan, G. G., and R. H. Kadlec, "Periodic Separating Reactors: Experiments and Theory," *AIChE J.*, **3**, 831 (1989).

61. Vavlitis, A. P., D. M. Ruthven, and K. F. Loughlin, "Sorption of n-Pentane, n-Octane, and n-Decane in 5A Zeolite Crystals," *J. Coll. Sci.*, **84**(2), 526-531 (1981).

62. Wakao, N., and S. Kaguei, *Heat and Mass Transfer in Packed Beds*, Gordon and Breach Science Publishers, New York, (1982).

63. Weisz, P. B., in "Advances in Catalysis and related Subjects," Vol. 13 (D. D. Eley, P. W Selwood, and P. B. Weisz, Eds.), p. 157, Academic Press, London, (1962).

64. Yang, R. T., *Gas Separation by Adsorption Process*, Butterworth, Boston, (1987).

# APPENDICES

## A.1 Computer Program for the Steady State Reactor Model

```
%
% This program solves the steady state reactor
% model, by the orthogonal collocation method
% N = 16 (number of collocation points);
%

%fixed given data**********************************************
yaf = 0.17;          % feed mol fraction of component A
ybf = 0.17;          % feed mol fraction of component B
tempf = 500;         % feed temperature; K
da = 1;              % Damkholer number
kc = 3.38;           % reaction equilibrium constant
alpha = 1+1/kc;
gama = yaf/kc+ybf/kc;
pe = 100;            % mass Peclet number
%**********************************************************

%Coefficients for A and B matrix
matrixab16;

% transferring the ODE into a set of algebraic equations:

   bb = [-yaf*pe
         da*gama
         da*gama
         da*gama
         da*gama
         da*gama
         da*gama
         da*gama
         da*gama
         da*gama
         da*gama
         da*gama
         da*gama
         da*gama
         da*gama
         da*gama
         da*gama
```

```
        da*gama
        0];


aa = [A(1,1)-pe, A(1,2:18)

-B(2,1)/pe+A(2,1), -B(2,2)/pe+A(2,2)+da*alpha,.....
(- B(2,3:18)+pe*A(2,3:18))/pe

(-B(3,1:2)+pe*A(3,1:2))/pe, -B(3,3)/pe+A(3,3)+da*alpha, .....
(-B(3,4:18)+pe*A(3,4:18))/pe

(-B(4,1:3)+pe*A(4,1:3))/pe, -B(4,4)/pe+A(4,4)+da*alpha, .....
(-B(4,5:18)+pe*A(4,5:18))/pe

(-B(5,1:4)+pe*A(5,1:4))/pe, -B(5,5)/pe+A(5,5)+da*alpha, .....
(-B(5,6:18)+pe*A(5,6:18))/pe

(-B(6,1:5)+pe*A(6,1:5))/pe, -B(6,6)/pe+A(6,6)+da*alpha, .....
(-B(6,7:18)+pe*A(6,7:18))/pe

(-B(7,1:6)+pe*A(7,1:6))/pe, -B(7,7)/pe+A(7,7)+da*alpha, .....
(-B(7,8:18)+pe*A(7,8:18))/pe

(-B(8,1:7)+pe*A(8,1:7))/pe, -B(8,8)/pe+A(8,8)+da*alpha, .....
(-B(8,9:18)+pe*A(8,9:18))/pe

(-B(9,1:8)+pe*A(9,1:8))/pe, -B(9,9)/pe+A(9,9)+da*alpha, .....
(-B(9,10:18)+pe*A(9,10:18))/pe

(-B(10,1:9)+pe*A(10,1:9))/pe,-B(10,10)/pe+A(10,10)+da*alpha,.....
(-B(10,11:18)+pe*A(10,11:18))/pe

(-B(11,1:10)+pe*A(11,1:10))/pe, .....
 -B(11,11)/pe+A(11,11)+da*alpha,.....
(-B(11,12:18)+pe*A(11,12:18))/pe

(-B(12,1:11)+pe*A(12,1:11))/pe, .....
 -B(12,12)/pe+A(12,12)+da*alpha, .....
(-B(12,13:18)+pe*A(12,13:18))/pe
```

```
(-B(13,1:12)+pe*A(13,1:12))/pe, .....
 -B(13,13)/pe+A(13,13)+da*alpha, .....
(-B(13,14:18)+pe*A(13,14:18))/pe

(-B(14,1:13)+pe*A(14,1:13))/pe, .....
 -B(14,14)/pe+A(14,14)+da*alpha, .....
(-B(14,15:18)+pe*A(14,15:18))/pe

(-B(15,1:14)+pe*A(15,1:14))/pe, .....
 -B(15,15)/pe+A(15,15)+da*alpha, .....
(-B(15,16:18)+pe*A(15,16:18))/pe

(-B(16,1:15)+pe*A(16,1:15))/pe, .....
 -B(16,16)/pe+A(16,16)+da*alpha, .....
(-B(16,17:18)+pe*A(16,17:18))/pe

(-B(17,1:16)+pe*A(17,1:16))/pe, .....
 -B(17,17)/pe+A(17,17)+da*alpha, -B(17,18)/pe+A(17,18)

A(18,1:18)];


h1 = aa\bb;

% dimensionless distance points in the reactor

      X( 1)=  .0000000E+00;
      X( 2)=  .5299533E-02;
      X( 3)=  .2771249E-01;
      X( 4)=  .6718440E-01;
      X( 5)=  .1222978E+00;
      X( 6)=  .1910619E+00;
      X( 7)=  .2709916E+00;
      X( 8)=  .3591982E+00;
      X( 9)=  .4524937E+00;
      X(10)=  .5475063E+00;
      X(11)=  .6408018E+00;
      X(12)=  .7290084E+00;
      X(13)=  .8089381E+00;
      X(14)=  .8777022E+00;
```

```
X(15)=  .9328156E+00;
X(16)=  .9722875E+00;
X(17)=  .9947005E+00;
X(18)=  .1000000E+01;

plot(X,h1,'-o')
xlabel('Dimensionless Distance (z/L)');
ylabel('YA');
legend('Pe=100')
```

## A.2 Computer Program for the Isothermal PSA Model

```
%
% this program solve the isothermal PSA model
% N = 20 (number of collocation points)
%

function yd = adsorption20AB(t,y);

% fixed given data**********************************************************
flux = 0.000015;  % feed molar flux; mol/cm^2/s
l = 100;          % adsorber length; cm
uf = 0.131;       % feed velocity at high pressure; cm/s
upf = 3;          % purge-to feed velocity ratio
yaf = 0.0815;     % feed mol fraction of component A
ybf = 0.2685;     % feed mol fraction of component B
tempf = 506;      % feed temperature; K
phetaref = 0.581; % coverage of adsorbent at feed conditions
kgL = 2.23;       % mass transfer coefficient at P_L ; cm/s
kgH = 0.62;       % mass transfer coefficient at P_H ; cm/s
time = 3.0;       % dimensionless pressurization time
plow = 2.0;       % low pressure; bar
phigh = 15;       % high pressure; bar

%ooooooooooooooooooooooooooooooooooooooooooooooooooooooooooooooooooo
pconstant = (phigh-plow)/time; % bar
R = 83.14;                     % ideal gas constant; bar*cm^3/mol/K
ctf = phigh/tempf/R; % total gas concentration at feed conditions; mol/cm^3
voidage = 0.32;      % bed porosity
density = 1.13;      % solid density; g/cm^3
mw = 72.15;          % molecular wieght for n-c5; g/mol
qmax = 13.0/100/mw ; % maximum adsorbed concentration; mol/g
qref = phetaref*qmax;  % adsorbed concentration at feed conditions; mol/g
zeta = ((1-voidage)/voidage)*density*qref/ctf;      % mass capacity
ap = 25;                       % specific area of the pellet; 1/cm
ko = 0.0000204/1.01325;  % limiting adsorption equilibrium constant; 1/bar
dh = 13.2*1000;                % heat of adsorption; cal/mol
kads = ko*exp(dh/1.987/tempf);  % adsorption equilibrium constant; 1/bar
%**************************************************************************
%**************************************************************************
```

```
p = phigh;      % pressure during this step; bar
press = 0;      % pressurization rate
kg = kgH;       % mass transfer coeficient; cm/s
uo = 1;         % dimensionless inlet velocity during this step
%*****************************************************************
ct = p/phigh;                          % dimensionless total gas concentration
nf = ((1-voidage)/voidage)*ap*kg*l/uf;     % no. of film-mass transfer unit
dm = 0.77*(2/p)*(tempf/498)^1.5;           % diffusion coefficient; cm^2/s
dl = 0.7*dm;                               % dispersion coefficient; cm^2/s
pe = uf*l/dl;                              % peclet number
%*****************************************************************

% coefficients for A and B matrix
matrixab20;

% matrix size
[m,n]=size(y);
yd=zeros(m,n);

% assign dummy variables
h2 = y(1);
h3 = y(2);
h4 = y(3);
h5 = y(4);
h6 = y(5);
h7 = y(6);
h8 = y(7);
h9 = y(8);
h10 = y(9);
h11 = y(10);
h12 = y(11);
h13 = y(12);
h14 = y(13);
h15 = y(14);
h16 = y 15);
h17 = y(16);
h18 = y(17);
h19 = y(18);
h20 = y(19);
h21 = y(20);
```

```
q1 = y(21);
q2 = y(22);
q3 = y(23);
q4 = y(24);
q5 = y(25);
q6 = y(26);
q7 = y(27);
q8 = y(28);
q9 = y(29);
q10 = y(30);
q11 = y(31);
q12 = y(32);
q13 = y(33);
q14 = y(34);
q15 = y(35);
q16 = y(36);
q17 = y(37);
q18 = y(38);
q19 = y(39);
q20 = y(40);
q21 = y(41);
q22 = y(42);

g2 = y(43);
g3 = y(44);
g4 = y(45);
g5 = y(46);
g6 = y(47);
g7 = y(48);
g8 = y(49);
g9 = y(50);
g10 = y(51);
g11 = y(52);
g12 = y(53);
g13 = y(54);
g14 = y(55);
g15 = y(56);
g16 = y(57);
g17 = y(58);
```

```
g18 = y(59);
g19 = y(60);
g20 = y(61);
g21 = y(62);

% algebraic equations to solve for velocity

x = [1,zeros(1,21)
    AX(2,1:22)
    AX(3,1:22)
    AX(4,1:22)
    AX(5,1:22)
    AX(6,1:22)
    AX(7,1:22)
    AX(8,1:22)
    AX(9,1:22)
    AX(10,1:22)
    AX(11,1:22)
    AX(12,1:22)
    AX(13,1:22)
    AX(14,1:22)
    AX(15,1:22)
    AX(16,1:22)
    AX(17,1:22)
    AX(18,1:22)
    AX(19,1:22)
    AX(20,1:22)
    AX(21,1:22)
    AX(22,1:22)];

 z = [ uo
    - press/ct - nf*(h2 - phetaref*y(22)/kads/p/(1 - phetaref*y(22))^5)
    - press/ct - nf*(h3 - phetaref*y(23)/kads/p/(1 - phetaref*y(23))^5)
    - press/ct - nf*(h4 - phetaref*y(24)/kads/p/(1 - phetaref*y(24))^5)
    - press/ct - nf*(h5 - phetaref*y(25)/kads/p/(1 - phetaref*y(25))^5)
    - press/ct - nf*(h6 - phetaref*y(26)/kads/p/(1 - phetaref*y(26))^5)
    - press/ct - nf*(h7 - phetaref*y(27)/kads/p/(1 - phetaref*y(27))^5)
    - press/ct - nf*(h8 - phetaref*y(28)/kads/p/(1 - phetaref*y(28))^5)
    - press/ct - nf*(h9 - phetaref*y(29)/kads/p/(1 - phetaref*y(29))^5)
    - press/ct - nf*(h10 - phetaref*y(30)/kads/p/(1 - phetaref*y(30))^5)
```

```
    - press/ct - nf*(h11 - phetaref*y(31)/kads/p/(1 - phetaref*y(31))^5)
    - press/ct - nf*(h12 - phetaref*y(32)/kads/p/(1 - phetaref*y(32))^5)
    - press/ct - nf*(h13 - phetaref*y(33)/kads/p/(1 - phetaref*y(33))^5)
    - press/ct - nf*(h14 - phetaref*y(34)/kads/p/(1 - phetaref*y(34))^5)
    - press/ct - nf*(h15 - phetaref*y(35)/kads/p/(1 - phetaref*y(35))^5)
    - press/ct - nf*(h16 - phetaref*y(36)/kads/p/(1 - phetaref*y(36))^5)
    - press/ct - nf*(h17 - phetaref*y(37)/kads/p/(1 - phetaref*y(37))^5)
    - press/ct - nf*(h18 - phetaref*y(38)/kads/p/(1 - phetaref*y(38))^5)
    - press/ct - nf*(h19 - phetaref*y(39)/kads/p/(1 - phetaref*y(39))^5)
    - press/ct - nf*(h20 - phetaref*y(40)/kads/p/(1 - phetaref*y(40))^5)
    - press/ct - nf*(h21 - phetaref*y(41)/kads/p/(1 - phetaref*y(41))^5)
     0];

  u = x\z;

% boundary conditions for mass balance eq of component A:
 hin = [ h2; h3; h4; h5; h6; h7; h8; h9; h10; h11; h12; h13; h14; .....
 h15; h16; h17; h18; h19; h20; h21]; % internal nodes

a1 = AX(1,1) - uo*pe;
a2 = AX(22,1);
b1 = AX(1,22);
b2 = AX(22,22);

phi1 = - AX(1,2:21)*hin - yaf*uo*pe ;
phi2 = - AX(22,2:21)*hin;

xx = [a1, b1
      a2, b2];

  zz = [phi1
        phi2];

    hh = xx\zz;
    h1 = hh(1);
    h22 = hh(2) ;
```

```
v = [u(1); u(2); u(3); u(4); u(5); u(6); u(7); u(8); u(9); u(10); u(11); u(12);....
u(13); u(14); u(15); u(16); u(17); u(18); u(19); u(20); u(21); u(22) ] ; % 
velocity at all nodes

h = [ h1; h2; h3; h4; h5; h6; h7; h8; h9; h10; h11; h12; h13; h14; h15;.....
 h16; h17; h18; h19; h20; h21; h22]; % mol fraction at all nodes


% boundary conditions for mass balance eq of component B:
gin = [g2;g3;g4;g5;g6;g7;g8;g9;g10;g11;g12;g13;g14;g15; .....
        g16;g17;g18;g19;g20;g21]; % internal nodes

phi1b = - AX(1,2:21)*gin - ybf*uo*pe;
phi2b = - AX(22,2:21)*gin;

  zz = [phi1b
        phi2b];

    gg = xx\zz;
    g1 = gg(1);
    g22 = gg(2) ;

g = [ g1;g2;g3;g4;g5;g6;g7;g8;g9;g10;g11;g12;g13;g14; .....
     g15;g16;g17;g18;g19;g20;g21;g22]; % internal nodes

%ODE

% mol fraction of component A in the gas phase

yd(1) =  (BX(2,:)*h)/pe - u(2)*(AX(2,:)*h) - h2*(AX(2,:)*v).....
          - h2*press/ct - nf*(h2-phetaref*y(22)/kads/p/(1-phetaref*y(22))^5);

yd(2) =  (BX(3,:)*h)/pe - u(3)*(AX(3,:)*h) - h3*(AX(3,:)*v).....
        - h3*press/ct - nf*(h3-phetaref*y(23)/kads/p/(1-phetaref*y(23))^5);

yd(3) =  (BX(4,:)*h)/pe - u(4)*(AX(4,:)*h) - h4*(AX(4,:)*v).....
          - h4*press/ct - nf*(h4-phetaref*y(24)/kads/p/(1-phetaref*y(24))^5);

yd(4) =  (BX(5,:)*h)/pe - u(5)*(AX(5,:)*h) - h5*(AX(5,:)*v).....
          - h5*press/ct - nf*(h5-phetaref*y(25)/kads/p/(1-phetaref*y(25))^5);
```

```
yd(5) =  (BX(6,:)*h)/pe - u(6)*(AX(6,:)*h) - h6*(AX(6,:)*v).....
          - h6*press/ct - nf*(h6-phetaref*y(26)/kads/p/(1-phetaref*y(26))^5);

yd(6) =  (BX(7,:)*h)/pe - u(7)*(AX(7,:)*h) - h7*(AX(7,:)*v).....
          - h7*press/ct - nf*(h7-phetaref*y(27)/kads/p/(1-phetaref*y(27))^5);

yd(7) =  (BX(8,:)*h)/pe - u(8)*(AX(8,:)*h) - h8*(AX(8,:)*v).....
          - h8*press/ct - nf*(h8-phetaref*y(28)/kads/p/(1-phetaref*y(28))^5);

yd(8) =  (BX(9,:)*h)/pe - u(9)*(AX(9,:)*h) - h9*(AX(9,:)*v).....
          - h9*press/ct - nf*(h9-phetaref*y(29)/kads/p/(1-phetaref*y(29))^5);

yd(9) =  (BX(10,:)*h)/pe - u(10)*(AX(10,:)*h) - h10*(AX(10,:)*v).....
          - h10*press/ct - nf*(h10-phetaref*y(30)/kads/p/(1-phetaref*y(30))^5);

yd(10) =  (BX(11,:)*h)/pe - u(11)*(AX(11,:)*h) - h11*(AX(11,:)*v).....
          - h11*press/ct - nf*(h11-phetaref*y(31)/kads/p/(1-phetaref*y(31))^5);

yd(11) =  (BX(12,:)*h)/pe - u(12)*(AX(12,:)*h) - h12*(AX(12,:)*v).....
          - h12*press/ct - nf*(h12-phetaref*y(32)/kads/p/(1-phetaref*y(32))^5);

yd(12) =  (BX(13,:)*h)/pe - u(13)*(AX(13,:)*h) - h13*(AX(13,:)*v).....
          - h13*press/ct - nf*(h13-phetaref*y(33)/kads/p/(1-phetaref*y(33))^5);

yd(13) =  (BX(14,:)*h)/pe - u(14)*(AX(14,:)*h) - h14*(AX(14,:)*v).....
          - h14*press/ct - nf*(h14-phetaref*y(34)/kads/p/(1-phetaref*y(34))^5);

yd(14) =  (BX(15,:)*h)/pe - u(15)*(AX(15,:)*h) - h15*(AX(15,:)*v).....
          - h15*press/ct - nf*(h15-phetaref*y(35)/kads/p/(1-phetaref*y(35))^5);

yd(15) =  (BX(16,:)*h)/pe - u(16)*(AX(16,:)*h) - h16*(AX(16,:)*v).....
          - h16*press/ct - nf*(h16-phetaref*y(36)/kads/p/(1-phetaref*y(36))^5);

yd(16) =  (BX(17,:)*h)/pe - u(17)*(AX(17,:)*h) - h17*(AX(17,:)*v).....
          - h17*press/ct - nf*(h17-phetaref*y(37)/kads/p/(1-phetaref*y(37))^5);

yd(17) =  (BX(18,:)*h)/pe - u(18)*(AX(18,:)*h) - h18*(AX(18,:)*v).....
          - h18*press/ct - nf*(h18-phetaref*y(38)/kads/p/(1-phetaref*y(38))^5);
```

```
yd(18) = (BX(19,:)*h)/pe - u(19)*(AX(19,:)*h) - h19*(AX(19,:)*v).....
       - h19*press/ct - nf*(h19-phetaref*y(39)/kads/p/(1-phetaref*y(39))^5);

yd(19) = (BX(20,:)*h)/pe - u(20)*(AX(20,:)*h) - h20*(AX(20,:)*v).....
       - h20*press/ct - nf*(h20-phetaref*y(40)/kads/p/(1-phetaref*y(40))^5);

yd(20) = (BX(21,:)*h)/pe - u(21)*(AX(21,:)*h) - h21*(AX(21,:)*v).....
       - h21*press/ct - nf*(h21-phetaref*y(41)/kads/p/(1-phetaref*y(41))^5);
```

% mol fraction of component A in the solid phase

```
yd(21) = ct*nf/zeta*(h1 - phetaref*y(21)/kads/p/(1 - phetaref*y(21))^5);
yd(22) = ct*nf/zeta*(h2 - phetaref*y(22)/kads/p/(1 - phetaref*y(22))^5);
yd(23) = ct*nf/zeta*(h3 - phetaref*y(23)/kads/p/(1 - phetaref*y(23))^5);
yd(24) = ct*nf/zeta*(h4 - phetaref*y(24)/kads/p/(1 - phetaref*y(24))^5);
yd(25) = ct*nf/zeta*(h5 - phetaref*y(25)/kads/p/(1 - phetaref*y(25))^5);
yd(26) = ct*nf/zeta*(h6 - phetaref*y(26)/kads/p/(1 - phetaref*y(26))^5);
yd(27) = ct*nf/zeta*(h7 - phetaref*y(27)/kads/p/(1 - phetaref*y(27))^5);
yd(28) = ct*nf/zeta*(h8 - phetaref*y(28)/kads/p/(1 - phetaref*y(28))^5);
yd(29) = ct*nf/zeta*(h9 - phetaref*y(29)/kads/p/(1 - phetaref*y(29))^5);
yd(30) = ct*nf/zeta*(h10 - phetaref*y(30)/kads/p/(1 - phetaref*y(30))^5);
yd(31) = ct*nf/zeta*(h11 - phetaref*y(31)/kads/p/(1 - phetaref*y(31))^5);
yd(32) = ct*nf/zeta*(h12 - phetaref*y(32)/kads/p/(1 - phetaref*y(32))^5);
yd(33) = ct*nf/zeta*(h13 - phetaref*y(33)/kads/p/(1 - phetaref*y(33))^5);
yd(34) = ct*nf/zeta*(h14 - phetaref*y(34)/kads/p/(1 - phetaref*y(34))^5);
yd(35) = ct*nf/zeta*(h15 - phetaref*y(35)/kads/p/(1 - phetaref*y(35))^5);
yd(36) = ct*nf/zeta*(h16 - phetaref*y(36)/kads/p/(1 - phetaref*y(36))^5);
yd(37) = ct*nf/zeta*(h17 - phetaref*y(37)/kads/p/(1 - phetaref*y(37))^5);
yd(38) = ct*nf/zeta*(h18 - phetaref*y(38)/kads/p/(1 - phetaref*y(38))^5);
yd(39) = ct*nf/zeta*(h19 - phetaref*y(39)/kads/p/(1 - phetaref*y(39))^5);
yd(40) = ct*nf/zeta*(h20 - phetaref*y(40)/kads/p/(1 - phetaref*y(40))^5);
yd(41) = ct*nf/zeta*(h21 - phetaref*y(41)/kads/p/(1 - phetaref*y(41))^5);
yd(42) = ct*nf/zeta*(h22 - phetaref*y(42)/kads/p/(1 - phetaref*y(42))^5);
```

% mol fraction of component B in the gas phase

```
yd(43) = (BX(2,:)*g)/pe - u(2)*(AX(2,:)*g) - g2*(AX(2,:)*v) - g2*press/ct;
yd(44) = (BX(3,:)*g)/pe - u(3)*(AX(3,:)*g) - g3*(AX(3,:)*v) - g3*press/ct;
yd(45) = (BX(4,:)*g)/pe - u(4)*(AX(4,:)*g) - g4*(AX(4,:)*v) - g4*press/ct;
yd(46) = (BX(5,:)*g)/pe - u(5)*(AX(5,:)*g) - g5*(AX(5,:)*v) - g5*press/ct;
```

```
yd(47) =  (BX(6,:)*g)/pe - u(6)*(AX(6,:)*g) - g6*(AX(6,:)*v) - g6*press/ct;
yd(48) =  (BX(7,:)*g)/pe - u(7)*(AX(7,:)*g) - g7*(AX(7,:)*v) - g7*press/ct;
yd(49) =  (BX(8,:)*g)/pe - u(8)*(AX(8,:)*g) - g8*(AX(8,:)*v) - g8*press/ct;
yd(50) =  (BX(9,:)*g)/pe - u(9)*(AX(9,:)*g) - g9*(AX(9,:)*v) - g9*press/ct;

yd(51) =  (BX(10,:)*g)/pe - u(10)*(AX(10,:)*g) - g10*(AX(10,:)*v) - ....
             g10*press/ct;

yd(52) =  (BX(11,:)*g)/pe - u(11)*(AX(11,:)*g) - g11*(AX(11,:)*v) - ....
             g11*press/ct;

yd(53) =  (BX(12,:)*g)/pe - u(12)*(AX(12,:)*g) - g12*(AX(12,:)*v) - .....
             g12*press/ct;

yd(54) =  (BX(13,:)*g)/pe - u(13)*(AX(13,:)*g) - g13*(AX(13,:)*v) - ....
             g13*press/ct;

yd(55) =  (BX(14,:)*g)/pe - u(14)*(AX(14,:)*g) - g14*(AX(14,:)*v) - ....
             g14*press/ct;

yd(56) =  (BX(15,:)*g)/pe - u(15)*(AX(15,:)*g) - g15*(AX(15,:)*v) - ....
             g15*press/ct;

yd(57) =  (BX(16,:)*g)/pe - u(16)*(AX(16,:)*g) - g16*(AX(16,:)*v) - ....
             g16*press/ct;

yd(58) =  (BX(17,:)*g)/pe - u(17)*(AX(17,:)*g) - g17*(AX(17,:)*v) - ....
             g17*press/ct;

yd(59) =  (BX(18,:)*g)/pe - u(18)*(AX(18,:)*g) - g18*(AX(18,:)*v) - ....
             g18*press/ct;

yd(60) =  (BX(19,:)*g)/pe - u(19)*(AX(19,:)*g) - g19*(AX(19,:)*v) - ....
             g19*press/ct;

yd(61) =  (BX(20,:)*g)/pe - u(20)*(AX(20,:)*g) - g20*(AX(20,:)*v) - ....
             g20*press/ct;

yd(62) =  (BX(21,:)*g)/pe - u(21)*(AX(21,:)*g) - g21*(AX(21,:)*v) - ....
             g21*press/ct;
```

## A.3 Computer Program for the Isothermal PSAR Model

```
%
% this program solve the isothermal PSAR model
% N = 20 (number of collocation points at each subdomain)
%

function yd = PSAR2d20ABxx(t,y);

% fixed given data**********************************************
flux = 0.000015;          % feed molar flux; mol/cm^2/s
l = 20;                   % adsorber length; cm
uf = 0.131;               % feed velocity at high pressure; cm/s
upf = 3;                  % purge-to feed velocity ratio
yaf = 0.17;               % feed mol fraction of component A
ybf = 0.17;               % feed mol fraction of component B
tempf = 506;              % feed temperature; K
phetaref = 0.539;         % coverage of adsorbent at feed conditions
kgL = 2.23;               % mass transfer coeficient at low pressure; cm/s
kgH = 0.62;               % mass transfer coeficient at high pressure; cm/s
time = 3.0;               % dimensionless pressurization time
plow = 2.0;               % low pressure; bar
phigh = 15;               % high pressure; bar
w = 0.5;                  % dimensionless catalyst length
beta = w/(1-w);           % catalyst-to adsorbent ratio
k1 = 0.025*1.13;          % reaction rate constant; 1/s
da = 5.18;                % Damkholer number
kc = 3.31;                % reaction equilibrium constant

%ooooooooooooooooooooooooooooooooooooooooooooooooooooooooooooooo
pconstant = (phigh-plow)/time;        % bar
R = 83.14;                            % ideal gas constant; bar*cm^3/mol/K
ctf = phigh/tempf/R;  % total gas concentration at feed conditions; mol/cm^3
voidage = 0.32;       % bed porosity
density = 1.13;       % solid density: g/cm^3
mw = 72.15;           % molecular wieght for n-c5; g/mol
qmax = 13.0/100/mw ;  % maximum adsorbed concentration; mol/g
qref = phetaref*qmax;  % adsorbed concentration at feed conditions; mol/g
zeta = ((1-voidage)/voidage)*density*qref/ctf;       % mass capacity
ap = 25;                    % specific area of the pellet; 1/cm
```

```
ko = 0.0000204/1.01325; % limiting adsorption equilibrium constant: 1/bar
dh = 13.2*1000;          % heat of adsorption; cal/mol
kads = ko*exp(dh/1.987/tempf);    % adsorption equilibrium constant; 1/bar
%**************************************************************************

p = phigh;        % pressure during this step: bar
press = 0;        % pressurization rate
kg = kgH;         % mass transfer coeficient; cm/s
uo = 1;           % dimensionless inlet velocity during this step
%**************************************************************************

ct = p/phigh;                          % dimensionless total gas concentration
nf = ((1-voidage)/voidage)*ap*kg*l/uf;    % no. of film-mass transfer unit
dm = 0.77*(2/p)*(tempf/498)^1.5;          % diffusion coefficient; cm^2/s
dl = 0.7*dm;        % dispersion coefficient; cm^2/s
pe = uf*l/dl;       % peclet number
%**************************************************************************

%  coefficients for A and B matrix

%  matrix size
[m,n]=size(y);
yd=zeros(m,n);

%  assign dummy variables
h2=y(1);
h3=y(2);
h4=y(3);
h5=y(4);
h6=y(5);
h7=y(6);
h8=y(7);
h9=y(8);
h10=y(9);
h11=y(10);
h12=y(11);
h13=y(12);
h14=y(13);
h15=y(14);
h16=y(15);
```

```
h17=y(16);
h18=y(17);
h19=y(18);
h20=y(19);
h21=y(20);

h23=y(21);
h24=y(22);
h25=y(23);
h26=y(24);
h27=y(25);
h28=y(26);
h29=y(27);
h30=y(28);
h31=y(29);
h32=y(30);
h33=y(31);
h34=y(32);
h35=y(33);
h36=y(34);
h37=y(35);
h38=y(36);
h39=y(37);
h40=y(38);
h41=y(39);
h42=y(40);

q1=y(41);
q2=y(42);
q3=y(43);
q4=y(44);
q5=y(45);
q6=y(46);
q7=y(47);
q8=y(48);
q9=y(49);
q10=y(50);
q11=y(51);
q12=y(52);
q13=y(53);
```

```
q14=y(54);
q15=y(55);
q16=y(56);
q17=y(57);
q18=y(58);
q19=y(59);
q20=y(60);
q21=y(61);
q22=y(62);

g2=y(63);
g3=y(64);
g4=y(65);
g5=y(66);
g6=y(67);
g7=y(68);
g8=y(69);
g9=y(70);
g10=y(71);
g11=y(72);
g12=y(73);
g13=y(74);
g14=y(75);
g15=y(76);
g16=y(77);
g17=y(78);
g18=y(79);
g19=y(80);
g20=y(81);
g21=y(82);

g23=y(83);
g24=y(84);
g25=y(85);
g26=y(86);
g27=y(87);
g28=y(88);
g29=y(89);
g30=y(90);
g31=y(91);
```

```
g32=y(92);
g33=y(93);
g34=y(94);
g35=y(95);
g36=y(96);
g37=y(97);
g38=y(98);
g39=y(99);
g40=y(100);
g41=y(101);
g42=y(102);

hfirstin = [h2; h3; h4; h5; h6; h7; h8; h9; h10; h11; h12; .....
            h13; h14; h15; h16; h17; h18; h19; h20; h21];

hsecondin = [h23; h24; h25; h26; h27; h28; h29; h30; .....
             h31; h32; h33; h34; h35; h36; h37; h38; h39; h40; h41; h42];

gfirstin = [g2; g3; g4; g5; g6; g7; g8; g9; g10; g11; .....
            g12; g13; g14; g15; g16; g17; g18; g19; g20; g21];

gsecondin = [g23; g24; g25; g26; g27; g28; g29; .....
             g30; g31; g32; g33; g34; g35; g36; g37; g38; g39; g40; g41; g42];

%boundary conditions for component A
a1= AX(1,1) - pe*w*uo;
a2= AX(22,1);
a3= 0;
b1= AX(1,22);
b2= AX(22,22) - beta*AX(1,1);
b3= AX(22,1);
c1= 0;
c2= - beta*AX(1,22);
c3= AX(22,22);
phi1= - AX(1,2:21)*hfirstin - pe*w*yaf*uo;
phi2= beta*AX(1,2:21)*hsecondin - AX(22,2:21)*hfirstin;
phi3= - AX(22,2:21)*hsecondin;

j = [a1  b1  c1
   a2  b2  c2
```

```
    a3  b3  c3 ];

    i = [phi1
         phi2
         phi3];

     h = j\i;

     h1  = h(1);
     h22 = h(2);
     h43 = h(3);

hfirst = [h1; h2; h3; h4; h5; h6; h7; h8; h9; h10; h11; h12; .....
          h13; h14; h15; h16; h17; h18; h19; h20; h21; h22];
hsecond = [h22; h23; h24; h25; h26; h27; h28; h29; h30; .....
           h31; h32; h33; h34; h35; h36; h37; h38; h39; h40; h41; h42; h43];

%boundary conditions for component B
phi1B= - AX(1,2:21)*gfirstin - pe*w*ybf*uo;
phi2B= beta*AX(1,2:21)*gsecondin - AX(22,2:21)*gfirstin;
phi3B= - AX(22,2:21)*gsecondin;


    iB = [ phi1B
           phi2B
           phi3B ];

     g = j\iB;

     g1  = g(1);
     g22 = g(2);
     g43 = g(3);

gfirst = [g1; g2; g3; g4; g5; g6; g7; g8; g9; g10; g11; g12; .....
          g13; g14; g15; g16; g17; g18; g19; g20; g21; g22];
gsecond = [g22; g23; g24; g25; g26; g27; g28; g29; g30; .....
           g31; g32; g33; g34; g35; g36; g37; g38; g39; g40; g41; g42; g43];

%algebric eqs to solve for velocity
```

```
x=[1,zeros(1,42)
    AX(2,1:22),zeros(1,21)
    AX(3,1:22),zeros(1,21)
    AX(4,1:22),zeros(1,21)
    AX(5,1:22),zeros(1,21)
    AX(6,1:22),zeros(1,21)
    AX(7,1:22),zeros(1,21)
    AX(8,1:22),zeros(1,21)
    AX(9,1:22),zeros(1,21)
    AX(10,1:22),zeros(1,21)
    AX(11,1:22),zeros(1,21)
    AX(12,1:22),zeros(1,21)
    AX(13,1:22),zeros(1,21)
    AX(14,1:22),zeros(1,21)
    AX(15,1:22),zeros(1,21)
    AX(16,1:22),zeros(1,21)
    AX(17,1:22),zeros(1,21)
    AX(18,1:22),zeros(1,21)
    AX(19,1:22),zeros(1,21)
    AX(20,1:22),zeros(1,21)
    AX(21,1:22),zeros(1,21)
    (1-w)*AX(22,1:21),(1-w)*AX(22,22) - w*AX(1,1), - w*AX(1,2:22)
    zeros(1,21),AX(2,1:22)
    zeros(1,21),AX(3,1:22)
    zeros(1,21),AX(4,1:22)
    zeros(1,21),AX(5,1:22)
    zeros(1,21),AX(6,1:22)
    zeros(1,21),AX(7,1:22)
    zeros(1,21),AX(8,1:22)
    zeros(1,21),AX(9,1:22)
    zeros(1,21),AX(10,1:22)
    zeros(1,21),AX(11,1:22)
    zeros(1,21),AX(12,1:22)
    zeros(1,21),AX(13,1:22)
    zeros(1,21),AX(14,1:22)
    zeros(1,21),AX(15,1:22)
    zeros(1,21),AX(16,1:22)
    zeros(1,21),AX(17,1:22)
    zeros(1,21),AX(18,1:22)
    zeros(1,21),AX(19,1:22)
```

```
    zeros(1,21),AX(20,1:22)
    zeros(1,21),AX(21,1:22)
    zeros(1,21),AX(22,1:22)];

 z = [ uo
  - w*press/ct
  - w*press/ct
  - w*press/ct
  - w*press/ct
  - w*press/ct
  - w*press/ct
  - w*press/ct
  - w*press/ct
  - w*press/ct
  - w*press/ct
  - w*press/ct
  - w*press/ct
  - w*press/ct
  - w*press/ct
  - w*press/ct
  - w*press/ct
  - w*press/ct
  - w*press/ct
  - w*press/ct
  - w*press/ct
  - w*press/ct
  0

 - (1-w)*press/ct - (1-w)*nf*(h23-phetaref*y(42)/kads/p/(1- .....
phetaref*y(42))^5)

 - (1-w)*press/ct - (1-w)*nf*(h24-phetaref*y(43)/kads/p/(1-....
phetaref*y(43))^5)

- (1-w)*press/ct - (1-w)*nf*(h25-phetaref*y(44)/kads/p/(1-....
phetaref*y(44))^5)

- (1-w)*press/ct - (1-w)*nf*(h26-phetaref*y(45)/kads/p/(1- ....
phetaref*y(45))^5)
```

- (1-w)*press/ct - (1-w)*nf*(h27-phetaref*y(46)/kads/p/(1- .... phetaref*y(46))^5)

- (1-w)*press/ct - (1-w)*nf*(h28-phetaref*y(47)/kads/p/(1- .... phetaref*y(47)/kads/p/(1phetaref*y(47))^5)

- (1-w)*press/ct - (1-w)*nf*(h29-phetaref*y(48)/kads/p/(1-.... phetaref*y(48))^5)

- (1-w)*press/ct - (1-w)*nf*(h30-phetaref*y(49)/kads/p/(1-..... phetaref*y(49))^5)

- (1-w)*press/ct - (1-w)*nf*(h31-phetaref*y(50)/kads/p/(1-..... phetaref*y(50))^5)

- (1-w)*press/ct - (1-w)*nf*(h32-phetaref*y(51)/kads/p/(1-..... phetaref*y(51))^5)

- (1-w)*press/ct - (1-w)*nf*(h33-phetaref*y(52)/kads/p/(1-..... phetaref*y(52))^5)

- (1-w)*press/ct - (1-w)*nf*(h34-phetaref*y(53)/kads/p/(1-..... phetaref*y(53))^5)

- (1-w)*press/ct - (1-w)*nf*(h35-phetaref*y(54)/kads/p/(1-..... phetaref*y(54))^5)

- (1-w)*press/ct - (1-w)*nf*(h36-phetaref*y(55)/kads/p/(1-..... phetaref*y(55))^5)

- (1-w)*press/ct - (1-w)*nf*(h37-phetaref*y(56)/kads/p/(1-..... phetaref*y(56))^5)

- (1-w)*press/ct - (1-w)*nf*(h38-phetaref*y(57)/kads/p/(1-..... phetaref*y(57))^5)

- (1-w)*press/ct - (1-w)*nf*(h39-phetaref*y(58)/kads/p/(1-..... phetaref*y(58))^5)

```
- (1-w)*press/ct - (1-w)*nf*(h40-phetaref*y(59)/kads/p/(1-.....
phetaref*y(59))^5)

- (1-w)*press/ct - (1-w)*nf*(h41-phetaref*y(60)/kads/p/(1-.....
phetaref*y(60))^5)

- (1-w)*press/ct - (1-w)*nf*(h42-phetaref*y(61)/kads/p/(1-.....
phetaref*y(61))^5)

0];

  u = x\z;

vfirst =  [u(1); u(2); u(3); u(4); u(5); u(6); u(7); u(8); u(9); u(10); u(11);
u(12); u(13); u(14); u(15); u(16); u(17); u(18); u(19); u(20); u(21); u(22) ];

vsecond =  [u(22); u(23); u(24); u(25); u(26); u(27); u(28); u(29); u(30);
u(31); u(32); u(33); u(34); u(35); u(36); u(37); u(38); u(39); u(40); u(41);
u(42); u(43) ];

%ODE

%mol fraction of component A in the gas phase in the catalyst region

yd(1)= (BX(2,:)*hfirst)/(w^2*pe) - u(2)*(AX(2,:)*hfirst)/w -
          h2*(AX(2,:)*vfirst)/w - da*(h2 - g2/kc) - h2*press/ct;

yd(2)= (BX(3,:)*hfirst)/(w^2*pe) - u(3)*(AX(3,:)*hfirst)/w -
          h3*(AX(3,:)*vfirst)/w - da*(h3 - g3/kc) - h3*press/ct;

yd(3)= (BX(4,:)*hfirst)/(w^2*pe) - u(4)*(AX(4,:)*hfirst)/w -
          h4*(AX(4,:)*vfirst)/w - da*(h4 - g4/kc) - h4*press/ct;

yd(4)= (BX(5,:)*hfirst)/(w^2*pe) - u(5)*(AX(5,:)*hfirst)/w -
          h5*(AX(5,:)*vfirst)/w - da*(h5 - g5/kc) - h5*press/ct;

yd(5)= (BX(6,:)*hfirst)/(w^2*pe) - u(6)*(AX(6,:)*hfirst)/w -
          h6*(AX(6,:)*vfirst)/w - da*(h6 - g6/kc) - h6*press/ct;
```

```
yd(6)= (BX(7,:)*hfirst)/(w^2*pe) - u(7)*(AX(7,:)*hfirst)/w -
          h7*(AX(7,:)*vfirst)/w - da*(h7 - g7/kc) - h7*press/ct;

yd(7)= (BX(8,:)*hfirst)/(w^2*pe) - u(8)*(AX(8,:)*hfirst)/w -
          h8*(AX(8,:)*vfirst)/w - da*(h8 - g8/kc) - h8*press/ct;

yd(8)= (BX(9,:)*hfirst)/(w^2*pe) - u(9)*(AX(9,:)*hfirst)/w -
          h9*(AX(9,:)*vfirst)/w - da*(h9 - g9/kc) - h9*press/ct;

yd(9)= (BX(10,:)*hfirst)/(w^2*pe) - u(10)*(AX(10,:)*hfirst)/w -
          h10*(AX(10,:)*vfirst)/w - da*(h10 - g10/kc) - h10*press/ct;

yd(10)= (BX(11,:)*hfirst)/(w^2*pe) - u(11)*(AX(11,:)*hfirst)/w -
          h11*(AX(11,:)*vfirst)/w - da*(h11 - g11/kc) - h11*press/ct;

yd(11)= (BX(12,:)*hfirst)/(w^2*pe) - u(12)*(AX(12,:)*hfirst)/w -
          h12*(AX(12,:)*vfirst)/w - da*(h12 - g12/kc) - h12*press/ct;

yd(12)= (BX(13,:)*hfirst)/(w^2*pe) - u(13)*(AX(13,:)*hfirst)/w -
          h13*(AX(13,:)*vfirst)/w - da*(h13 - g13/kc) - h13*press/ct;

yd(13)= (BX(14,:)*hfirst)/(w^2*pe) - u(14)*(AX(14,:)*hfirst)/w -
          h14*(AX(14,:)*vfirst)/w - da*(h14 - g14/kc) - h14*press/ct;

yd(14)= (BX(15,:)*hfirst)/(w^2*pe) - u(15)*(AX(15,:)*hfirst)/w -
          h15*(AX(15,:)*vfirst)/w - da*(h15 - g15/kc) - h15*press/ct;

yd(15)= (BX(16,:)*hfirst)/(w^2*pe) - u(16)*(AX(16,:)*hfirst)/w -
          h16*(AX(16,:)*vfirst)/w - da*(h16 - g16/kc) - h16*press/ct;

yd(16)= (BX(17,:)*hfirst)/(w^2*pe) - u(17)*(AX(17,:)*hfirst)/w -
          h17*(AX(17,:)*vfirst)/w - da*(h17 - g17/kc) - h17*press/ct;

yd(17)= (BX(18,:)*hfirst)/(w^2*pe) - u(18)*(AX(18,:)*hfirst)/w -
          h18*(AX(18,:)*vfirst)/w - da*(h18 - g18/kc) - h18*press/ct;

yd(18)= (BX(19,:)*hfirst)/(w^2*pe) - u(19)*(AX(19,:)*hfirst)/w -
          h19*(AX(19,:)*vfirst)/w - da*(h19 - g19/kc) - h19*press/ct;
```

```
yd(19)= (BX(20,:)*hfirst)/(w^2*pe) - u(20)*(AX(20,:)*hfirst)/w -
        h20*(AX(20,:)*vfirst)/w - da*(h20 - g20/kc) - h20*press/ct;

yd(20)= (BX(21,:)*hfirst)/(w^2*pe) - u(21)*(AX(21,:)*hfirst)/w -
        h21*(AX(21,:)*vfirst)/w - da*(h21 - g21/kc) - h21*press/ct;

% mol fraction of component A in the gas phase in the adsorbent region

yd(21)= (BX(2,:)*hsecond)/((1-w)^2*pe) - u(23)*(AX(2,:)*hsecond)/(1-w) -
        h23*(AX(2,:)*vsecond)/(1-w) - h23*press/ct - nf*(h23-
        phetaref*y(42)/kads/p/(1-phetaref*y(42))^5);

yd(22)= (BX(3,:)*hsecond)/((1-w)^2*pe) - u(24)*(AX(3,:)*hsecond)/(1-w) -
        h24*(AX(3,:)*vsecond)/(1-w) - h24*press/ct - nf*(h24-
        phetaref*y(43)/kads/p/(1-phetaref*y(43))^5);

yd(23)= (BX(4,:)*hsecond)/((1-w)^2*pe) - u(25)*(AX(4,:)*hsecond)/(1-w) -
        h25*(AX(4,:)*vsecond)/(1-w) - h25*press/ct - nf*(h25-
        phetaref*y(44)/kads/p/(1-phetaref*y(44))^5);

yd(24)= (BX(5,:)*hsecond)/((1-w)^2*pe) - u(26)*(AX(5,:)*hsecond)/(1-w) -
        h26*(AX(5,:)*vsecond)/(1-w) - h26*press/ct - nf*(h26-
        phetaref*y(45)/kads/p/(1-phetaref*y(45))^5);

yd(25)= (BX(6,:)*hsecond)/((1-w)^2*pe) - u(27)*(AX(6,:)*hsecond)/(1-w) -
        h27*(AX(6,:)*vsecond)/(1-w) - h27*press/ct - nf*(h27-
        phetaref*y(46)/kads/p/(1-phetaref*y(46))^5);

yd(26)= (BX(7,:)*hsecond)/((1-w)^2*pe) - u(28)*(AX(7,:)*hsecond)/(1-w) -
        h28*(AX(7,:)*vsecond)/(1-w) - h28*press/ct - nf*(h28-
        phetaref*y(47)/kads/p/(1-phetaref*y(47))^5);

yd(27)= (BX(8,:)*hsecond)/((1-w)^2*pe) - u(29)*(AX(8,:)*hsecond)/(1-w) -
        h29*(AX(8,:)*vsecond)/(1-w) - h29*press/ct - nf*(h29-
        phetaref*y(48)/kads/p/(1-phetaref*y(48))^5);

yd(28)= (BX(9,:)*hsecond)/((1-w)^2*pe) - u(30)*(AX(9,:)*hsecond)/(1-w) -
        h30*(AX(9,:)*vsecond)/(1-w) - h30*press/ct - nf*(h30-
        phetaref*y(49)/kads/p/(1-phetaref*y(49))^5);
```

```
yd(29)= (BX(10,:)*hsecond)/((1-w)^2*pe) - u(31)*(AX(10,:)*hsecond)/(1-
        w) - h31*(AX(10,:)*vsecond)/(1-w) - h31*press/ct - nf*(h31-
        phetaref*y(50)/kads/p/(1-phetaref*y(50))^5);

yd(30)= (BX(11,:)*hsecond)/((1-w)^2*pe) - u(32)*(AX(11,:)*hsecond)/(1-
        w) - h32*(AX(11,:)*vsecond)/(1-w) - h32*press/ct - nf*(h32-
        phetaref*y(51)/kads/p/(1-phetaref*y(51))^5);

yd(31)= (BX(12,:)*hsecond)/((1-w)^2*pe) - u(33)*(AX(12,:)*hsecond)/(1-
        w) - h33*(AX(12,:)*vsecond)/(1-w) - h33*press/ct - nf*(h33-
        phetaref*y(52)/kads/p/(1-phetaref*y(52))^5);

yd(32)= (BX(13,:)*hsecond)/((1-w)^2*pe) - u(34)*(AX(13,:)*hsecond)/(1-
        w) - h34*(AX(13,:)*vsecond)/(1-w) - h34*press/ct - nf*(h34-
        phetaref*y(53)/kads/p/(1-phetaref*y(53))^5);

yd(33)= (BX(14,:)*hsecond)/((1-w)^2*pe) - u(35)*(AX(14,:)*hsecond)/(1-
        w) - h35*(AX(14,:)*vsecond)/(1-w) - h35*press/ct - nf*(h35-
        phetaref*y(54)/kads/p/(1-phetaref*y(54))^5);

yd(34)= (BX(15,:)*hsecond)/((1-w)^2*pe) - u(36)*(AX(15,:)*hsecond)/(1-
        w) - h36*(AX(15,:)*vsecond)/(1-w) - h36*press/ct - nf*(h36-
        phetaref*y(55)/kads/p/(1-phetaref*y(55))^5);

yd(35)= (BX(16,:)*hsecond)/((1-w)^2*pe) - u(37)*(AX(16,:)*hsecond)/(1-
        w) - h37*(AX(16,:)*vsecond)/(1-w) - h37*press/ct - nf*(h37-
        phetaref*y(56)/kads/p/(1-phetaref*y(56))^5);

yd(36)= (BX(17,:)*hsecond)/((1-w)^2*pe) - u(38)*(AX(17,:)*hsecond)/(1-
        w) - h38*(AX(17,:)*vsecond)/(1-w) - h38*press/ct - nf*(h38-
        phetaref*y(57)/kads/p/(1-phetaref*y(57))^5);

yd(37)= (BX(18,:)*hsecond)/((1-w)^2*pe) - u(39)*(AX(18,:)*hsecond)/(1-
        w) - h39*(AX(18,:)*vsecond)/(1-w) - h39*press/ct - nf*(h39-
        phetaref*y(58)/kads/p/(1-phetaref*y(58))^5);

yd(38)= (BX(19,:)*hsecond)/((1-w)^2*pe) - u(40)*(AX(19,:)*hsecond)/(1-
        w) - h40*(AX(19,:)*vsecond)/(1-w) - h40*press/ct - nf*(h40-
        phetaref*y(59)/kads/p/(1-phetaref*y(59))^5);
```

```
yd(39)= (BX(20,:)*hsecond)/((1-w)^2*pe) - u(41)*(AX(20,:)*hsecond)/(1-
        w) - h41*(AX(20,:)*vsecond)/(1-w) - h41*press/ct - nf*(h41-
        phetaref*y(60)/kads/p/(1-phetaref*y(60))^5);

yd(40)= (BX(21,:)*hsecond)/((1-w)^2*pe) - u(42)*(AX(21,:)*hsecond)/(1-
        w) - h42*(AX(21,:)*vsecond)/(1-w) - h42*press/ct - nf*(h42-
        phetaref*y(61)/kads/p/(1-phetaref*y(61))^5);

%mol fraction of component A in the solid phase in the adsorbent region

yd(41)= ct*nf/zeta*(h22-phetaref*y(41)/kads/p/(1-phetaref*y(41))^5);
yd(42)= ct*nf/zeta*(h23-phetaref*y(42)/kads/p/(1-phetaref*y(42))^5);
yd(43)= ct*nf/zeta*(h24-phetaref*y(43)/kads/p/(1-phetaref*y(43))^5);
yd(44)= ct*nf/zeta*(h25-phetaref*y(44)/kads/p/(1-phetaref*y(44))^5);
yd(45)= ct*nf/zeta*(h26-phetaref*y(45)/kads/p/(1-phetaref*y(45))^5);
yd(46)= ct*nf/zeta*(h27-phetaref*y(46)/kads/p/(1-phetaref*y(46))^5);
yd(47)= ct*nf/zeta*(h28-phetaref*y(47)/kads/p/(1-phetaref*y(47))^5);
yd(48)= ct*nf/zeta*(h29-phetaref*y(48)/kads/p/(1-phetaref*y(48))^5);
yd(49)= ct*nf/zeta*(h30-phetaref*y(49)/kads/p/(1-phetaref*y(49))^5);
yd(50)= ct*nf/zeta*(h31-phetaref*y(50)/kads/p/(1-phetaref*y(50))^5);
yd(51)= ct*nf/zeta*(h32-phetaref*y(51)/kads/p/(1-phetaref*y(51))^5);
yd(52)= ct*nf/zeta*(h33-phetaref*y(52)/kads/p/(1-phetaref*y(52))^5);
yd(53)= ct*nf/zeta*(h34-phetaref*y(53)/kads/p/(1-phetaref*y(53))^5);
yd(54)= ct*nf/zeta*(h35-phetaref*y(54)/kads/p/(1-phetaref*y(54))^5);
yd(55)= ct*nf/zeta*(h36-phetaref*y(55)/kads/p/(1-phetaref*y(55))^5);
yd(56)= ct*nf/zeta*(h37-phetaref*y(56)/kads/p/(1-phetaref*y(56))^5);
yd(57)= ct*nf/zeta*(h38-phetaref*y(57)/kads/p/(1-phetaref*y(57))^5);
yd(58)= ct*nf/zeta*(h39-phetaref*y(58)/kads/p/(1-phetaref*y(58))^5);
yd(59)= ct*nf/zeta*(h40-phetaref*y(59)/kads/p/(1-phetaref*y(59))^5);
yd(60)= ct*nf/zeta*(h41-phetaref*y(60)/kads/p/(1-phetaref*y(60))^5);
yd(61)= ct*nf/zeta*(h42-phetaref*y(61)/kads/p/(1-phetaref*y(61))^5);
yd(62)= ct*nf/zeta*(h43-phetaref*y(62)/kads/p/(1-phetaref*y(62))^5);

%mol fraction of component B in the gas phase in the catalyst region

yd(63)= (BX(2,:)*gfirst)/(w^2*pe) - u(2)*(AX(2,:)*gfirst)/w -
        g2*(AX(2,:)*vfirst)/w + da*(h2 - g2/kc) - g2*press/ct;

yd(64)= (BX(3,:)*gfirst)/(w^2*pe) - u(3)*(AX(3,:)*gfirst)/w -
        g3*(AX(3,:)*vfirst)/w + da*(h3 - g3/kc) - g3*press/ct;
```

```
yd(65)= (BX(4,:)*gfirst)/(w^2*pe) - u(4)*(AX(4,:)*gfirst)/w -
        g4*(AX(4,:)*vfirst)/w + da*(h4 - g4/kc) - g4*press/ct;

yd(66)= (BX(5,:)*gfirst)/(w^2*pe) - u(5)*(AX(5,:)*gfirst)/w -
        g5*(AX(5,:)*vfirst)/w + da*(h5 - g5/kc) - g5*press/ct;

yd(67)= (BX(6,:)*hfirst)/(w^2*pe) - u(6)*(AX(6,:)*gfirst)/w -
        g6*(AX(6,:)*vfirst)/w  + da*(h6 - g6/kc) - g6*press/ct;

yd(68)= (BX(7,:)*gfirst)/(w^2*pe) - u(7)*(AX(7,:)*gfirst)/w -
        g7*(AX(7,:)*vfirst)/w  + da*(h7 - g7/kc) - g7*press/ct;

yd(69)= (BX(8,:)*gfirst)/(w^2*pe) - u(8)*(AX(8,:)*gfirst)/w -
        g8*(AX(8,:)*vfirst)/w + da*(h8 - g8/kc) - g8*press/ct;

yd(70)= (BX(9,:)*gfirst)/(w^2*pe) - u(9)*(AX(9,:)*gfirst)/w -
        g9*(AX(9,:)*vfirst)/w  + da*(h9 - g9/kc) - g9*press/ct;

yd(71)= (BX(10,:)*gfirst)/(w^2*pe) - u(10)*(AX(10,:)*gfirst)/w -
        g10*(AX(10,:)*vfirst)/w + da*(h10 - g10/kc) - g10*press/ct;

yd(72)= (BX(11,:)*gfirst)/(w^2*pe) - u(11)*(AX(11,:)*gfirst)/w -
        g11*(AX(11,:)*vfirst)/w + da*(h11 - g11/kc) - g11*press/ct;

yd(73)= (BX(12,:)*gfirst)/(w^2*pe) - u(12)*(AX(12,:)*gfirst)/w -
        g12*(AX(12,:)*vfirst)/w + da*(h12 - g12/kc) - g12*press/ct;

yd(74)= (BX(13,:)*gfirst)/(w^2*pe) - u(13)*(AX(13,:)*gfirst)/w -
        g13*(AX(13,:)*vfirst)/w + da*(h13 - g13/kc) - g13*press/ct;

yd(75)= (BX(14,:)*gfirst)/(w^2*pe) - u(14)*(AX(14,:)*gfirst)/w -
        g14*(AX(14,:)*vfirst)/w + da*(h14 - g14/kc) - g14*press/ct;

yd(76)= (BX(15,:)*gfirst)/(w^2*pe) - u(15)*(AX(15,:)*gfirst)/w -
        g15*(AX(15,:)*vfirst)/w + da*(h15 - g15/kc) - g15*press/ct;

yd(77)= (BX(16,:)*gfirst)/(w^2*pe) - u(16)*(AX(16,:)*gfirst)/w -
        g16*(AX(16,:)*vfirst)/w + da*(h16 - g16/kc) - g16*press/ct;
```

```
yd(78)= (BX(17,:)*gfirst)/(w^2*pe) - u(17)*(AX(17,:)*gfirst)/w -
        g17*(AX(17,:)*vfirst)/w + da*(h17 - g17/kc) - g17*press/ct;

yd(79)= (BX(18,:)*gfirst)/(w^2*pe) - u(18)*(AX(18,:)*gfirst)/w -
        g18*(AX(18,:)*vfirst)/w + da*(h18 - g18/kc) - g18*press/ct;

yd(80)= (BX(19,:)*gfirst)/(w^2*pe) - u(19)*(AX(19,:)*gfirst)/w -
        g19*(AX(19,:)*vfirst)/w + da*(h19 - g19/kc) - g19*press/ct;

yd(81)= (BX(20,:)*gfirst)/(w^2*pe) - u(20)*(AX(20,:)*gfirst)/w -
        g20*(AX(20,:)*vfirst)/w + da*(h20 - g20/kc) - g20*press/ct;

yd(82)= (BX(21,:)*gfirst)/(w^2*pe) - u(21)*(AX(21,:)*gfirst)/w -
        g21*(AX(21,:)*vfirst)/w + da*(h21 - g21/kc) - g21*press/ct;

%mol fraction of component B in the gas phase in the adsorbent region

yd(83)= (BX(2,:)*gsecond)/((1-w)^2*pe) - u(23)*(AX(2,:)*gsecond)/(1-w) -
        g23*(AX(2,:)*vsecond)/(1-w) - g23*press/ct ;

yd(84)= (BX(3,:)*gsecond)/((1-w)^2*pe) - u(24)*(AX(3,:)*gsecond)/(1-w) -
        g24*(AX(3,:)*vsecond)/(1-w) - g24*press/ct ;

yd(85)= (BX(4,:)*gsecond)/((1-w)^2*pe) - u(25)*(AX(4,:)*gsecond)/(1-w) -
        g25*(AX(4,:)*vsecond)/(1-w) - g25*press/ct ;

yd(86)= (BX(5,:)*gsecond)/((1-w)^2*pe) - u(26)*(AX(5,:)*gsecond)/(1-w) -
        g26*(AX(5,:)*vsecond)/(1-w) - g26*press/ct ;

yd(87)= (BX(6,:)*gsecond)/((1-w)^2*pe) - u(27)*(AX(6,:)*gsecond)/(1-w) -
        g27*(AX(6,:)*vsecond)/(1-w) - g27*press/ct ;

yd(88)= (BX(7,:)*gsecond)/((1-w)^2*pe) - u(28)*(AX(7,:)*gsecond)/(1-w) -
        g28*(AX(7,:)*vsecond)/(1-w) - g28*press/ct ;

yd(89)= (BX(8,:)*gsecond)/((1-w)^2*pe) - u(29)*(AX(8,:)*gsecond)/(1-w) -
        g29*(AX(8,:)*vsecond)/(1-w) - g29*press/ct ;

yd(90)= (BX(9,:)*gsecond)/((1-w)^2*pe) - u(30)*(AX(9,:)*gsecond)/(1-w) -
        g30*(AX(9,:)*vsecond)/(1-w) - g30*press/ct ;
```

```
yd(91)= (BX(10,:)*gsecond)/((1-w)^2*pe) - u(31)*(AX(10,:)*gsecond)/(1-
        w) - g31*(AX(10,:)*vsecond)/(1-w) - g31*press/ct ;

yd(92)= (BX(11,:)*gsecond)/((1-w)^2*pe) - u(32)*(AX(11,:)*gsecond)/(1-
        w) - g32*(AX(11,:)*vsecond)/(1-w) - g32*press/ct ;

yd(93)= (BX(12,:)*gsecond)/((1-w)^2*pe) - u(33)*(AX(12,:)*gsecond)/(1-
        w) - g33*(AX(12,:)*vsecond)/(1-w) - g33*press/ct ;

yd(94)= (BX(13,:)*gsecond)/((1-w)^2*pe) - u(34)*(AX(13,:)*gsecond)/(1-
        w) - g34*(AX(13,:)*vsecond)/(1-w) - g34*press/ct ;

yd(95)= (BX(14,:)*gsecond)/((1-w)^2*pe) - u(35)*(AX(14,:)*gsecond)/(1-
        w) - g35*(AX(14,:)*vsecond)/(1-w)  - g35*press/ct ;

yd(96)= (BX(15,:)*gsecond)/((1-w)^2*pe) - u(36)*(AX(15,:)*gsecond)/(1-
        w) - g36*(AX(15,:)*vsecond)/(1-w) - g36*press/ct ;

yd(97)= (BX(16,:)*gsecond)/((1-w)^2*pe) - u(37)*(AX(16,:)*gsecond)/(1-
        w) - g37*(AX(16,:)*vsecond)/(1-w) - g37*press/ct ;

yd(98)= (BX(17,:)*gsecond)/((1-w)^2*pe) - u(38)*(AX(17,:)*gsecond)/(1-
        w) - g38*(AX(17,:)*vsecond)/(1-w) - g38*press/ct ;

yd(99)= (BX(18,:)*gsecond)/((1-w)^2*pe) - u(39)*(AX(18,:)*gsecond)/(1-
        w) - g39*(AX(18,:)*vsecond)/(1-w) - g39*press/ct ;

yd(100)= (BX(19,:)*gsecond)/((1-w)^2*pe) - u(40)*(AX(19,:)*gsecond)/(1-
        w) - g40*(AX(19,:)*vsecond)/(1-w) - g40*press/ct ;

yd(101)= (BX(20,:)*gsecond)/((1-w)^2*pe) - u(41)*(AX(20,:)*gsecond)/(1-
        w) - g41*(AX(20,:)*vsecond)/(1-w) - g41*press/ct ;

yd(102)= (BX(21,:)*gsecond)/((1-w)^2*pe) - u(42)*(AX(21,:)*gsecond)/(1-
        w) - g42*(AX(21,:)*vsecond)/(1-w) - g42*press/ct ;
```

## A.4 Computer Program for the Nonisothermal PSA Model

```
%
% this program solve the nonisothermal PSA model
% N = 20 (number of collocation points)
%

function yd=adsorption20ABT(t,y);

% fixed given data**********************************************
flux = 0.000015;          % feed molar flux; mol/cm^2/s
l = 20;                   % adsorber length; cm
dc = 3.35;                % adsorber diameter; cm
uf = 0.131;               % feed velocity at high pressure; cm/s
upf = 3;                  % purge-to feed velocity ratio
yaf = 0.17;               %feed mol fraction of component A
ybf = 0.17;               %feed mol fraction of component B
tempf = 506;              % feed temperature; K
phetaref = 0.539;         % coverage of adsorbent at feed conditions
kgL = 2.23;               % mass transfer coeficient at low pressure; cm/s
kgH = 0.62;               % mass transfer coeficient at high pressure; cm/s
time = 3.0;               % dimensionless pressurization time
plow = 2.0;               % low pressure; bar
phigh = 15;               % high pressure; bar

kl = 0.01;                % axial thermal conductivity; W/cm/K
cpg = 82.06;              % heat capacity of the gas; J/mol/K
cps = 0.9;                % heat capacity of the solid; J/g/K
hw = 0.002;               % heat transfer coeficient; W/cm^2/K

%ooooooooooooooooooooooooooooooooooooooooooooooooooooooooooooo
pconstant = (phigh-plow)/time;      % bar
R = 83.14;                          % ideal gas constant; bar*cm^3/mol/K
ctf = phigh/tempf/R;  % total gas concentration at feed conditions; mol/cm^3
voidage = 0.32;           % bed porosity
density = 1.13;           % solid density; g/cm^3
mw = 72.15;               % molecular wieght for n-c5; g/mol
qmax = 13.0/100/mw ;   % maximum adsorbed concentration; mol/g
qref = phetaref*qmax;   % adsorbed concentration at feed conditions; mol/g
zeta = ((1-voidage)/voidage)*density*qref/ctf;    % mass capacity factor
```

```
ap = 25;                        % specific area of the pellet; 1/cm
ko = 0.0000204/1.01325;  % limiting adsorption equilibrium constant; 1/bar
dh = 13.2*1000;                % heat of adsorption; cal/mol
kads = ko*exp(dh/1.987/tempf);  % adsorption equilibrium constant; 1/bar
%**********************************************************

p = phigh;      % pressure during this step; bar
press = 0;      % pressurization rate
kg = kgH;       % mass transfer coeficient; cm/s
uo = 1;         % dimensionless inlet velocity during this step
%**********************************************************

ct = p/phigh;                                % dimensionless total gas concentration
nf = ((1-voidage)/voidage)*ap*kg*l/uf;    % no. of film-mass transfer unit
dm = 0.77*(2/p)*(tempf/498)^1.5;          % diffusion coefficient; cm^2/s
dl = 0.7*dm;                                 % dispersion coefficient; cm^2/s
pe = uf*l/dl;                                % mass peclet number

peh = l*uf*ctf*cpg/kl;                       % heat peclet number
zetah = ((1-voidage)/voidage)*density*cps/ctf/cpg;  % heat capacity factor
B = dh*qref/tempf/cps;                       % adiabatic temperature rise
nw = 4*hw*l/voidage/dc/uf/ctf/cpg;           % no. of wall-heat transfer unit
arh = dh/1.987/tempf;                        % arhenius number
%**********************************************************

% coefficients for A and B matrix
matrixab20

% matrix size
[m,n]=size(y);
yd=zeros(m,n);

% assign dummy variables
h2=y(1);
h3=y(2);
h4=y(3);
h5=y(4);
h6=y(5);
h7=y(6);
h8=y(7);
```

```
h9=y(8);
h10=y(9);
h11=y(10);
h12=y(11);
h13=y(12);
h14=y(13);
h15=y(14);
h16=y(15);
h17=y(16);
h18=y(17);
h19=y(18);
h20=y(19);
h21=y(20);

q1=y(21);
q2=y(22);
q3=y(23);
q4=y(24);
q5=y(25);
q6=y(26);
q7=y(27);
q8=y(28);
q9=y(29);
q10=y(30);
q11=y(31);
q12=y(32);
q13=y(33);
q14=y(34);
q15=y(35);
q16=y(36);
q17=y(37);
q18=y(38);
q19=y(39);
q20=y(40);
q21=y(41);
q22=y(42);

g2=y(43);
g3=y(44);
g4=y(45);
```

```
g5=y(46);
g6=y(47);
g7=y(48);
g8=y(49);
g9=y(50);
g10=y(51);
g11=y(52);
g12=y(53);
g13=y(54);
g14=y(55);
g15=y(56);
g16=y(57);
g17=y(58);
g18=y(59);
g19=y(60);
g20=y(61);
g21=y(62);

t2=y(63);
t3=y(64);
t4=y(65);
t5=y(66);
t6=y(67);
t7=y(68);
t8=y(69);
t9=y(70);
t10=y(71);
t11=y(72);
t12=y(73);
t13=y(74);
t14=y(75);
t15=y(76);
t16=y(77);
t17=y(78);
t18=y(79);
t19=y(80);
t20=y(81);
t21=y(82);

% boundary conditions for heat balance eq.:
```

```
tin = [ t2; t3; t4; t5; t6; t7; t8; t9; t10; t11; t12; t13; t14; t15; t16; t17; t18;
        t19; t20; t21];

a1= AX(1,1) - peh;
a2= AX(22,1);
b1= AX(1,22);
b2= AX(22,22);

phi1= - AX(1,2:21)*tin;
phi2= - AX(22,2:21)*tin;

xx = [a1, b1
      a2, b2];

  zz = [phi1
        phi2];

    tt = xx\zz;
    t1 = tt(1);
    t22 = tt(2) ;

temp = [ t1; t2; t3; t4; t5; t6; t7; t8; t9; t10; t11; t12; t13; t14; t15; t16; t17;
           t18; t19; t20; t21; t22];

% temperature dependance of adsorption equlibrium constant
kads1 = ko*exp(arh/(t1+1));
kads2 = ko*exp(arh/(t2+1));
kads3 = ko*exp(arh/(t3+1));
kads4 = ko*exp(arh/(t4+1));
kads5 = ko*exp(arh/(t5+1));
kads6 = ko*exp(arh/(t6+1));
kads7 = ko*exp(arh/(t7+1));
kads8 = ko*exp(arh/(t8+1));
kads9 = ko*exp(arh/(t9+1));
kads10 = ko*exp(arh/(t10+1));
kads11 = ko*exp(arh/(t11+1));
kads12 = ko*exp(arh/(t12+1));
kads13 = ko*exp(arh/(t13+1));
kads14 = ko*exp(arh/(t14+1));
```

```
kads15 = ko*exp(arh/(t15+1));
kads16 = ko*exp(arh/(t16+1));
kads17 = ko*exp(arh/(t17+1));
kads18 = ko*exp(arh/(t18+1));
kads19 = ko*exp(arh/(t19+1));
kads20 = ko*exp(arh/(t20+1));
kads21 = ko*exp(arh/(t21+1));
kads22 = ko*exp(arh/(t22+1));

%algebraic eqs to solve for velocity

x = [1,zeros(1,21)
    AX(2,1:22)
    AX(3,1:22)
    AX(4,1:22)
    AX(5,1:22)
    AX(6,1:22)
    AX(7,1:22)
    AX(8,1:22)
    AX(9,1:22)
    AX(10,1:22)
    AX(11,1:22)
    AX(12,1:22)
    AX(13,1:22)
    AX(14,1:22)
    AX(15,1:22)
    AX(16,1:22)
    AX(17,1:22)
    AX(18,1:22)
    AX(19,1:22)
    AX(20,1:22)
    AX(21,1:22)
    AX(22,1:22)];

z=[ uo
    - press/ct - nf*(h2-phetaref*y(22)/kads2/p/(1-phetaref*y(22))^5)
    - press/ct - nf*(h3-phetaref*y(23)/kads3/p/(1-phetaref*y(23))^5)
    - press/ct - nf*(h4-phetaref*y(24)/kads4/p/(1-phetaref*y(24))^5)
    - press/ct - nf*(h5-phetaref*y(25)/kads5/p/(1-phetaref*y(25))^5)
    - press/ct - nf*(h6-phetaref*y(26)/kads6/p/(1-phetaref*y(26))^5)
```

```
      - press/ct - nf*(h7-phetaref*y(27)/kads7/p/(1-phetaref*y(27))^5)
      - press/ct - nf*(h8-phetaref*y(28)/kads8/p/(1-phetaref*y(28))^5)
      - press/ct - nf*(h9-phetaref*y(29)/kads9/p/(1-phetaref*y(29))^5)
      - press/ct - nf*(h10-phetaref*y(30)/kads10/p/(1-phetaref*y(30))^5)
      - press/ct - nf*(h11-phetaref*y(31)/kads11/p/(1-phetaref*y(31))^5)
      - press/ct - nf*(h12-phetaref*y(32)/kads12/p/(1-phetaref*y(32))^5)
      - press/ct - nf*(h13-phetaref*y(33)/kads13/p/(1-phetaref*y(33))^5)
      - press/ct - nf*(h14-phetaref*y(34)/kads14/p/(1-phetaref*y(34))^5)
      - press/ct - nf*(h15-phetaref*y(35)/kads15/p/(1-phetaref*y(35))^5)
      - press/ct - nf*(h16-phetaref*y(36)/kads16/p/(1-phetaref*y(36))^5)
      - press/ct - nf*(h17-phetaref*y(37)/kads17/p/(1-phetaref*y(37))^5)
      - press/ct - nf*(h18-phetaref*y(38)/kads18/p/(1-phetaref*y(38))^5)
      - press/ct - nf*(h19-phetaref*y(39)/kads19/p/(1-phetaref*y(39))^5)
      - press/ct - nf*(h20-phetaref*y(40)/kads20/p/(1-phetaref*y(40))^5)
      - press/ct - nf*(h21-phetaref*y(41)/kads21/p/(1-phetaref*y(41))^5)
       0];

  u = x\z;

% boundary conditions for mass balance eq of component A:
hin = [ h2; h3; h4; h5; h6; h7; h8; h9; h10; h11; h12; h13; h14; h15; h16;
          h17; h18; h19; h20; h21]; % internal nodes

a1= AX(1,1) - uo*pe;
a2= AX(22,1);
b1= AX(1,22);
b2= AX(22,22);

phi1= - AX(1,2:21)*hin - yaf*uo*pe ;
phi2= - AX(22,2:21)*hin;

xx = [a1, b1
      a2, b2];

  zz = [phi1
        phi2];

    hh = xx\zz;
    h1 = hh(1);
    h22 = hh(2) ;
```

```
v = [u(1); u(2); u(3); u(4); u(5); u(6); u(7); u(8); u(9); u(10); u(11); u(12);
        u(13); u(14); u(15); u(16); u(17); u(18); u(19); u(20); u(21); u(22) ] ;
        % velocity at all nodes

h = [ h1; h2; h3; h4; h5; h6; h7; h8; h9; h10; h11; h12; h13; h14; h15; h16;
        h17; h18; h19; h20; h21; h22]; % mol fraction at all nodes


% boundary conditions for mass balance eq of component B:
gin = [g2;g3;g4;g5;g6;g7;g8;g9;g10;g11;g12;g13;g14;
        g15;g16;g17;g18;g19;g20;g21]; % internal nodes

phi1b = - AX(1,2:21)*gin - ybf*uo*pe;
phi2b = - AX(22,2:21)*gin;

xx = [a1, b1
      a2, b2];

  zz = [phi1b
        phi2b];

    gg = xx\zz;
    g1 = gg(1);
    g22 = gg(2) ;

g = [g1;g2;g3;g4;g5;g6;g7;g8;g9;g10;g11;g12;g13;g14;
     g15;g16;g17;g18;g19;g20;g21;g22]; % internal nodes

%ODE

% mol fraction of component A in the gas phase

yd(1)= (BX(2,:)*h)/pe - u(2)*(AX(2,:)*h) - h2*(AX(2,:)*v)...
     - h2*press/ct - nf*(h2-phetaref*y(22)/kads2/p/(1-phetaref*y(22))^5);

yd(2)= (BX(3,:)*h)/pe - u(3)*(AX(3,:)*h) - h3*(AX(3,:)*v)...
     - h3*press/ct - nf*(h3-phetaref*y(23)/kads3/p/(1-phetaref*y(23))^5);
```

```
yd(3)= (BX(4,:)*h)/pe - u(4)*(AX(4,:)*h) - h4*(AX(4,:)*v)...
      - h4*press/ct - nf*(h4-phetaref*y(24)/kads4/p/(1-phetaref*y(24))^5);

yd(4)= (BX(5,:)*h)/pe - u(5)*(AX(5,:)*h) - h5*(AX(5,:)*v)...
      - h5*press/ct - nf*(h5-phetaref*y(25)/kads5/p/(1-phetaref*y(25))^5);

yd(5)= (BX(6,:)*h)/pe - u(6)*(AX(6,:)*h) - h6*(AX(6,:)*v)...
      - h6*press/ct - nf*(h6-phetaref*y(26)/kads6/p/(1-phetaref*y(26))^5);

yd(6)= (BX(7,:)*h)/pe - u(7)*(AX(7,:)*h) - h7*(AX(7,:)*v)...
      - h7*press/ct - nf*(h7-phetaref*y(27)/kads7/p/(1-phetaref*y(27))^5);

yd(7)= (BX(8,:)*h)/pe - u(8)*(AX(8,:)*h) - h8*(AX(8,:)*v)...
      - h8*press/ct - nf*(h8-phetaref*y(28)/kads8/p/(1-phetaref*y(28))^5);

yd(8)= (BX(9,:)*h)/pe - u(9)*(AX(9,:)*h) - h9*(AX(9,:)*v) - h9*press/ct -
        nf*(h9-phetaref*y(29)/kads9/p/(1-phetaref*y(29))^5);

yd(9)= (BX(10,:)*h)/pe - u(10)*(AX(10,:)*h) - h10*(AX(10,:)*v) -
        h10*press/ct - nf*(h10-phetaref*y(30)/kads10/p/(1-
        phetaref*y(30))^5);

yd(10)= (BX(11,:)*h)/pe - u(11)*(AX(11,:)*h) - h11*(AX(11,:)*v)...
      - h11*press/ct - nf*(h11-phetaref*y(31)/kads11/p/(1-
        phetaref*y(31))^5);

yd(11)= (BX(12,:)*h)/pe - u(12)*(AX(12,:)*h) - h12*(AX(12,:)*v)...
      - h12*press/ct - nf*(h12-phetaref*y(32)/kads12/p/(1-
        phetaref*y(32))^5);

yd(12)= (BX(13,:)*h)/pe - u(13)*(AX(13,:)*h) - h13*(AX(13,:)*v)...
      - h13*press/ct - nf*(h13-phetaref*y(33)/kads13/p/(1-
        phetaref*y(33))^5);

yd(13)= (BX(14,:)*h)/pe - u(14)*(AX(14,:)*h) - h14*(AX(14,:)*v)...
      - h14*press/ct - nf*(h14-phetaref*y(34)/kads14/p/(1-
        phetaref*y(34))^5);
```

```
yd(14)= (BX(15,:)*h)/pe - u(15)*(AX(15,:)*h) - h15*(AX(15,:)*v)...
      - h15*press/ct - nf*(h15-phetaref*y(35)/kads15/p/(1-
        phetaref*y(35))^5);

yd(15)= (BX(16,:)*h)/pe - u(16)*(AX(16,:)*h) - h16*(AX(16,:)*v)...
      - h16*press/ct - nf*(h16-phetaref*y(36)/kads16/p/(1-
        phetaref*y(36))^5);

yd(16)= (BX(17,:)*h)/pe - u(17)*(AX(17,:)*h) - h17*(AX(17,:)*v)...
      - h17*press/ct - nf*(h17-phetaref*y(37)/kads17/p/(1-
        phetaref*y(37))^5);

yd(17)= (BX(18,:)*h)/pe - u(18)*(AX(18,:)*h) - h18*(AX(18,:)*v)...
      - h18*press/ct - nf*(h18-phetaref*y(38)/kads18/p/(1-
        phetaref*y(38))^5);

yd(18)= (BX(19,:)*h)/pe - u(19)*(AX(19,:)*h) - h19*(AX(19,:)*v)...
      - h19*press/ct - nf*(h19-phetaref*y(39)/kads19/p/(1-
        phetaref*y(39))^5);

yd(19)= (BX(20,:)*h)/pe - u(20)*(AX(20,:)*h) - h20*(AX(20,:)*v)...
      - h20*press/ct - nf*(h20-phetaref*y(40)/kads20/p/(1-
        phetaref*y(40))^5);

yd(20)= (BX(21,:)*h)/pe - u(21)*(AX(21,:)*h) - h21*(AX(21,:)*v)...
      - h21*press/ct - nf*(h21-phetaref*y(41)/kads21/p/(1-
        phetaref*y(41))^5);


% mol fraction of component A in the solid phase

yd(21)= ct*nf/zeta*(h1-phetaref*y(21)/kads1/p/(1-phetaref*y(21))^5);
yd(22)= ct*nf/zeta*(h2-phetaref*y(22)/kads2/p/(1-phetaref*y(22))^5);
yd(23)= ct*nf/zeta*(h3-phetaref*y(23)/kads3/p/(1-phetaref*y(23))^5);
yd(24)= ct*nf/zeta*(h4-phetaref*y(24)/kads4/p/(1-phetaref*y(24))^5);
yd(25)= ct*nf/zeta*(h5-phetaref*y(25)/kads5/p/(1-phetaref*y(25))^5);
yd(26)= ct*nf/zeta*(h6-phetaref*y(26)/kads6/p/(1-phetaref*y(26))^5);
yd(27)= ct*nf/zeta*(h7-phetaref*y(27)/kads7/p/(1-phetaref*y(27))^5);
yd(28)= ct*nf/zeta*(h8-phetaref*y(28)/kads8/p/(1-phetaref*y(28))^5);
yd(29)= ct*nf/zeta*(h9-phetaref*y(29)/kads9/p/(1-phetaref*y(29))^5);
```

```
yd(30)= ct*nf/zeta*(h10-phetaref*y(30)/kads10/p/(1-phetaref*y(30))^5);
yd(31)= ct*nf/zeta*(h11-phetaref*y(31)/kads11/p/(1-phetaref*y(31))^5);
yd(32)= ct*nf/zeta*(h12-phetaref*y(32)/kads12/p/(1-phetaref*y(32))^5);
yd(33)= ct*nf/zeta*(h13-phetaref*y(33)/kads13/p/(1-phetaref*y(33))^5);
yd(34)= ct*nf/zeta*(h14-phetaref*y(34)/kads14/p/(1-phetaref*y(34))^5);
yd(35)= ct*nf/zeta*(h15-phetaref*y(35)/kads15/p/(1-phetaref*y(35))^5);
yd(36)= ct*nf/zeta*(h16-phetaref*y(36)/kads16/p/(1-phetaref*y(36))^5);
yd(37)= ct*nf/zeta*(h17-phetaref*y(37)/kads17/p/(1-phetaref*y(37))^5);
yd(38)= ct*nf/zeta*(h18-phetaref*y(38)/kads18/p/(1-phetaref*y(38))^5);
yd(39)= ct*nf/zeta*(h19-phetaref*y(39)/kads19/p/(1-phetaref*y(39))^5);
yd(40)= ct*nf/zeta*(h20-phetaref*y(40)/kads20/p/(1-phetaref*y(40))^5);
yd(41)= ct*nf/zeta*(h21-phetaref*y(41)/kads21/p/(1-phetaref*y(41))^5);
yd(42)= ct*nf/zeta*(h22-phetaref*y(42)/kads22/p/(1-phetaref*y(42))^5);

% mol fraction of component B in the gas phase

yd(43)= (BX(2,:)*g)/pe - u(2)*(AX(2,:)*g) - g2*(AX(2,:)*v) - g2*press/ct;
yd(44)= (BX(3,:)*g)/pe - u(3)*(AX(3,:)*g) - g3*(AX(3,:)*v) - g3*press/ct;
yd(45)= (BX(4,:)*g)/pe - u(4)*(AX(4,:)*g) - g4*(AX(4,:)*v) - g4*press/ct;
yd(46)= (BX(5,:)*g)/pe - u(5)*(AX(5,:)*g) - g5*(AX(5,:)*v) - g5*press/ct;
yd(47)= (BX(6,:)*g)/pe - u(6)*(AX(6,:)*g) - g6*(AX(6,:)*v) - g6*press/ct;
yd(48)= (BX(7,:)*g)/pe - u(7)*(AX(7,:)*g) - g7*(AX(7,:)*v) - g7*press/ct;
yd(49)= (BX(8,:)*g)/pe - u(8)*(AX(8,:)*g) - g8*(AX(8,:)*v) - g8*press/ct;
yd(50)= (BX(9,:)*g)/pe - u(9)*(AX(9,:)*g) - g9*(AX(9,:)*v) - g9*press/ct;

yd(51)= (BX(10,:)*g)/pe - u(10)*(AX(10,:)*g) - g10*(AX(10,:)*v) -
        g10*press/ct;

yd(52)= (BX(11,:)*g)/pe - u(11)*(AX(11,:)*g) - g11*(AX(11,:)*v) -
        g11*press/ct;
yd(53)= (BX(12,:)*g)/pe - u(12)*(AX(12,:)*g) - g12*(AX(12,:)*v) -
g12*press/ct;

yd(54)= (BX(13,:)*g)/pe - u(13)*(AX(13,:)*g) - g13*(AX(13,:)*v) -
        g13*press/ct;

yd(55)= (BX(14,:)*g)/pe - u(14)*(AX(14,:)*g) - g14*(AX(14,:)*v) -
        g14*press/ct;
```

```
yd(56)= (BX(15,:)*g)/pe - u(15)*(AX(15,:)*g) - g15*(AX(15,:)*v) -
        g15*press/ct;

yd(57)= (BX(16,:)*g)/pe - u(16)*(AX(16,:)*g) - g16*(AX(16,:)*v) -
        g16*press/ct;

yd(58)= (BX(17,:)*g)/pe - u(17)*(AX(17,:)*g) - g17*(AX(17,:)*v) -
        g17*press/ct;

yd(59)= (BX(18,:)*g)/pe - u(18)*(AX(18,:)*g) - g18*(AX(18,:)*v) -
        g18*press/ct;

yd(60)= (BX(19,:)*g)/pe - u(19)*(AX(19,:)*g) - g19*(AX(19,:)*v) -
        g19*press/ct;

yd(61)= (BX(20,:)*g)/pe - u(20)*(AX(20,:)*g) - g20*(AX(20,:)*v) -
        g20*press/ct;

yd(62)= (BX(21,:)*g)/pe - u(21)*(AX(21,:)*g) - g21*(AX(21,:)*v) -
        g21*press/ct;

%**********************************************************************

% temperature profile eqs in the gas phase:

yd(63)= (BX(2,:)*temp)/peh/(ct+zetah) - u(2)*(AX(2,:)*temp)*ct/(ct+zetah)
        - (t2+1)*(AX(2,:)*v)*ct/(ct+zetah) - nw*t2/(ct+zetah)
        +B*zetah*ct*nf/zeta/(ct+zetah)*(h2-phetaref*y(22)/kads2/p/(1-
        phetaref*y(22))^5);

yd(64)= (BX(3,:)*temp)/peh/(ct+zetah) - u(3)*(AX(3,:)*temp)*ct/(ct+zetah)
        - (t3+1)*(AX(3,:)*v)*ct/(ct+zetah) - nw*t3/(ct+zetah) +
        B*zetah*ct*nf/zeta/(ct+zetah)*(h3-phetaref*y(23)/kads3/p/(1-
        phetaref*y(23))^5);

yd(65)= (BX(4,:)*temp)/peh/(ct+zetah) - u(4)*(AX(4,:)*temp)*ct/(ct+zetah)
          - (t4+1)*(AX(4,:)*v)*ct/(ct+zetah) - nw*t4/(ct+zetah) +
          B*zetah*ct*nf/zeta/(ct+zetah)*(h4-phetaref*y(24)/kads4/p/(1-
          phetaref*y(24))^5);
```

```
yd(66)= (BX(5,:)*temp)/peh/(ct+zetah) - u(5)*(AX(5,:)*temp)*ct/(ct+zetah)
        - (t5+1)*(AX(5,:)*v)*ct/(ct+zetah) - nw*t5/(ct+zetah) +
        B*zetah*ct*nf/zeta/(ct+zetah)*(h5-phetaref*y(25)/kads5/p/(1-
        phetaref*y(25))^5);

yd(67)= (BX(6,:)*temp)/peh/(ct+zetah) - u(6)*(AX(6,:)*temp)*ct/(ct+zetah)
        - (t6+1)*(AX(6,:)*v)*ct/(ct+zetah) - nw*t6/(ct+zetah) +
        B*zetah*ct*nf/zeta/(ct+zetah)*(h6-phetaref*y(26)/kads6/p/(1-
        phetaref*y(26))^5);

yd(68)= (BX(7,:)*temp)/peh/(ct+zetah) - u(7)*(AX(7,:)*temp)*ct/(ct+zetah)
        - (t7+1)*(AX(7,:)*v)*ct/(ct+zetah) - nw*t7/(ct+zetah) +
        B*zetah*ct*nf/zeta/(ct+zetah)*(h7-phetaref*y(27)/kads7/p/(1-
        phetaref*y(27))^5);

yd(69)= (BX(8,:)*temp)/peh/(ct+zetah) - u(8)*(AX(8,:)*temp)*ct/(ct+zetah)
        - (t8+1)*(AX(8,:)*v)*ct/(ct+zetah) - nw*t8/(ct+zetah) +
        B*zetah*ct*nf/zeta/(ct+zetah)*(h8-phetaref*y(28)/kads8/p/(1-
        phetaref*y(28))^5);

yd(70)= (BX(9,:)*temp)/peh/(ct+zetah) - u(9)*(AX(9,:)*temp)*ct/(ct+zetah)
        - (t9+1)*(AX(9,:)*v)*ct/(ct+zetah) - nw*t9/(ct+zetah) +
        B*zetah*ct*nf/zeta/(ct+zetah)*(h9-phetaref*y(29)/kads9/p/(1-
        phetaref*y(29))^5);

yd(71)= (BX(10,:)*temp)/peh/(ct+zetah) -
        u(10)*(AX(10,:)*temp)*ct/(ct+zetah) -
        (t10+1)*(AX(10,:)*v)*ct/(ct+zetah)  - nw*t10/(ct+zetah) +
        B*zetah*ct*nf/zeta/(ct+zetah)*(h10-phetaref*y(30)/kads10/p/(1-
        phetaref*y(30))^5);

yd(72)= (BX(11,:)*temp)/peh/(ct+zetah)
        u(11)*(AX(11,:)*temp)*ct/(ct+zetah) -
        (t11+1)*(AX(11,:)*v)*ct/(ct+zetah) - nw*t11/(ct+zetah) +
        B*zetah*ct*nf/zeta/(ct+zetah)*(h11-phetaref*y(31)/kads11/p/(1-
        phetaref*y(31))^5);
```

```
yd(73)= (BX(12,:)*temp)/peh/(ct+zetah) -
        u(12)*(AX(12,:)*temp)*ct/(ct+zetah) -
        (t12+1)*(AX(12,:)*v)*ct/(ct+zetah) - nw*t12/(ct+zetah) +
        B*zetah*ct*nf/zeta/(ct+zetah)*(h12-phetaref*y(32)/kads12/p/(1-
        phetaref*y(32))^5);

yd(74)= (BX(13,:)*temp)/peh/(ct+zetah) -
        u(13)*(AX(13,:)*temp)*ct/(ct+zetah) -
        (t13+1)*(AX(13,:)*v)*ct/(ct+zetah) - nw*t13/(ct+zetah) +
        B*zetah*ct*nf/zeta/(ct+zetah)*(h13-phetaref*y(33)/kads13/p/(1-
        phetaref*y(33))^5);

yd(75)= (BX(14,:)*temp)/peh/(ct+zetah) -
        u(14)*(AX(14,:)*temp)*ct/(ct+zetah) -
        (t14+1)*(AX(14,:)*v)*ct/(ct+zetah) - nw*t14/(ct+zetah) +
        B*zetah*ct*nf/zeta/(ct+zetah)*(h14-phetaref*y(34)/kads14/p/(1-
        phetaref*y(34))^5);

yd(76)= (BX(15,:)*temp)/peh/(ct+zetah) -
        u(15)*(AX(15,:)*temp)*ct/(ct+zetah) -
        (t15+1)*(AX(15,:)*v)*ct/(ct+zetah) - nw*t15/(ct+zetah) +
        B*zetah*ct*nf/zeta/(ct+zetah)*(h15-phetaref*y(35)/kads15/p/(1-
        phetaref*y(35))^5);

yd(77)= (BX(16,:)*temp)/peh/(ct+zetah) -
        u(16)*(AX(16,:)*temp)*ct/(ct+zetah) -
        (t16+1)*(AX(16,:)*v)*ct/(ct+zetah) - nw*t16/(ct+zetah) +
        B*zetah*ct*nf/zeta/(ct+zetah)*(h16-phetaref*y(36)/kads16/p/(1-
        phetaref*y(36))^5);

yd(78)= (BX(17,:)*temp)/peh/(ct+zetah) -
        u(17)*(AX(17,:)*temp)*ct/(ct+zetah) -
        (t17+1)*(AX(17,:)*v)*ct/(ct+zetah) - nw*t17/(ct+zetah) +
        B*zetah*ct*nf/zeta/(ct+zetah)*(h17-phetaref*y(37)/kads17/p/(1-
        phetaref*y(37))^5);
```

```
yd(79)= (BX(18,:)*temp)/peh/(ct+zetah) -
        u(18)*(AX(18,:)*temp)*ct/(ct+zetah) -
        (t18+1)*(AX(18,:)*v)*ct/(ct+zetah) - nw*t18/(ct+zetah) +
        B*zetah*ct*nf/zeta/(ct+zetah)*(h18-phetaref*y(38)/kads18/p/(1-
        phetaref*y(38))^5);

yd(80)= (BX(19,:)*temp)/peh/(ct+zetah) -
        u(19)*(AX(19,:)*temp)*ct/(ct+zetah) -
        (t19+1)*(AX(19,:)*v)*ct/(ct+zetah) - nw*t19/(ct+zetah) +
        B*zetah*ct*nf/zeta/(ct+zetah)*(h19-phetaref*y(39)/kads19/p/(1-
        phetaref*y(39))^5);

yd(81)= (BX(20,:)*temp)/peh/(ct+zetah) -
        u(20)*(AX(20,:)*temp)*ct/(ct+zetah) -
        (t20+1)*(AX(20,:)*v)*ct/(ct+zetah) - nw*t20/(ct+zetah) +
        B*zetah*ct*nf/zeta/(ct+zetah)*(h20-phetaref*y(40)/kads20/p/(1-
        phetaref*y(40))^5);

yd(82)= (BX(21,:)*temp)/peh/(ct+zetah) -
        u(21)*(AX(21,:)*temp)*ct/(ct+zetah) -
        (t21+1)*(AX(21,:)*v)*ct/(ct+zetah) - nw*t21/(ct+zetah) +
        B*zetah*ct*nf/zeta/(ct+zetah)*(h21-phetaref*y(41)/kads21/p/(1-
        phetaref*y(41))^5);
```

## A.5 Energy Balance Equations Needed to Include Heat Effect for the PSAR System

The normalized equations developed in Chapter 4 are re-written in terms of the two-space variables defined in chapter 3. The model assumptions of Chapter 4 are valid here, with the addition that the continuity of concentration, mass flux, heat flux, and velocity are applicable at the junction of the two subdomains.

Thus, the fluid phase heat balance equation in the catalyst region is

$$\frac{\partial \overline{T}}{\partial \nu_1} = 0 \tag{A.1}$$

and the fluid phase heat balance equation in the adsorbent region is

$$\frac{\partial \overline{T}}{\partial \tau} = \frac{1}{Pe_H (C_T + \zeta_H)(1-\omega)^2} \frac{\partial^2 \overline{T}}{\partial \nu_2^{\,2}} - \frac{C_T}{(C_T + \zeta_H)(1-\omega)} \frac{\partial}{\partial \nu_2} [U(\overline{T}+1)]$$

$$+ \frac{B\zeta_H}{(C_T + \zeta_H)} \frac{\partial Q_A}{\partial \tau} - \frac{N_w}{(C_T + \zeta_H)} \overline{T} \tag{A.2}$$

The boundary conditions for pressurization and adsorption steps are

$$\nu_1 = 1, (\nu_2 = 0), \tau > 0 \qquad (1-\omega) \frac{\partial \overline{T}}{\partial \nu_1} = \omega \frac{\partial \overline{T}}{\partial \nu_2} \tag{A.3a}$$

$$\nu_2 = 1, \tau > 0 \qquad \frac{\partial \overline{T}}{\partial \nu_2} = 0 \tag{A.3b}$$

The boundary conditions for blowdown step are

$$\nu_2 = 0, \tau > 0 \qquad \frac{\partial \overline{T}}{\partial \nu_2} = 0 \tag{A.4a}$$

$$\nu_2 = 1, (\nu_1 = 0), \tau > 0 \qquad (1-\omega)\frac{\partial \overline{T}}{\partial \nu_1} = \omega \frac{\partial \overline{T}}{\partial \nu_2} \tag{A.4b}$$

The boundary conditions for desorption step are

$$\nu_2 = 0, \tau > 0 \qquad -\frac{1}{Pe_H}\frac{\partial \overline{T}}{\partial \nu_2} = U\big|_{x=0}(1-\omega)C_T\overline{T} \tag{A.5a}$$

$$\nu_2 = 1, (\nu_1 = 0), \tau > 0 \qquad (1-\omega)\frac{\partial \overline{T}}{\partial \nu_1} = \omega \frac{\partial \overline{T}}{\partial \nu_2} \tag{A.5b}$$

The initial condition is

$$\overline{T}(x, \tau = 0) = 0 \tag{A.6}$$